

AERODYNAMIC OPTIMIZATION OF BUILDING AUGMENTED WIND TURBINES

by

John Adam MacQuarrie

Bachelor Aerospace Engineering, Ryerson, 2008

A thesis

presented to Ryerson University

in partial fulfillment of the
requirements for the degree of
Master of Applied Science
in the Program of
Aerospace Engineering

Toronto, Ontario, Canada, 2011

©John Adam MacQuarrie 2011

I hereby declare that I am the sole author of this thesis.

I authorize Ryerson University to lend this thesis to other institutions or individuals for the purpose of scholarly research.

I further authorize Ryerson University to reproduce this thesis by photocopying or by other means, in total or in part, at the request of other institutions or individuals for the purpose of scholarly research.

Aerodynamic Optimization of Building Augmented Wind Turbines

Master of Applied Science 2011

John Adam MacQuarrie

Aerospace Engineering

Ryerson University

Abstract

The omnipresence of wind, low production cost and much advancement within the field, wind power provides a vast and promising renewable energy resource. With the current high prices of oil and pressure to reduce carbon emissions, wind energy has achieved great interest creating high demands for innovative wind technology. Additionally, producing energy at the door step of consumers, such as at consumer dwellings in urban areas, wind power provides a means of producing efficient and reliable energy.

The use of architectural structures to provide an augmentation source for the wind has been pursued by some ambitious architects but the effects of building augmentation are still uncertain. This study used computational fluid dynamic models to analyze varying building geometries and their effects on power augmentation. A porous region was used to model a wind turbine back pressure across the gap between the buildings. Results show augmentation increases power production one to two times compared to equivalent size free-standing wind turbines. Results also show that certain wind incidence angles provide the best augmentation indicating that building geometry is optimal when design takes into consideration winds regularity azimuth.

Acknowledgements

I would like to thank my advisor Dr. Paul Walsh for giving me the opportunity to work with him on this insightful thesis.

I would also like to extend my gratitude to Dr. Jasson Lassaline for his technical support needed for the completion on this thesis.

I would like to thank the Shared Hierarchical Academic Research Computing Network (SHARCNET, www.sharcnet.ca) and Compute/Calcul Canada for providing me with the facilities to perform this immense study.

Lastly, I would like to extend tremendous gratitude to my mentor and friend Alberto Bueron for his wealth of support, guidance and voice of reason throughout this thesis.

Dedication

This thesis is dedicated to my close friends and family for giving me the support and encouragement needed in the pursuit of this degree.

Contents

1	Introduction	1
1.1	Ducted Wind Turbines	4
1.2	Building Augmented Wind Turbines	6
1.3	Betz Limit	6
2	Background	13
2.1	Flow Between Cylinder Pair	13
2.2	Strouhal Number	14
2.3	Von Karman Street	15
2.4	2D Optimized BAWT Footprint	17
2.5	Statement of Purpose	18
3	Model and Mesh Development	19
3.1	Modeling	19
3.1.1	Domain Boundaries	19
3.1.2	Bodies of Influence	24
3.2	Meshing	29
3.3	Inflation Layers	29
3.4	Sponge Layer	33
3.5	Element sizing	33
3.6	Grid and Time Step Study	34
3.6.1	Steady State Grid Convergence	34
3.7	Time Step Study	38
3.8	Grid-Time Step Study	39
4	Methodology	41
4.1	Boundary Conditions	41
4.2	Solution Parameters	43
4.3	Solution Criteria	43
4.4	Augmented Power	47

5	Results	49
5.1	Velocity Augmentation	49
5.2	Augmented Power	53
5.2.1	Total Power	53
5.2.2	Power Augmentation Factor	55
5.3	Power Rating	55
5.3.1	Even Frequency Regimes	57
5.3.2	Wind Regime Case Study	61
6	Conclusion	65
6.1	Future Work	65
	Bibliography	106

List of Tables

2.1	Strouhal numbers and frequencies in flow of Reynolds number 10^6	14
2.2	Optimal parameters for different wind variations	17
3.1	Various model cases	23
3.2	Element size controls	34
3.3	Steady state grid convergence and associated errors	38
3.4	Convergence of power with respect to time step size	39
3.5	Steady state grid convergence	40
5.1	Incidence angles and relative frequencies of wind regimes	57
5.2	Wind regime of Toronto Island	61
5.3	Power rating for the wind regimes	64
B.1	Vortex propagation distances after three periods with respect to Strouhal numbers	69

List of Figures

1.1	Global temperature change	2
1.2	Bahrain World Trade Center (Manama, Bahrain)	3
1.3	Schematic sketch of mean flow stream line pattern around a building	4
1.4	Ducted turbines: Left: Roof top mounted, Right: Building integrated	5
1.5	Building integrated ducted turbine with spoiler	5
1.6	Two buildings used as concentrators	7
1.7	Project WEB	8
1.8	Project WEB performance	9
1.9	Turbine performance	10
1.10	Betz limit	11
2.1	Vortex street from cylinder pair	14
2.2	Iso-surface of Q-criterion depicting von Karman street and associated pressure	15
2.3	Oscillation of measured power for results of case ($R_t = 0, R_x = 0, R_y = 0, \alpha = 60^\circ$)	16
2.4	Varying parameters on a 2D building footprint	18
3.1	Variation of 3D BAWT parameters	21
3.2	Variation of taper ratio R_t	22
3.3	Variations of variables R_x and R_y	22
3.4	Front view of BAWT and simulated turbine capture area	23
3.5	Top view of turbine spans across and extends height of the BAWT	24
3.6	Side and top views of the domain	25
3.7	Isometric view of the domain	26
3.8	Close view of BAWT system with plain simulating turbines	27
3.9	Bodies of influence defining the vortex street defined	28
3.10	Inflation layers against building facade	30
3.11	Unwrapped building surface's y^+ values along building height	32
3.12	Sponge layer defining the outlet boundary	33
3.13	Surface mesh of <i>Walls, Turbine</i> and <i>Ground</i>	35
3.14	Mesh sliced lengthwise across <i>Turbine</i>	36
3.15	Steady state mesh convergence	37

3.16	Grid convergence at $t_i = 1s$	40
4.1	Log-Law velocity profile of ABL	42
4.2	Mean time power coverage study ($R_t = 0.33, R_x = 0, R_y = 1, \alpha = 0^\circ$)	44
4.3	Error coverage study ($R_t = 0.33, R_x = 0, R_y = 1, \alpha = 0^\circ$)	45
4.4	Mean time power coverage study ($R_t = 0.33, R_x = 0.5, R_y = 1, \alpha = 60^\circ$)	46
5.1	Results	50
5.2	Results continued	51
5.3	Velocity augmentation factors	52
5.4	Total Power	54
5.5	Power augmentation factors	56
5.6	Power rating for high regime	58
5.7	Power rating for medium regime	59
5.8	Power rating for low regime	60
5.9	Toronto Island yearly average wind rose plot	62
5.10	BAWT azimuth on wind rose plot	63
5.11	Power rating for Toronto Island case study	64
B.1	Body of influence	70
B.2	Q-Criterion Iso Surface with Turbulent kinetic energy variations ($R_t = 0.33, R_x = 0.5,$ $R_y = 0.5$ and $\alpha = 0^\circ$)	71
B.3	Q-Criterion Iso Surface with Turbulent kinetic energy variations ($R_t = 0$ and $\alpha = 60^\circ$)	72
C.1	Pressure reading through BAWT a model	74
D.1	Contour of pressure on BAWT walls the pressure contour through the mid-plane projected on the domain side wall	77
D.2	Flow stream lines ($R_t = 0, R_x = 0, R_y = 0$ and $\alpha = 0$)	78

List of Appendices

A	Parabolic BAWT Profile Formulation	67
B	Bodies of Influence	69
C	Porous Jump	73
D	Figures	77
E	Velocity Inlet ABL UDF	79
F	FLUENT Journal Scripting	81
G	Shell Bash Script	83
H	FLUENT CFD Code Settings	85
I	Sample Output File	95

List of Symbols

Re	Reynolds number
S_t	Strouhal number
Δy	Distance of first element off the wall
α	Permeability of the porous media
μ	Fluid viscosity
τ	Shear stress
n	Number of inflated prism layers
y^+	Nondimensional distance
l_{vp}	Vortex propagation distance
N_i	Number of iterations
P_i	Power at i^{th} iteration
R_t	taper ratio
R_x	forward lean
R_y	building spread
t	Time
t_i	Time at i^{th} timestep
u	Velocity in the x -direction
u_p	Potential Velocity
z	z -displacement
z_o	Surface roughness height

χ	Placeholder
\varnothing	diameter
C_2	Coefficient of pressure
Δm	Porous jump thickness
ΔP	Pressure drop
ρ	Density

Chapter 1

Introduction

Wind power is generating interest amongst many nations to produce cheaper and sustainable electrical power to combat the soaring prices on fossil fuels and to reduce CO_2 emissions [20]. It is well known and documented that CO_2 emissions from burning fossil fuels is contributing to global warming which has been felt all around the world. Figure 1.1 shows the average global temperature change documented by NASA indicating a dramatic rise in temperature caused by CO_2 emissions [3]. Fox [6] stated the world's energy demand has increased two fold from 1971 to 2003, and currently will increase 40% by the year 2020. It is imperative that renewable energies is further developed and integrated into power systems to reduce fossil fuel emissions.

Compared to other renewable energies such as hydro, wave energy and solar, wind energy is the most promising form of renewable energy. It has sustained a 25% compounded rate of growth for over a decade and has exceeded a total capacity of 60,000MW [6]. The winds ability to produce power any hour of the day and season makes it a good source of energy [6]. Vast wind farms far from city centers have been constructed to mitigate the pressure of increased power demands due to growing urban areas. However, the great lengths of transmission lines used in power delivery to the areas are expensive to build and maintain, which makes wind farm energy less of an economical energy resource.

The problem of the integration of wind turbines into the urban environment is the spatial constraints imposed on the turbine size. Wind turbines extract kinetic energy from the wind through the turbine capture area and power increases capture area. Imposing size limit constrains turbines to produce little energy and making wind energy in urban environments not appealing.

A way to combat the size constraints was to increase power by increasing kinetic energy of the air. One method was to accelerate air velocities through a duct and a turbine by means of a pressure drop. It was shown ducted turbines boosted power and became integrated into the roof tops of some commercial building.

Research has been done by Campbell [22] to utilize the airflow between buildings where wind speeds increase to pass through narrow gaps. The increased wind velocity that occurs between building structures is known as the venturi effect which many researchers are utilizing to increase kinetic energy of the wind to drive smaller turbines to produce equivalent energy yields to larger turbines in open fields.

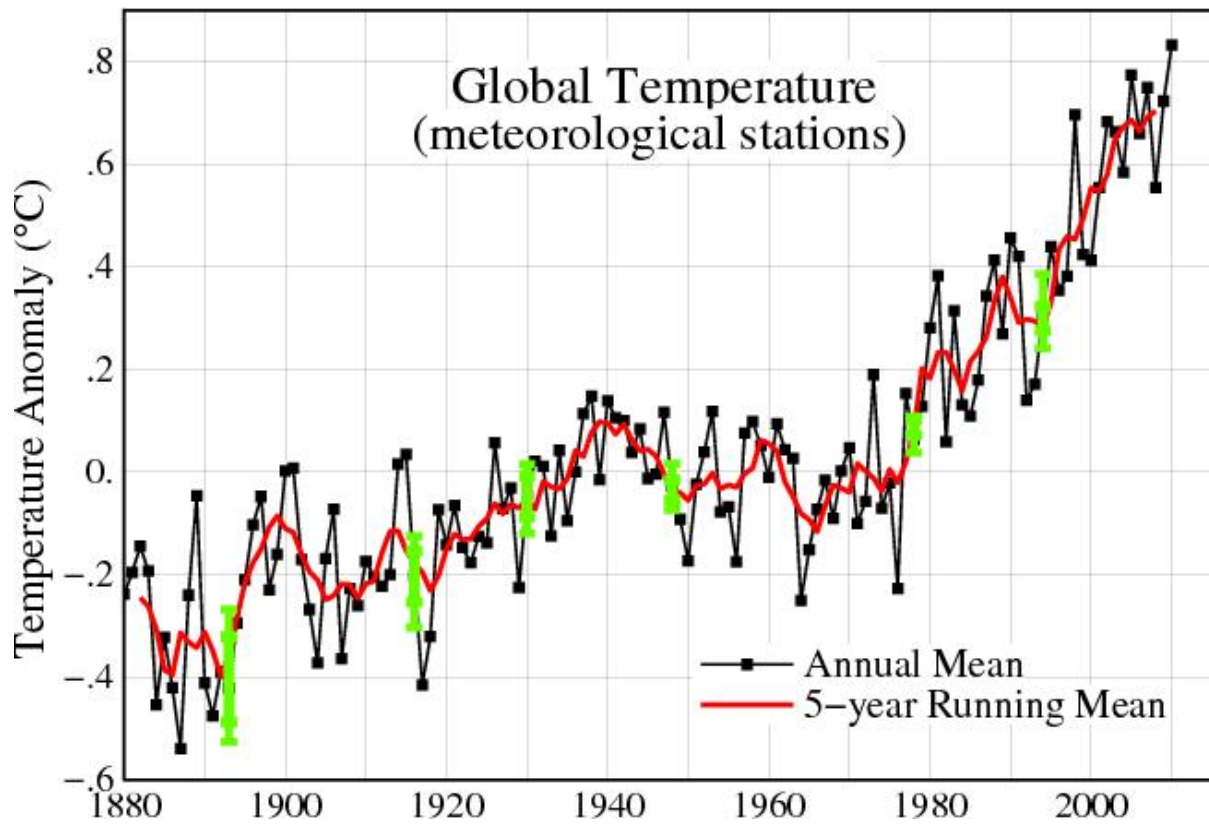


Figure 1.1: Global temperature change
[3]

The size of urban turbines are constrained by space in which makes them less viable compared with their larger stand alone counterparts [22]. Concerns with the implementation of turbine into urban areas are the energy yield and the return on investment.

A system where two buildings are used to increase the winds kinetic energy is called building augmented wind turbine (BAWT). The Bahrain World Trade Center (BWTC) shown in Figure 1.2, was the first BAWT system to have been erected in 2008. Three 29m diameter turbines are suspended between its two tower facing north to take advantage of the blowing winds from the Persian Gulf from a 90° azimuth. The BWTC was shown to produce 11%–15% of the buildings electrical power [22]. Reasonings for the architectural building shape and optimized performance test results were not obtained.

Campbell [22] found in his research an optimal shape that would generate best power augmentation. He derived his shape using computational fluid dynamics (CFD) to analyse the shapes of the buildings and verified his results with scaled wind tunnel and field tests.



Figure 1.2: Bahrain World Trade Center (Manama, Bahrain)

This study uses CFD (computational fluid dynamics) software to compute the mass flow of air driven through a series of BAWT configurations with a simplified turbine model and compares the total power captured by the various configurations. This thesis will show that building shapes can be varied for maximizing power generation by wind augmentation.

Wind turbines are only 60% effective which is called the Betz limit and will be derived in subsequent

sections. It should be noted that some published studies made the mistake to state that the augmentation increases performance past Betz limit. An augmentation of the wind has only taken place to accelerate velocities through the rotor where the turbine can extract a maximum power factor of 59.3%.

1.1 Ducted Wind Turbines

Ducted wind turbines are categorized as small wind turbines which are situated inside or at the end of an air duct. These turbines are mounted generally on a roof top or integrated into the buildings facade. One end receives ambient air to be accelerated through the duct and directed to the turbine and the exit flow is directed perpendicular to the outside wind. This is done to utilize the separated flow from the leading edge of the turbine unit or the buildings roof. Such a setup produces a low pressure region which increases the mass flow and energy potential in the air. A schematic of the flow streamline passing over a building is shown in Figure 1.3. Figure 1.4 is the first model of a ducted wind turbine produced in 1979 by a Glaswegian engineer [9].

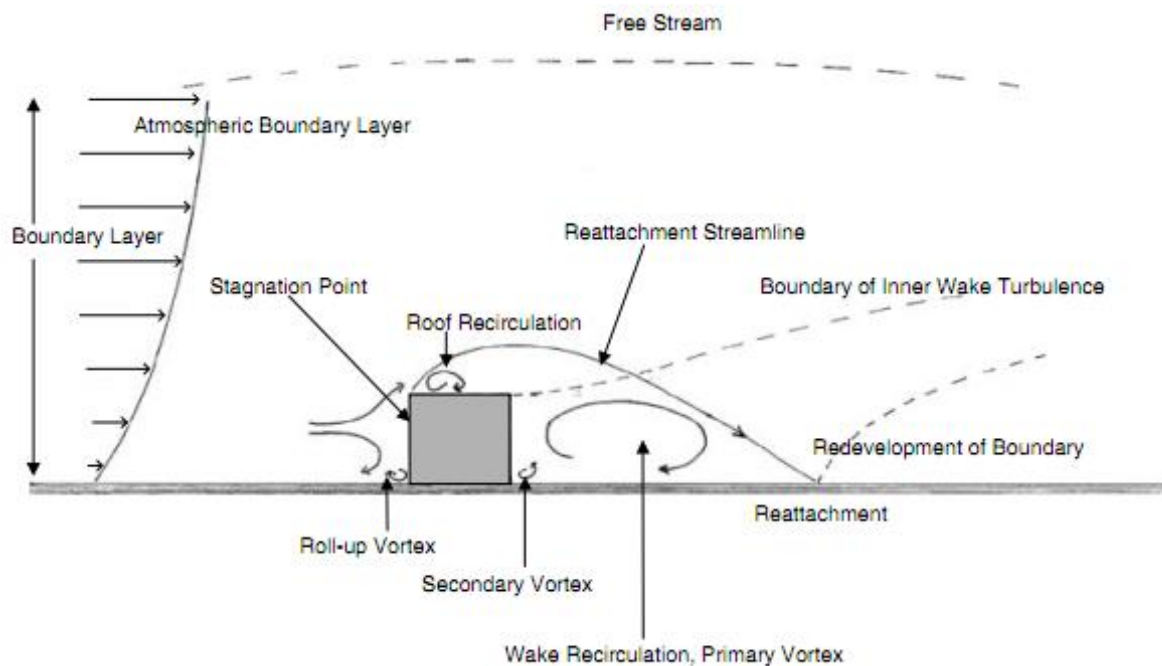


Figure 1.3: Schematic sketch of mean flow stream line pattern around a building [9]

Building integrated ducts increase air velocity from outside ambient air to the turbine by 20% and provide a 1.7 power increase compared to a bare stand-alone turbine of equal size. Spoilers can also be added to the top of the inlet to increase the performance. Spoilers slightly increase velocities from 30% to 40% at wind incidence angles up to 40° with a power increase to 2.2 to 2.7 [9]. Figure 1.5 shows a

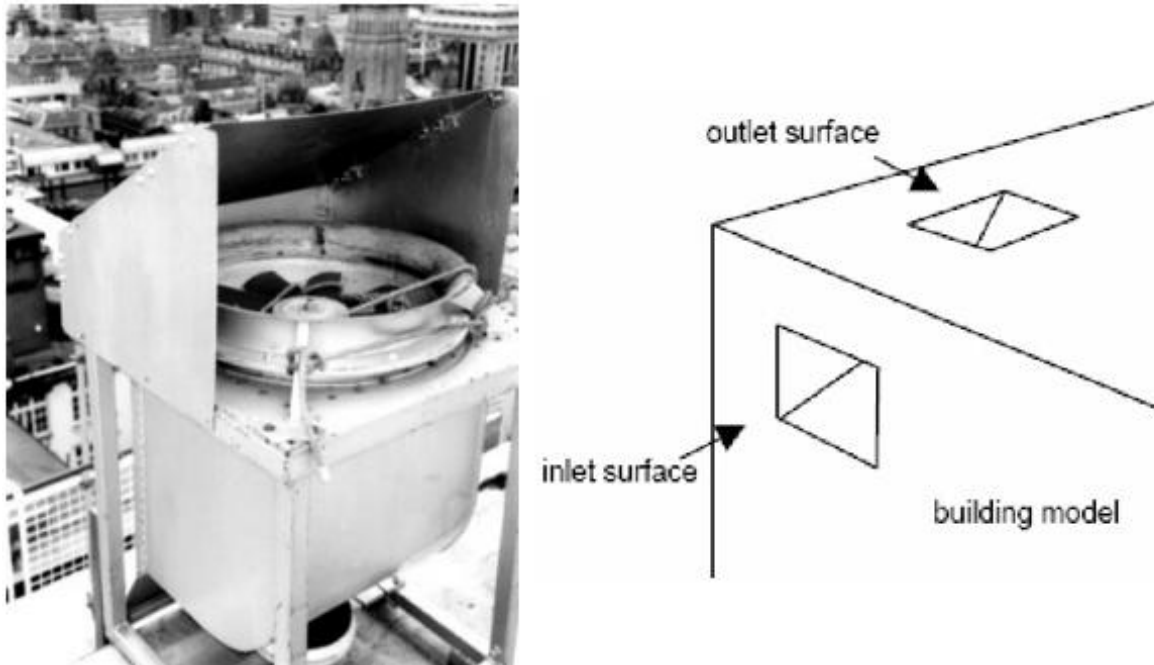


Figure 1.4: Ducted turbines: Left: Roof top mounted, Right: Building integrated [9]

spoiler mounted above the inlet of a building integrated wind turbine. Due to the size of ducted wind turbines, they are considered a small scale energy producer ranging from 250W–500W.

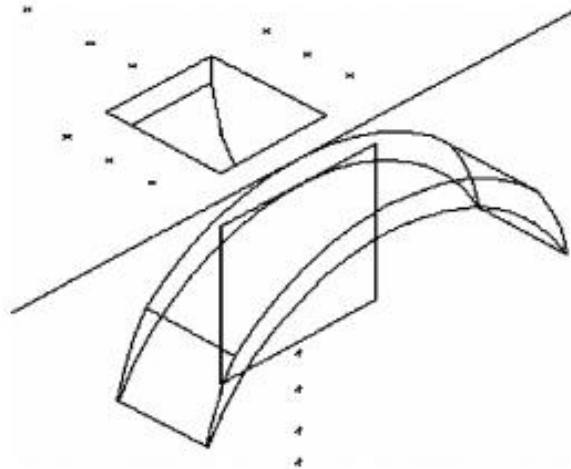


Figure 1.5: Building integrated ducted turbine with spoiler [9]

1.2 Building Augmented Wind Turbines

A building augmented wind turbine (BAWT) system utilizes the venturi effect where the facade of the building is used to create a pressure drop through the system to increase the kinetic energy of the wind at the turbine rotor. Augmentation of the wind using buildings can be done either by integrating and retro-fitting existing buildings with wind turbines or designing buildings aerodynamically.

There are different types of BAWT system that are in use today where turbines are mounted on the side or top of a building. This study is focused on BAWT systems where two buildings are acting as a wind augmentser with turbines suspended between the buildings. This type of BAWT is shown in Figure 1.6.

Several studies have been performed in the exploration of two-building BAWT systems. Imperial College [5] developed and tested BAWT systems where the building designs were contrived by the aerodynamic performance of the augmenters. This project is known as Wind Energy for the Built Environment (Project WEB) [22] and is shown in Figure 1.7 . The key findings from that research were that optimal augmentser geometries were smooth, rounded and resembled a structural footprint of a ‘kidney’ or ‘boomerang’ shape. It was also found that losses due to flow separation could be reduced by incorporating closely fitted wings or an infill to shroud the turbine and good wind augmentation could be obtained at high angles of incidences up to 75° [5].

Results from the Project WEB are shown in Figure 1.8. Substantial power enhancement up to 2.5 was obtained for low velocities and considerable power enhancement around 1.5 was obtained for speeds greater than 5m/s. Figure 1.8 also shows good power enhancements at 0° , 30° , and 60° incidence and power generation still occurs at a wind incidence angle of 90° .

There were some issues raised by Campbell [22] concerning the environmental integration of the BAWT systems. Aerodynamically optimal designs may prove suboptimal economically and the buildings performance may not be energy efficient. Floor plans may not provide practical living space for the occupying residence. Spaces adjacent to the turbines would be less inviting due to concerns over noise, flickering of rotating blades and electromagnetic interference with electronic devices. Campbell suggested the possible solutions to tackle these concerns by placing service areas such as elevators and stairs adjacent to the turbines where these service areas could act as a buffer to the occupied spaces [22].

1.3 Betz Limit

The principle of wind turbines is to extract kinetic energy from the prevailing wind and convert it into electricity. A limit to the maximum extractable kinetic energy from the wind by a wind turbine was theorized to be 59.3% by Betz in 1919 [13], and is appropriately termed the Betz limit. Betz formulated the limit using simple one dimensional Bernoulli equation to model incompressible wind flow across the rotor. The assumptions used in the derivation were a constant, uniformly distributed velocity and pressure profile across the turbine’s seeping area. Due to this model is one dimensional, tip losses due to rotational effects and viscous dissipation are neglected.



Figure 1.6: Two buildings used as concentrators

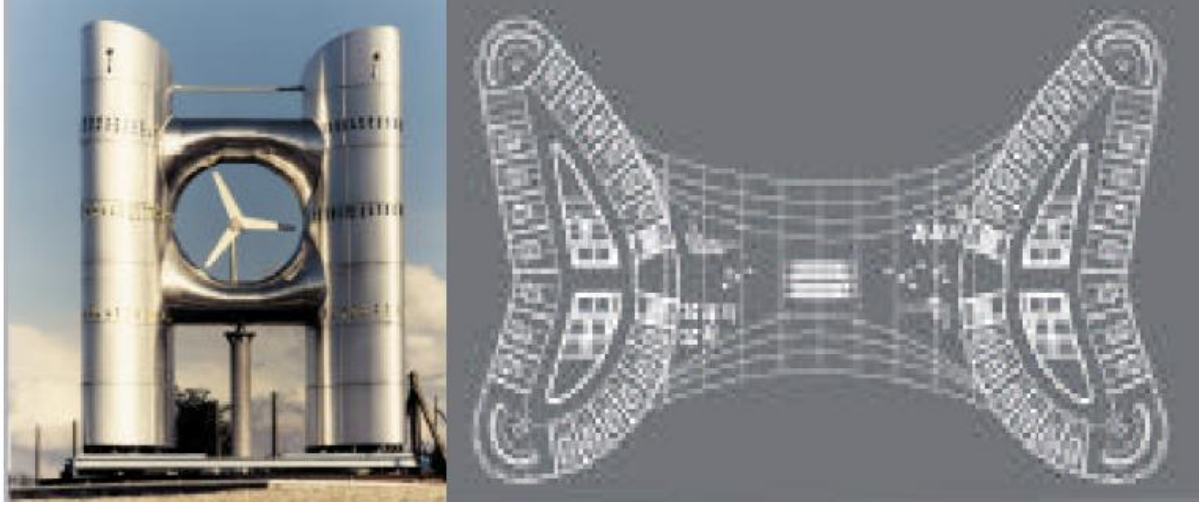


Figure 1.7: Project WEB
[22]

Referring to Figure 1.9, Betz assumed a stream tube of constant mass flow starting with the undisturbed wind flow defined as V_1 , and V_2 as the velocity of the wind before and aft of the rotor. Also it was assumed the wind velocity at the turbines rotor is the mean velocity of the wind before and aft of the rotor. Thus the mean wind speed at the rotor is given as

$$V = \frac{1}{2}(V_1 + V_2) \quad (1.1)$$

The assumption of incompressibility makes the mass flow of the given stream tube to be constant at the rotor inlet and is defined as

$$\dot{m} = \rho A_r V \quad (1.2)$$

where, ρ is density of air, A_r is the rotor sweeping area, \dot{m} is the mass flow through turbine rotor area and V is the mean velocity of air at the rotor. The kinetic energy extracted by the turbine is defined by the change in kinetic energy of the inlet and exit of the stream tube.

The Betz limit is defined as the ratio of change in kinetic energy to the undisturbed kinetic energy. Simplified, the power ratio is defined as

$$PR = \frac{P}{P_o} = \frac{1}{2}(1 - VR^2)(1 + VR) \quad (1.3)$$

where $VR = V_2/V_1$ is considered the velocity ratio. A graphical representation of Equation 1.3 is presented in Figure 1.10. The inflection point is the Bezt limit and is found by the minimization of the

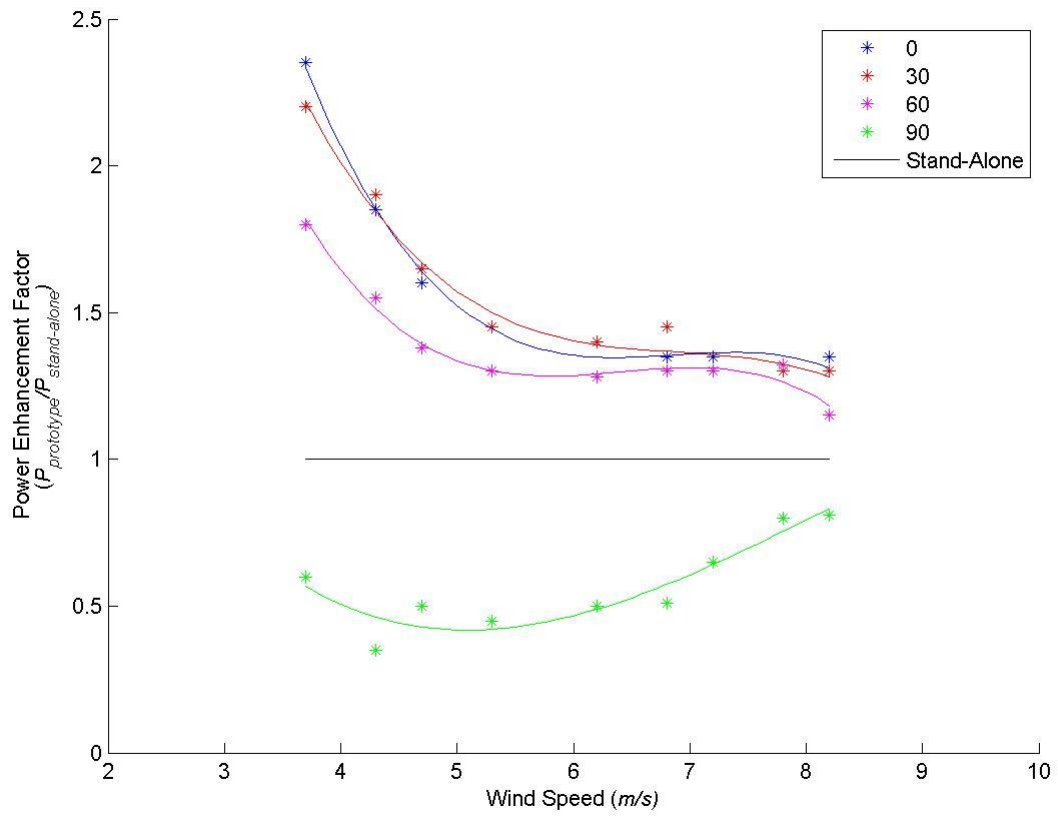


Figure 1.8: Project WEB performance [22]

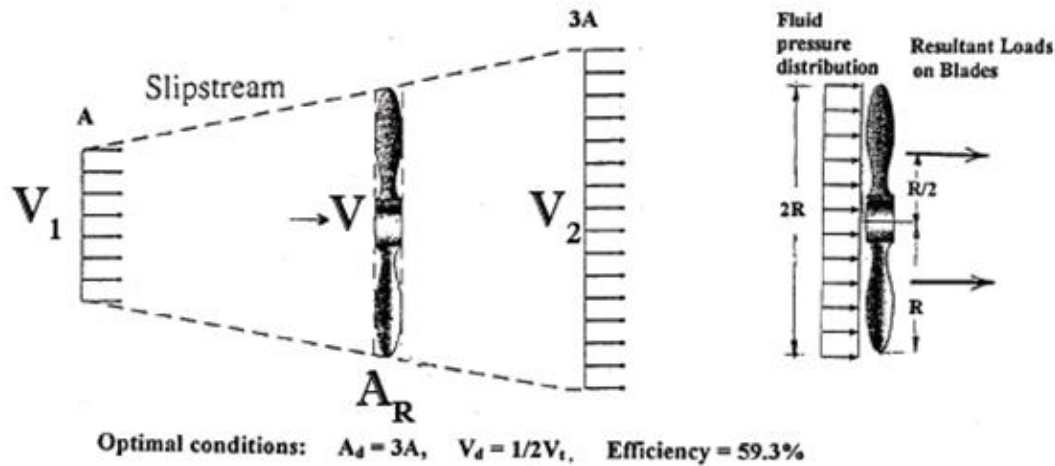


Figure 1.9: Turbine performance
[13]

differential form of Equation 1.3 to yield the velocity ratio corresponding to the maximum power ratio. Maximum power ratio of 0.593 is the Betz limit and is represented in Figure 1.10.

In reality the Betz limit cannot be achieved with a wind turbine alone due to aerodynamic losses, viscous dissipation, and efficiency losses through mechanical and electrical power converting devices. Such losses arise due to mechanical efficiency losses which reduces the power to 35%–45%. There are energy converters, transmitters, generators and storage devices, the energy extracted drops to 10%–30% of the available potential wind power. However, engineers are using shrouded and ducted turbines to increase the overall mass flow to the turbines increasing the flow's kinetic energy. These devices are known as wind augmentation devices because they increase the mass flow and kinetic energy at the rotor plane by utilizing the pressure differential to increase the energy density of the flow.

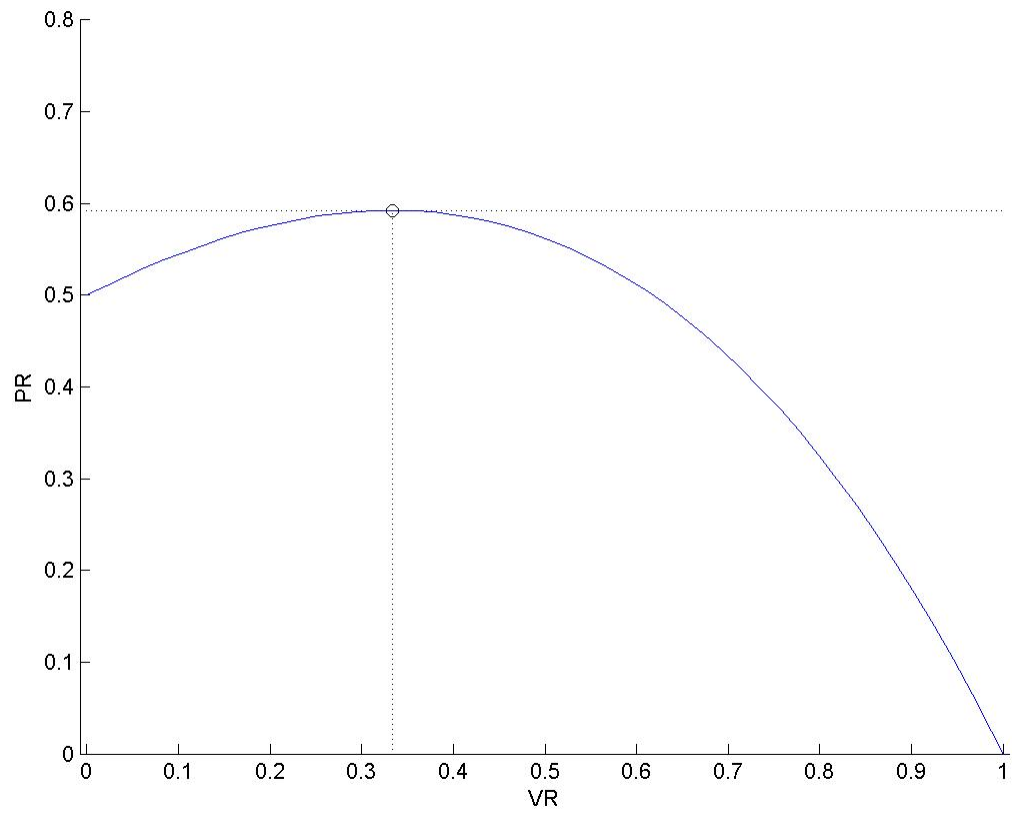


Figure 1.10: Betz limit

Chapter 2

Background

It is well known that turbulence generated aft of an obstacle can affect the upstream flow characteristics and therefore proper modeling techniques of the turbulence aft of the BAWT systems were utilized. Vortex shedding occurs in a fluid as it passes blunt objects. Alternating low-pressure regions form behind objects which curls the flow into these regions creating a vortex. The vortex low-pressure regions propagate downstream and affect the pressure throughout the solution domain which is known as a pressure cascade. Modeling this pressure cascade from vortex shedding will influence the flow characteristics upstream of the BAWT which affects the velocity of the flow passing through the *Turbine* boundary. This chapter presents the background information for the formulation of methods used to model vortex shedding in the subsequent sections.

2.1 Flow Between Cylinder Pair

Investigation into flow around paired cylinders had been studied by many researchers like Bearman and Wadcock [7], and Kim and Durbin [17]. Figure 2.1 shows the von Karman street aft of cylinder pairs in low flow Reynolds numbers.

The spatial distance separating the cylinder normalized by the cylinder diameter (gap ratio) was the subject of study. They concluded that with gap ratios of 0.5 to 1, the flow is deflected from one body and back to the other in an alternating manner and becomes asymmetric downstream. For gap ratios less than 0.5, the flow around the two cylinders resembled a flow around a single bluff body and produced a single vortex street. The studies also noted that there were multiple modes and Strouhal Numbers for the quasi-stable and alternating behaviours complicating the determination of the vortex shedding period [7, 17].

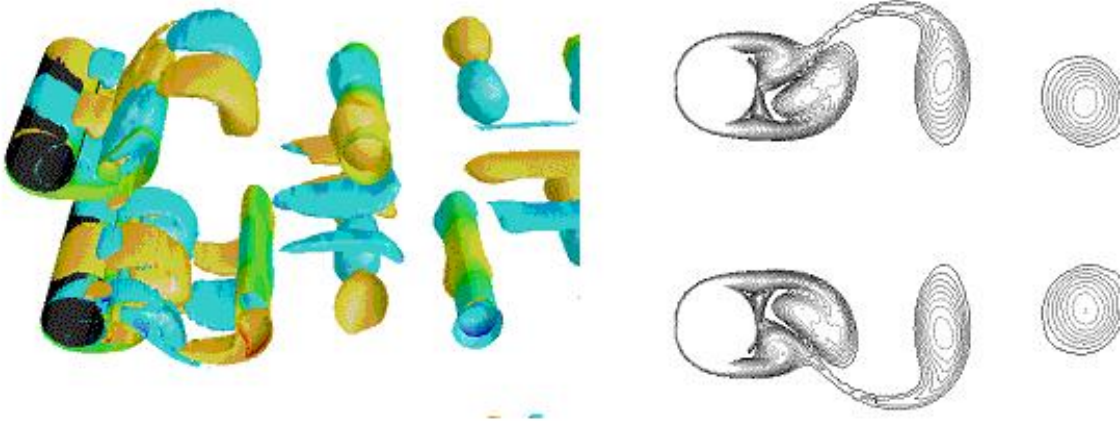


Figure 2.1: Vortex street from cylinder pair
[8]

Strouhal Numbers	Frequency [Hz]
0.18	0.0374
0.50	0.1040

Table 2.1: Strouhal numbers and frequencies in flow of Reynolds number 10^6
[24]

2.2 Strouhal Number

The von Karman street which forms aft of the BAWT will develop regular periodic oscillation of vortex shedding. Physicist Strouhal described these oscillating frequencies of the vortex street from a circular cylinder as a dimensionless number appropriately named the Strouhal number. The formula for the Strouhal number is shown in Equation 2.1

$$S_t = \frac{f_r L}{V} \quad (2.1)$$

where f_r is the frequency of the vortex shedding, L is the characteristic length of the circular cylinders and V is the velocity of the fluid. For Strouhal numbers high as 1 represent flows dominated by viscosity where slow oscillating motion happens. For Strouhal numbers to the order of 10^{-4} , high speeds dominates the flow and intermediate number characterise turbulent flow with build up of shedding vortices [23]. Experimental results from Zdravkovich [24] on for flow over a cylinder at a Reynolds number of 10^6 give Strouhal numbers ranging from 0.18–0.50 and relative frequencies are given in Tabletab::Strouhal numbers.

For the purpose of this study a Strouhal number of 0.18 is used to predict the vortex shedding

frequency using $L = 20\text{m}$ and $V = 4.16\text{m/s}$ giving a frequency of 0.0374Hz or and a shed period of 26.7s . Flow simulation accuracy can be achieved by using low order time steps to analyse the vortex structures. Due to the computational resources needed, CFD simulations were performed using 1s time step, one order less than the shedding period.

2.3 Von Karman Street

This study is focused on the augmented power ratio resultant of the BAWT geometry and transient pressure fluctuations created by the resultant von Karman street. The technique used in viewing vortices was given by [2] wherein creating an isoplot of the Q-Criterion at the lowest calculated value. The Q-criterion is a factor used in determining vortex structures in turbulence where flow rotation dominates strain [18]. Using the ANSYS post processing program, an isoplot of the Q-Criterion at the lowest calculated value is created to describe the von Karman street generated downstream as shown in Figure 2.2.

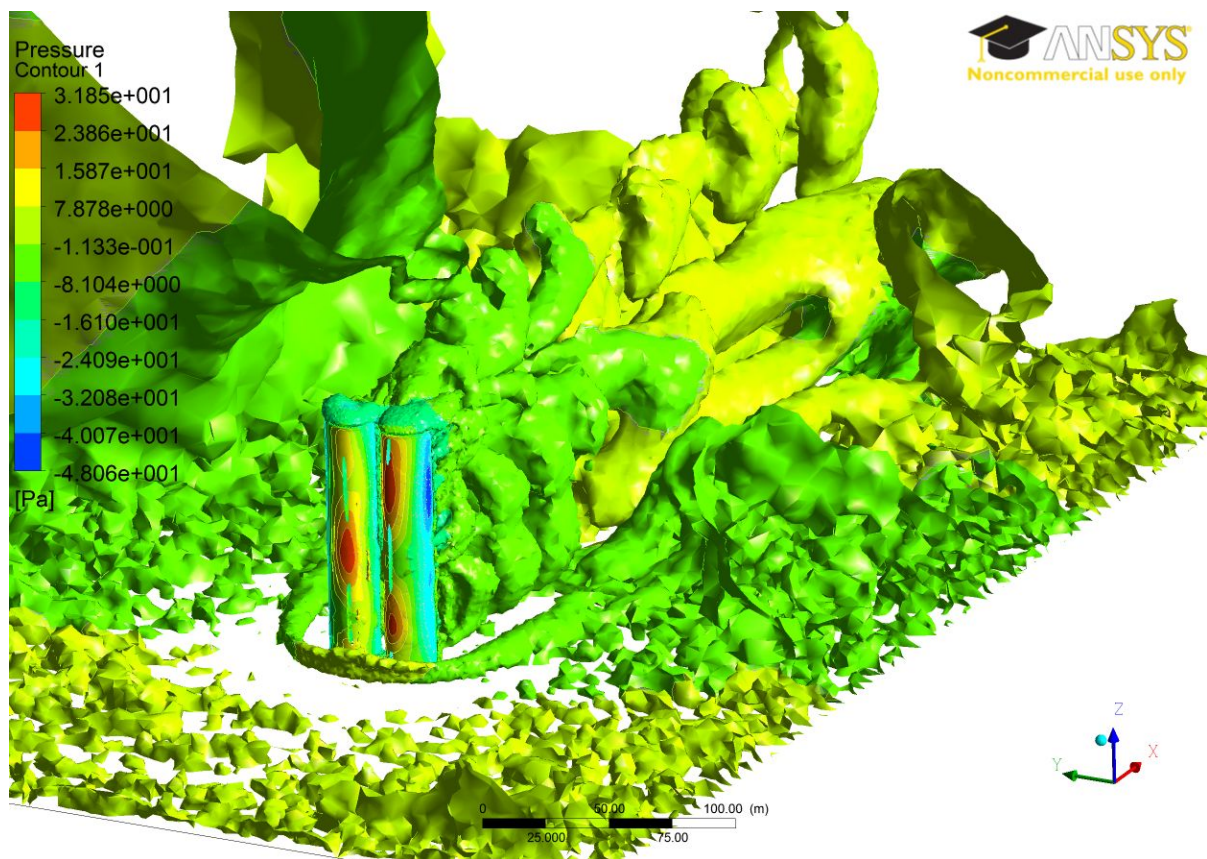


Figure 2.2: Iso-surface of Q-criterion depicting von Karman street and associated pressure

The technique used describes the von Karman street quite well and conforms to the size and frequency

of the shed vortices previously mentioned in Table 2.1. It is shown in Figure 2.2 a periodic von Karman street forms downstream. The bubble formations are vortex rollups which occur after its been shed from the building. There are three vortecies within the designated vortex street clearly defined by the bodies of influence. Von Karman street conforms to the belief that the vortex size does not have considerable change downstream and falls within the expected Strouhal numbers.

Fluctuations of the measured augmented power were either small or insignificant at low wind incidence angles. Where at wind incidence angles of 40° and 60° , oscillations in the measured augmented power are evident. Figure 2.3 is a look at a solution oscillating with respect at 60° wind incidence angle.

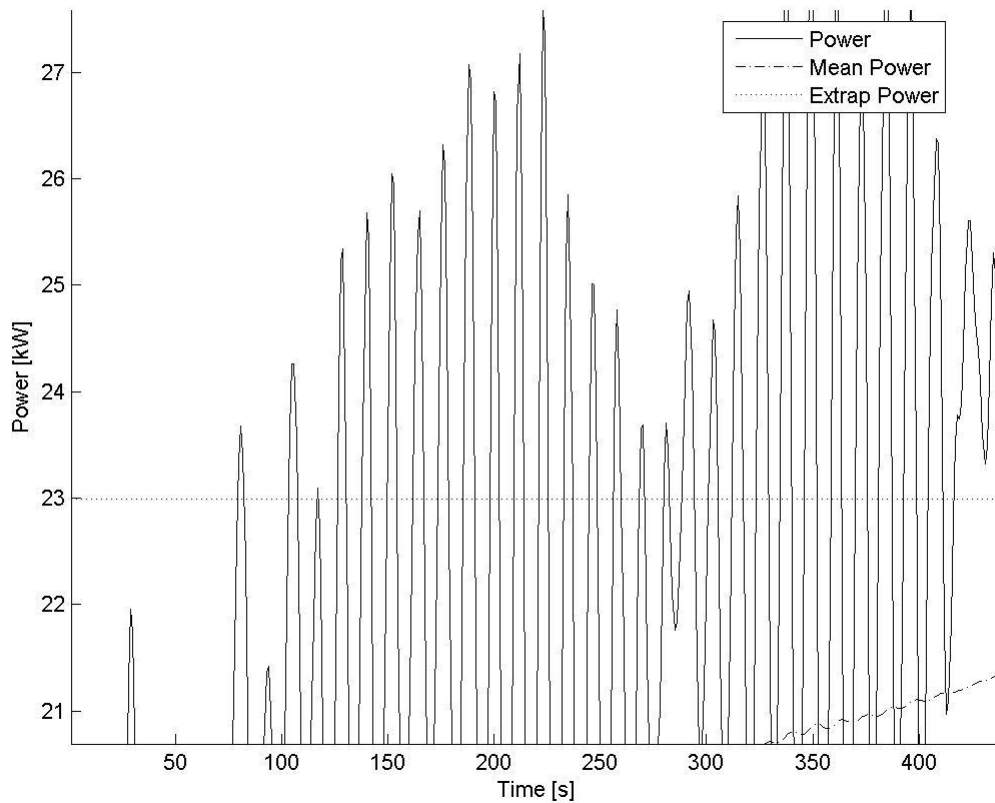


Figure 2.3: Oscillation of measured power for results of case ($R_t = 0$, $R_x = 0$, $R_y = 0$, $\alpha = 60^\circ$)

Scrutinizing the solution oscillations in Figure 2.3, there are 8–9 periods in a span of 100s resulting in shedding frequencies within the range of 0.08Hz–0.09Hz. The range of Strouhal numbers corresponding to the shedding frequency range is 0.385Hz–0.433Hz respectively. The measured Strouhal number fall within the range given by Zdrakovich in Table 2.1 thus verifies the solution model of this study.

Parameters	Wind Variations	
	Low	High
Thickness (b_x/D_o)	20/20	40/20
Oblatness (a/D_o)	15/20	5/20
Gap (g/D_o)	3/20	3/20

Table 2.2: Optimal parameters for different wind variations [14]

$$\begin{aligned}
 S_t &= \frac{f_r L}{V} \\
 &= \frac{0.08(20)}{4.16} \\
 &= 0.385
 \end{aligned}$$

After three periods and shedding frequency of 0.08Hz a vortex propagates 156m downstream, which is within the mesh body of influence defining the von Karman street. A vortex propagation distance was calculated by

$$\begin{aligned}
 L_p &= 3(P)V \\
 &= 3(12.5)4.16 \\
 &= 156m
 \end{aligned}$$

2.4 2D Optimized BAWT Footprint

Research of a 2D BAWT was performed by Hans Hamm [14]. His model consists of a base 2D geometry where he obtained through a CFD study optimal designs that provides the greatest wind augmentation factors in cases with high and low wind incidence angles.

Figure 2.4 is Hamm's illustration of the optimal two dimensional BAWT configuration at low variations in wind incidence angles. The dimensions parameters are nondimensionalized with respect to the base diameter of the BAWT.

Hamm's [14] research was a study on deriving geometries for best wind augmentation. However a configuration which produces best wind augmentation may not necessarily be the best for power production. The total power produced by wind turbines should also be taking into consideration for BAWT optimization studies. Wind speeds were shown to increase with the reduction of the gap distance but limits the wind turbines rotor diameter to produce small amounts of energy. Maximizing the rotor

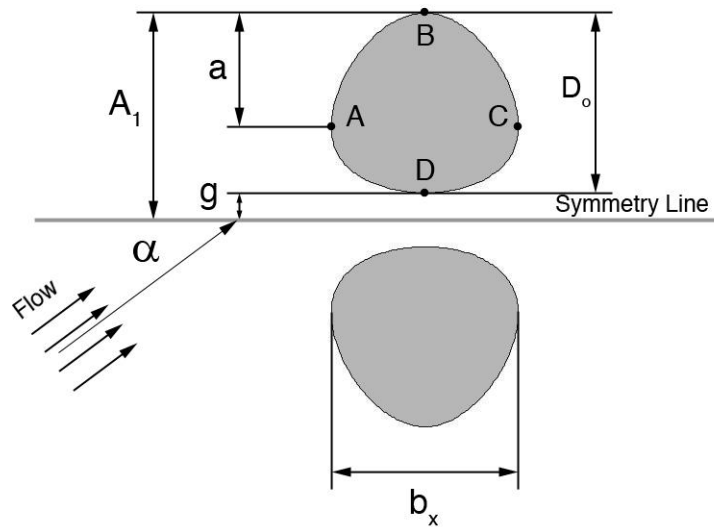


Figure 2.4: Varying parameters on a 2D building footprint
[14]

diameter to increase energy yields is the main factor when for wind farming and should be taken into consideration for optimizing BAWT systems.

2.5 Statement of Purpose

This research is intended to analyse variations of building facades with respect to three different parameters to determine their effects on power augmentation performance at various wind incidence angles. The BAWT will be modeled from a base two-dimensional building footprint where a controlled extruded three-dimensional building facade is varied under the three parameters of: taper (R_t), forward lean (R_x) and spread (R_y). All BAWT configurations were analysed with wind incidence angle as a factor in the overall performance.

The goals of this research are:

1. Determine power variations of different BAWT configuration using three varying parameters such as; taper (R_t), forward lean (R_x), and spread (R_y)
2. Determine increase of power that can be achieved using building facades as augmenters/concentrators
3. Determine the augmentation factors for each configuration
4. Determine the best BAWT configuration for three varying wind regimes
5. Determine the overall BAWT power ratings

Chapter 3

Model and Mesh Development

This section discusses the approach used in the development of the models and the mesh. Nineteen BAWT model configurations were created varying in shape using three parabolic parameters with associated constraints and contained within a solution domain. The grids were created to adequately defined the boundary layer along BAWT walls and the resulting turbulent flow structures downstream of the domain.

3.1 Modeling

Modeling was done using Design Modeller from ANSYS Workbench. The dimensional BAWT footprint generated by Hans Hamm is used as for the cross-section of the 3D model. Hamm's geometry was optimized for greatest velocity augmentation at low wind incidence angles which makes it a good starting point for this 3D optimization study. The 3D model was created by extruding and varying a 2D footprint geometry 100m in height. Multiple BAWT configurations were generated by controlling the extrusion process using three parameters to create nineteen BAWT models. Also described is the turbine capture area to simulate the presence of a wind turbine. Lastly the size of the domain will be discussed.

3.1.1 Domain Boundaries

Urban landscapes are densely packed with tall residential and commercial buildings separated by roadways. The separation gaps between adjacent buildings provide corridors for wind to flow through. Since wind directions in urban landscapes are constrained to the orientations of the surrounding buildings, this study assumed low variation of wind incidence angles approaching the BAWT.

The base footprint for all contrived 3D BAWT models will be the optimized two-dimensional geometry for low varying wind incidence angles generated by the work of Hans Hamm. The optimal footprint parameters for low wind incidence are listed below:

1. a moderate thickness ($b_x/D_o = 20/20$)

2. high oblateness ($a/D_o = 15/20$)

3. small gap ratio ($g/D_o = 3/20$)

The footprint was extruded in the vertical z axis to create *Wall* boundaries and was controlled using three normalized parameters with respect to the base characteristic diameter \varnothing_o of 20m which was equivalent to D_o characteristic diameter of Hans Hamm. The parameters governing the vertical taper (R_t), forward lean (R_x), and spread (R_y) are:

$$R_t = 1 - \varnothing_t/\varnothing_o \quad (3.1)$$

$$R_x = x_t/(R_t\varnothing_o) \quad (3.2)$$

$$R_y = y_t/(R_t\varnothing_o) \quad (3.3)$$

Where \varnothing_t is the building diameter at 100m height, \varnothing_o is the buildings base diameter, x_t is the forward shift if the building top with respect to the building base and y_t is the distance from the symmetry plane to the edge of the building top.

Parabolic profiles were chosen to define the vertical profile of the BAWT systems. The parabolic profile was inspired from the velocity profile of the atmospheric boundary layer (ABL) which will be discussed in subsequent sections. It was thought that a uniform velocity profile normal to the turbine capture area could be achieved in augmentation to provide uniform loading distribution to the turbines. This would require higher velocity augmentation of the low elevations and lower velocity augmentation of the high elevations of the ABL.

Parabolic inflection point is constrained to the roof top of the BAWT with respect to their coordinate systems. Constraints are imposed to limit the values of R_x and R_y . These constraints are imposed to maintain a configuration where there is no overhang of the building over the referenced footprint. The governing system of equations defining the profiles given in Equation 3.6

$$P_{taper}(z) = \frac{z(200-z)}{500}\chi \quad (3.4)$$

$$P_{lean}(z) = \frac{z(200-z)}{500}\chi \quad (3.5)$$

$$P_{spread}(z) = \frac{z(200-z)}{500}\chi + 3 \quad (3.6)$$

$$\chi = \begin{cases} R_t & \text{for } 0 \leq \varnothing(z) < \varnothing_o \\ R_t R_x & \text{for } 0 \leq x(z) \leq R_t \varnothing_o \\ R_t R_y & \text{for } g\varnothing_o \leq y(z) \leq (R_t + g)\varnothing_o \end{cases}$$

where χ is a place holder for various cases. Parabolic profile derivation can be found in Appendix A. Figure 3.1 illustrates the use of each parameter. Figures 3.2 and 3.3 represent the geometric variations of the BAWT with respect to each parameter.

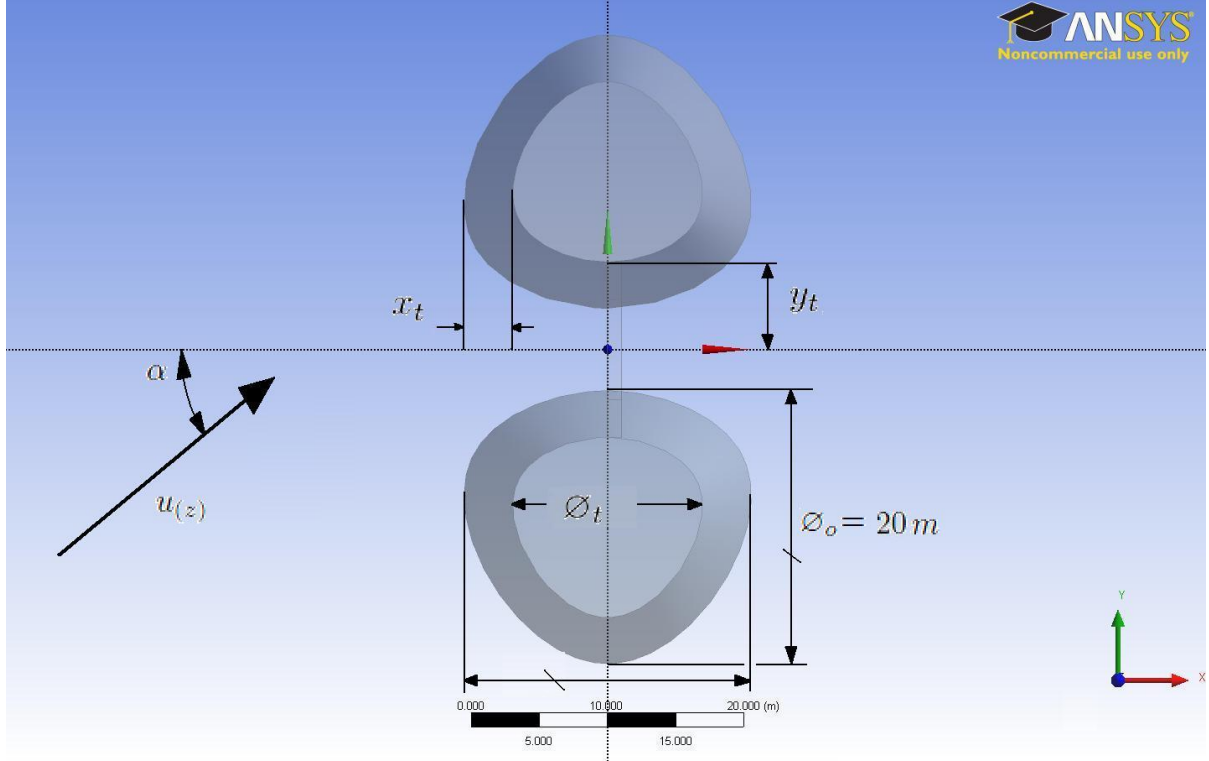
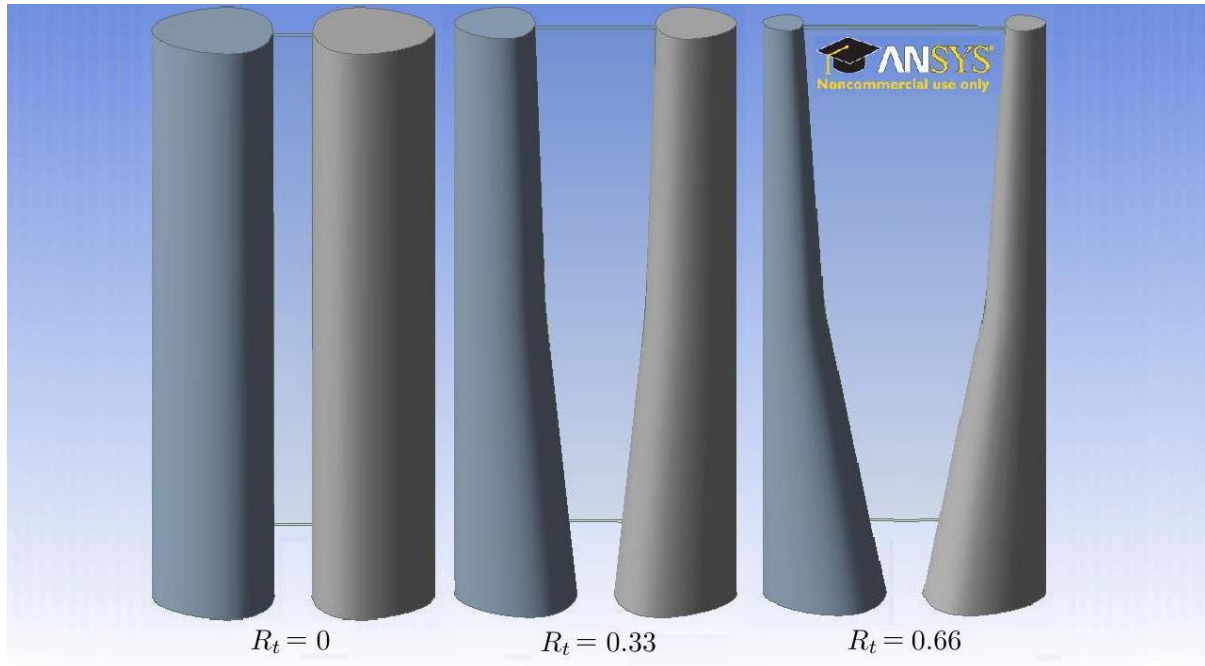
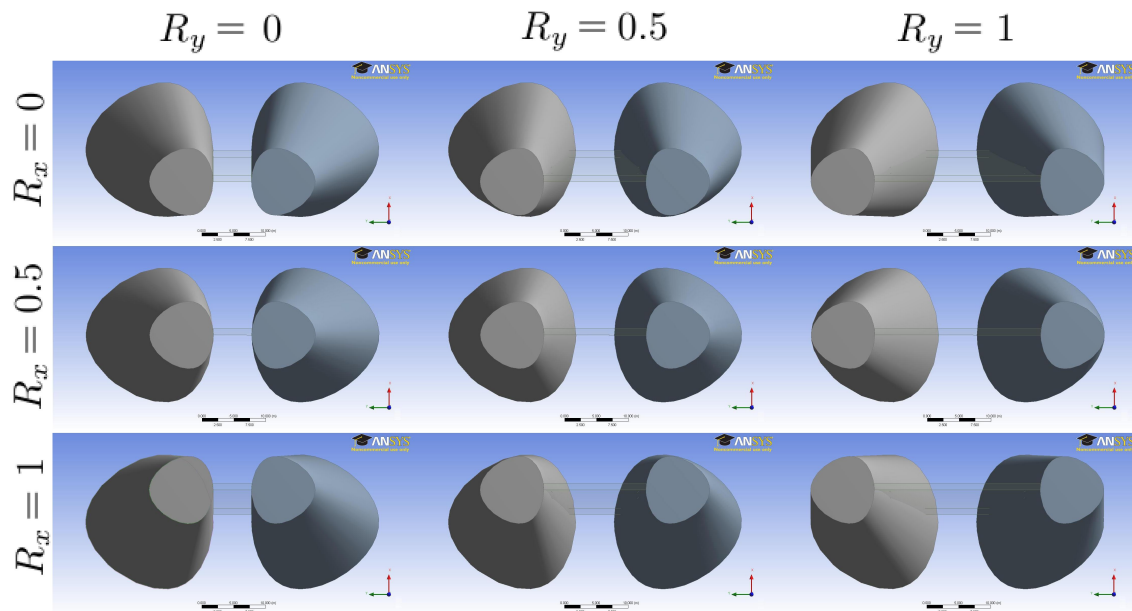


Figure 3.1: Variation of 3D BAWT parameters

The cases analysed used each building parameter at three different points of interest: minimum (0), medium (0.5) and maximum (1) values for R_x and R_y ; 0, 0.33 and 0.66 for R_t and where subject to four incidence angles of 0° , 20° , 40° , and 60° . The different variations of models totalled to 76 and are shown in Table 3.1 with their respective incidence angles.

The velocity profile also defined the starting location of the modeled turbine above a referenced potential wind speed, u_p at 10m height. The potential wind speed equated to the bottom speed limit of a HAWT at 4.16m/s [1] and modeling turbines under this limit below 10m is not appropriate. The turbine is also constrained at the augments throat where the maximum wind augmentation occurs. Thus it is constrained to Equation 3.6 for case $x(z)$ when $10\text{m} \leq z \leq 100\text{m}$ and is illustrated in Figures 3.4 and 3.5.

The domain sizing is critical for the proper analysis of flow characteristics such as pressure to diffuse throughout the domain without any adverse effects from the boundaries of domain. Appropriate domain sizing for flows above Reynolds number $3.5 \cdot 10^6$ are suggested by Grinstein [10]. The *Inlet* boundary is

Figure 3.2: Variation of taper ratio R_t Figure 3.3: Variations of variables R_x and R_y

R_t	R_x	R_y	Wind Incidence Angles (α)			
			0°	20°	40°	60°
0	0	0	0°	20°	40°	60°
0.33	0	0	0°	20°	40°	60°
		0.5	0°	20°	40°	60°
		1	0°	20°	40°	60°
0.33	0.5	0	0°	20°	40°	60°
		0.5	0°	20°	40°	60°
		1	0°	20°	40°	60°
0.33	1	0	0°	20°	40°	60°
		0.5	0°	20°	40°	60°
		1	0°	20°	40°	60°
0.66	0	0	0°	20°	40°	60°
		0.5	0°	20°	40°	60°
		1	0°	20°	40°	60°
0.66	0.5	0	0°	20°	40°	60°
		0.5	0°	20°	40°	60°
		1	0°	20°	40°	60°
0.66	1	0	0°	20°	40°	60°
		0.5	0°	20°	40°	60°
		1	0°	20°	40°	60°

Table 3.1: Various model cases

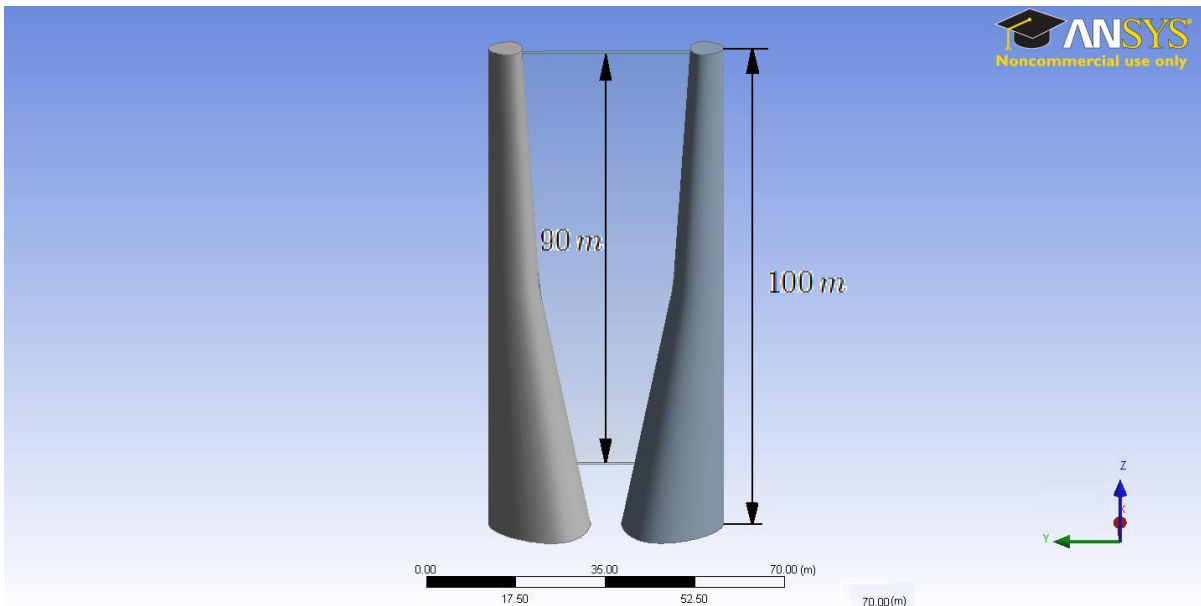


Figure 3.4: Front view of BAWT and simulated turbine capture area

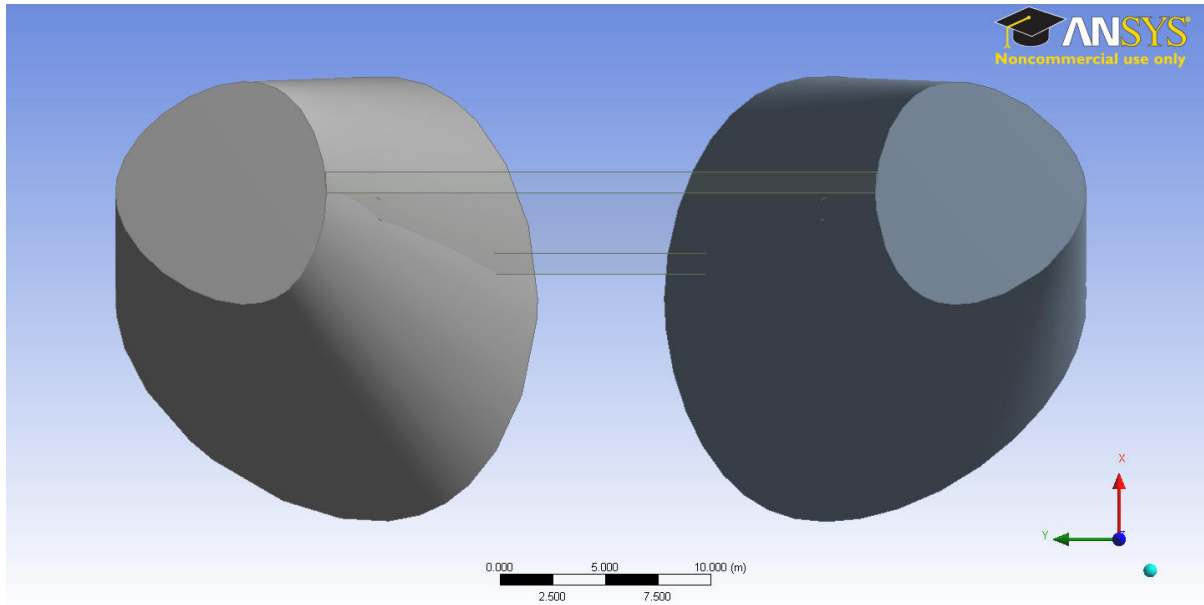


Figure 3.5: Top view of turbine spans across and extends height of the BAWT

located 200m upstream, *Outlet* boundary is 400m downstream, *Side* boundaries are 200m cross-stream and *Top* is 300m above the boundary *Ground*. Domain sizing is illustrated in Figure 3.6 and Figures 3.7 3.8 show the domain and turbine boundary locations.

3.1.2 Bodies of Influence

The fidelity of the solution of the BAWT configurations is dependent on the mesh resolution of the defining von Karman street. The latter occurs from the resulting shedding and propagation of vortex structures downstream from bluff bodies. Grid resolution must define these turbulent structures well enough to accurately model the pressure cascade of the von Karman street. Tapered cylinders produces varying vortex structures which are described to be a linear function of taper by Piccirillo and Van Atta [11, 12, 21]. Two bodies of influence will refine the mesh to resolve the varying shed vortex scales.

The size of the body of influence to define the von Karman street from a cylinder for Reynolds numbers above $5.5 \cdot 10^5$ was suggested to be three times the cylinder diameter by Grinstein [10]. A coarse body of influence was defined by a sphere of diameter 120m extending its centroid from the *Ground* at the center of the BAWT extending to 100m in height, and spanning the length of the *Domain* downstream 400m. The fine body of influence is defined by a sphere of 80m also extending its centroid from the *Ground* at the center of the BAWT extending 100m in height and spanning 250m downstream. Figure 3.9 shows the *Bodies of Influence* defining the von Karman vortex street.

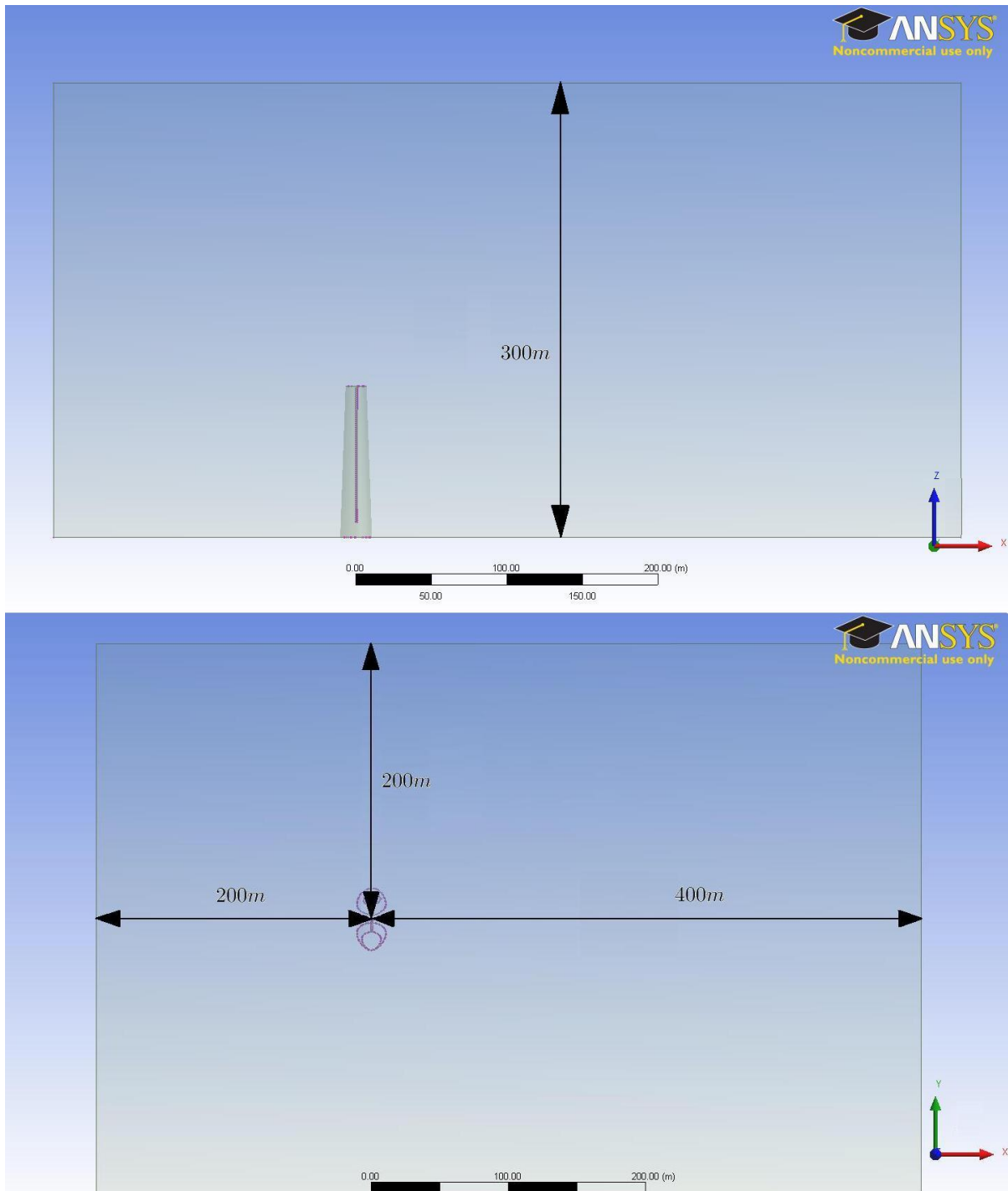


Figure 3.6: Side and top views of the domain

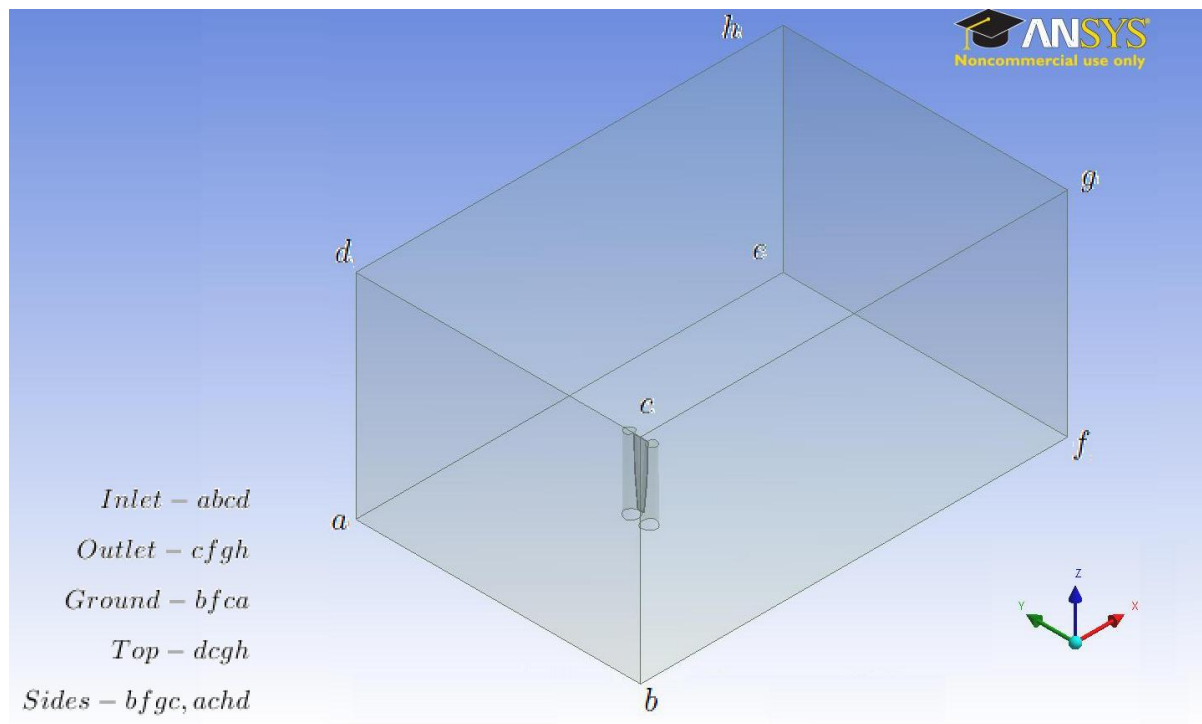


Figure 3.7: Isometric view of the domain

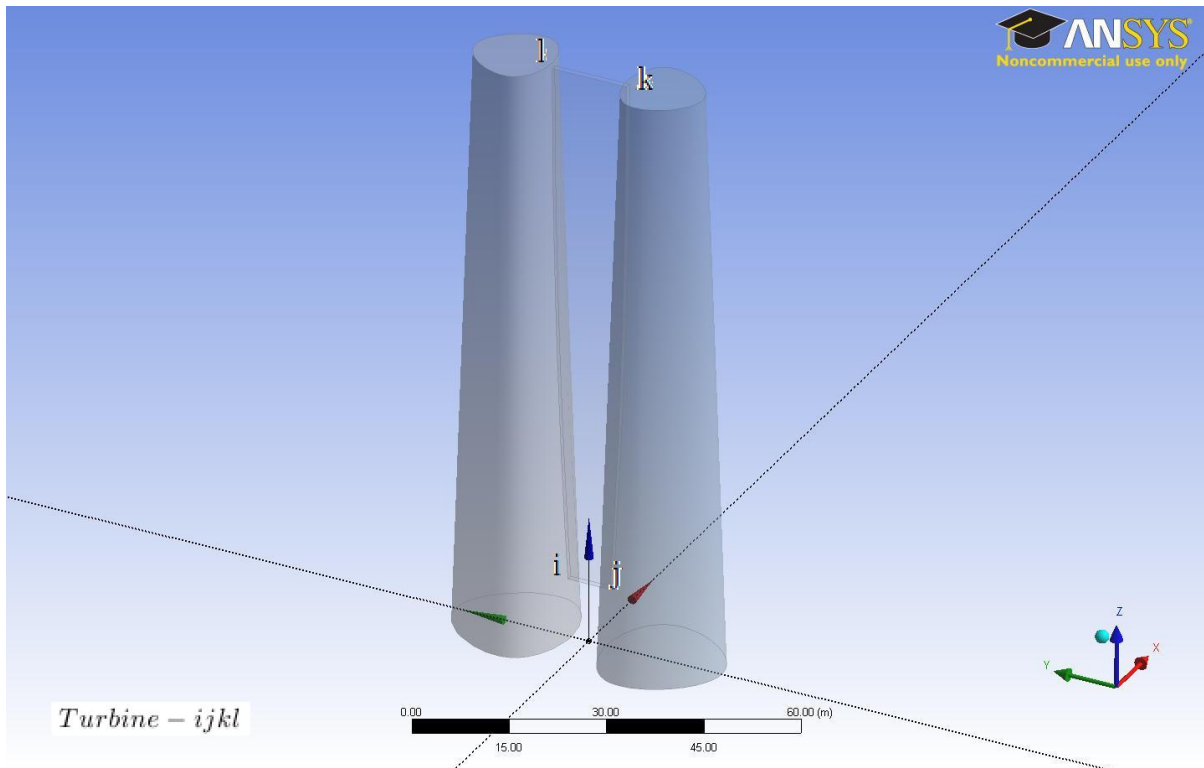


Figure 3.8: Close view of BAWT system with plain simulating turbines

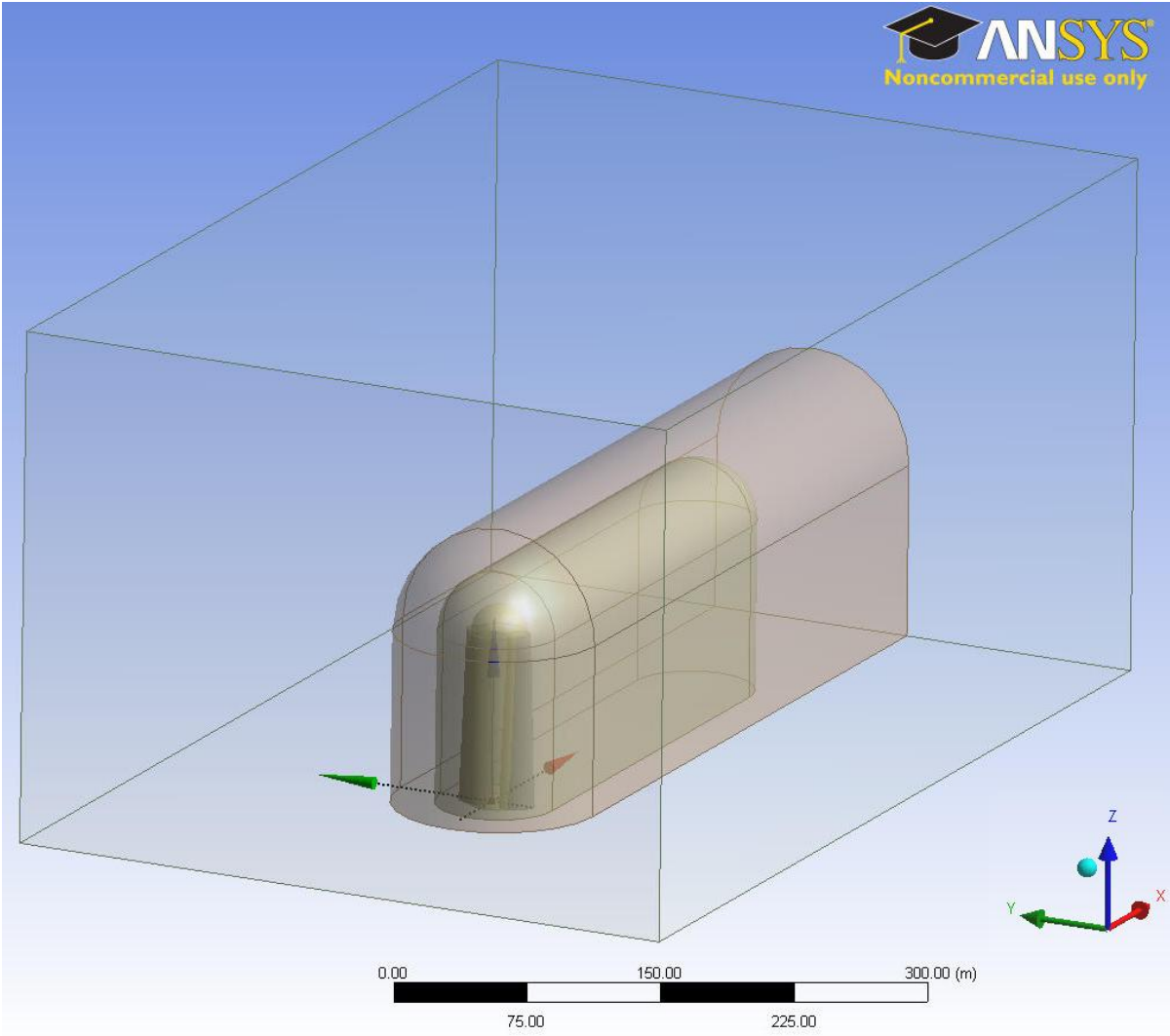


Figure 3.9: Bodies of influence defining the vortex street defined

3.2 Meshing

CFD requires the computational domain to be discretized into elements for the solver to apply the discrete RANS fluid equations at each element interface. ANSYS MESH was used to discretize the solution domain around the various BAWT geometries.

An unstructured grid system was chosen for its suitability to model complex turbulent flow structures within the von Karman street [16]. Modeling of the von Karman street relies on accurate modeling of the adverse pressure gradients of vortex shedding and requires adequate boundary layer resolution on the *Wall* boundaries. A near-wall model was used to approximate transition to laminar boundary layer where boundary layer accuracy can be reduced to y^+ values from 1–10. The boundary layer was defined at the first prism height, Δy of 0.001m with 25 inflated prism layers at an expansion ratio of 1.2.

3.3 Inflation Layers

Inflation layers were used to capture the velocity gradient of the boundary layer developed by shear friction occurring from a no-slip wall condition of the domain *Walls*. Also it is critical to capture the laminar separation with appropriate mesh refinement to capture the separation bubble from the shed vortex.

To resolve flow calculations to a degree of accuracy, FLUENT uses an enhanced wall treatment for the selected $k-\omega$ shear stress transport (SST) model. This wall treatment uses a near-wall approximation method predicts the boundary's viscous and transition layers. This reduces the need to extensively refine the mesh near a *Wall* boundary to capture the boundary layer profile, and also reduces computational cost. Figure 3.10 shows inflation layers surrounding a cross section of the buildings facade,

$$y^+ = \frac{\rho u_\tau y_p}{\mu} \quad (3.7)$$

where $u_\tau = \sqrt{\frac{\tau_\omega}{\rho_\omega}}$ is the friction velocity, and τ_ω is the shear stress and ρ_ω is the density of the fluid at the surface wall, y_p is the displacement of the first adjacent nodal point P from the wall and ρ is the density of the fluid.

For the $k-\omega$ (SST) turbulence model, Fluent recommends when using the enhanced wall treatment to obtain a y^+ value of the first adjacent nodes to be within $1 \leq y^+ \leq 5$. FLUENT approximates the first inflation layer height with Equation 3.8,

$$\Delta y = Ly^+ \sqrt{80} Re^{(-13/14)} \quad (3.8)$$

where y^+ is the targeted value of the first adjacent node, L is the structural cord length and Re is

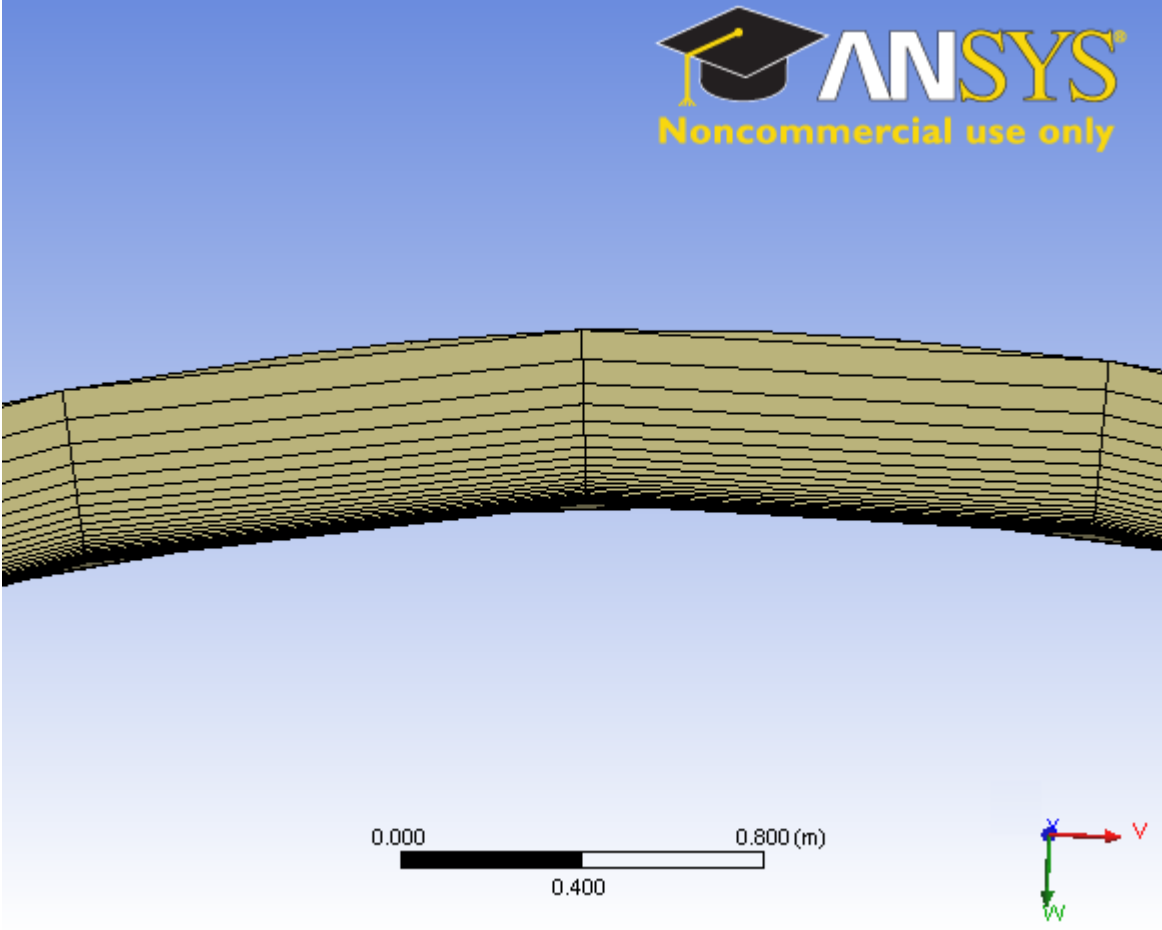


Figure 3.10: Inflation layers against building facade

the average flows Reynolds number. Reynolds number is defined as

$$Re = \frac{\rho V L}{\mu} \quad (3.9)$$

A $y^+ \approx 10$ was used to define the first non-dimensional off-wall spacing. The reference y^+ of 5 was not used for the purpose of reducing mesh size and computational time. The first node spacing off the wall with respect to a Reynolds number of $5.5 \cdot 10^6$ is calculated to be,

$$\begin{aligned} \Delta y &= 20(10)\sqrt{80}(5.5 \cdot 10^6)^{(-13/14)} \\ &= 0.000984 \\ &\approx 0.001m \end{aligned}$$

The number of inflation layers was selected in FLUENT MESH operation to define the resultant inflation around the buildings. The final inflation layer thickness of 0.1m was assumed to generate a cell height to length ratio of 10 to provide good solution transition from the inflation layers to the domain elements sized at 1m. Inflation layer height was increased by the standard growth factor of 1.2, thus the number of inflation layers is calculated by Equation 3.10,

$$h_n = \Delta y(1.2)^n \quad (3.10)$$

$$\begin{aligned} \left(\frac{h_n}{\Delta y}\right) &= (1.2)^n \\ \ln\left(\frac{h_n}{\Delta y}\right) &= n \ln(1.2) \\ n &= \frac{\ln\left(\frac{0.1}{0.001}\right)}{\ln(1.2)} \\ &\approx 25 \end{aligned}$$

Thus the inflation applied to the building in this study uses 25 layers, with a starting inflation height of 0.001m and a growth factor of 1.2. Figure 3.11 shows a plot of the y^+ values up along the building height for transient solutions. The y^+ values in Figure 3.11 are shown to be within the reasonable range which FLUENT determines to be good for near-wall approximations to take effect.

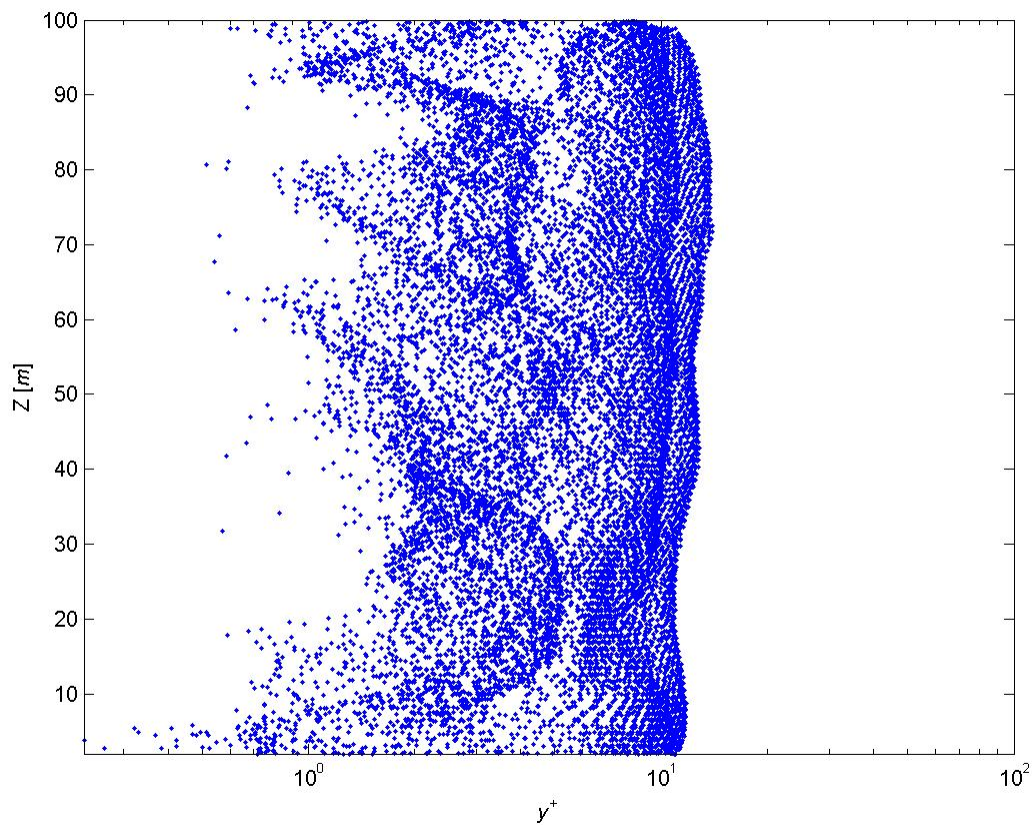


Figure 3.11: Unwrapped building surface's y^+ values along building height

3.4 Sponge Layer

For transient flows, turbulence poses problems where the residuals of the scalar quantities at the outlet boundary can reflect back into the solution domain by the solver. Grinstein suggests the use of a sponge layer to manipulate the multidimensional vertical structures to approach normal to the *Outlet* domain [10]. A single 5m inflated prism layer called a ‘sponge layer’ shown in Figure 3.12 was used.

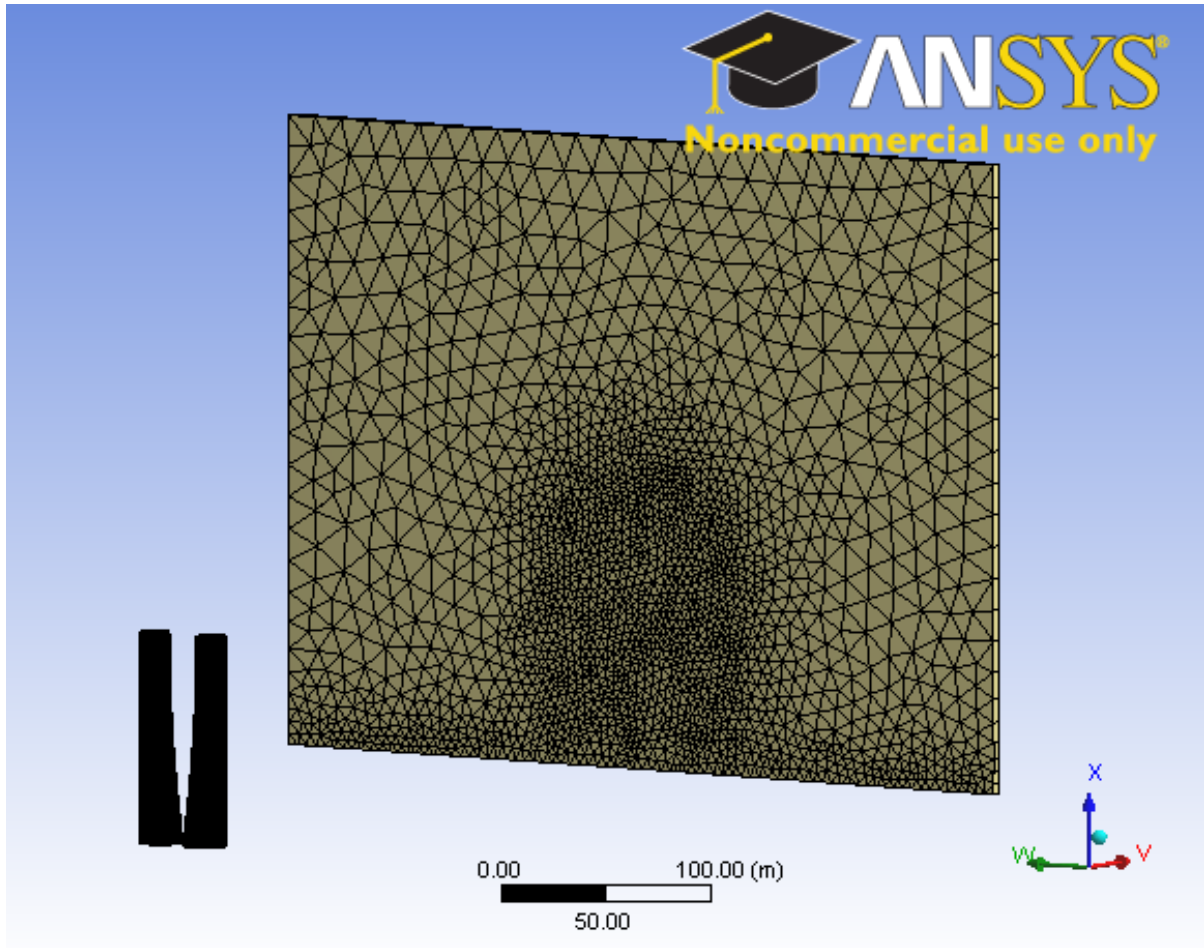


Figure 3.12: Sponge layer defining the outlet boundary

3.5 Element sizing

Face and element sizing specified for the model domains and boundaries were obtained from a grid study analysis. The resulting element sizings are shown in Table 3.2. A surface mesh of the *Walls*, *Turbine* and *Ground* is shown in Figure 3.13. It can be seen the *Fine Body of Influence* refines the face sizing of

	Bodies	Size (m)
	Domain	15
Coarse body of influence		5
Fine body of influence		2.5
Turbine		1
	Faces	Size (m)
	Ground	5
	Walls	1

Table 3.2: Element size controls

the *Ground* at the base and downstream of the BAWT to define the vortex path. Figure 3.14 illustrates the element growth factor produced from the bodies of influence.

3.6 Grid and Time Step Study

The accuracy a numerical simulation has is dependent on the grid resolution. Through parametric studies of grid resolutions, insight is gained into when the physics modeled becomes independent of grid spacing and does not change with increased grid refinement.

Steady state simulations are conducted for this preliminary grid independence study. This study conducted tests using four grids ranging in density of $0.66 \cdot 10^6$ – $3.9 \cdot 10^6$ elements. The power within the wind at the *Turbine* plane was the monitored parameter in determining solution convergence.

This study looks into the concentrator affects of a BAWT under time averaged conditions. Transient simulations are used to perform time step simulations where the solution is found for a series of time-step for a specified time interval. Just like the grid independence study, a time-step study is performed with the derived grid from the grid independence study. The three time-step sizes used in this study were 0.1s, 1s and 10s.

Lastly a verification of the resultant time-step was used in conjunction with the parametric grid study under a transient simulation. This study will verify mesh independence with the resultant time-step.

3.6.1 Steady State Grid Convergence

The grid study used four meshes with all the same controls applied to them but are different in their scaling parameters. This parameter allows all elements to be adjusted in scale, varying in the x , y , and z directions.

The initial mesh was scaled by factors of 0.5, 0.75, 1 and 1.4 where a scaling less than 1 represents a stretch factor, and a factor above 1 is shrinkage factor. Each scaled mesh was tested until convergence

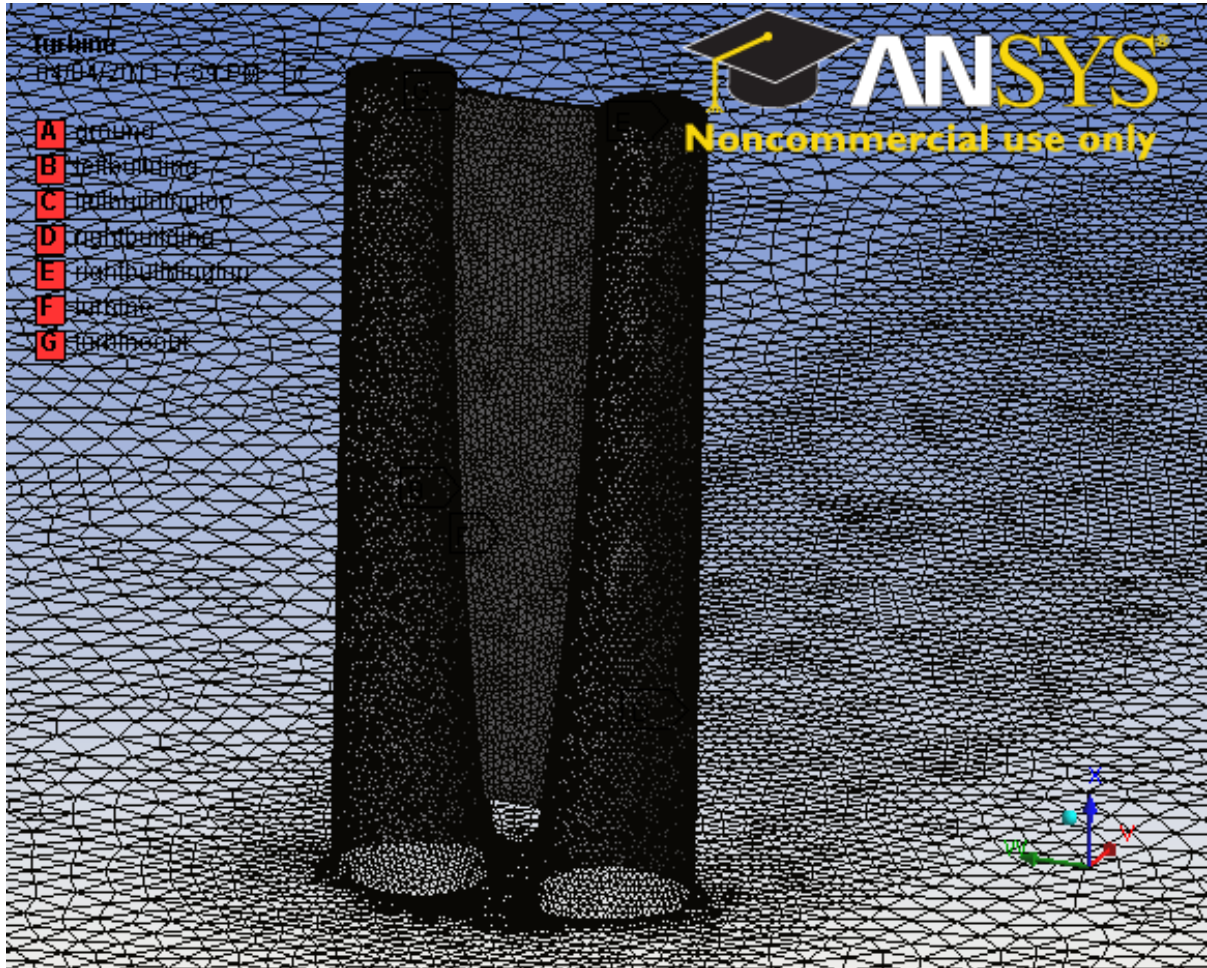


Figure 3.13: Surface mesh of *Walls, Turbine* and *Ground*

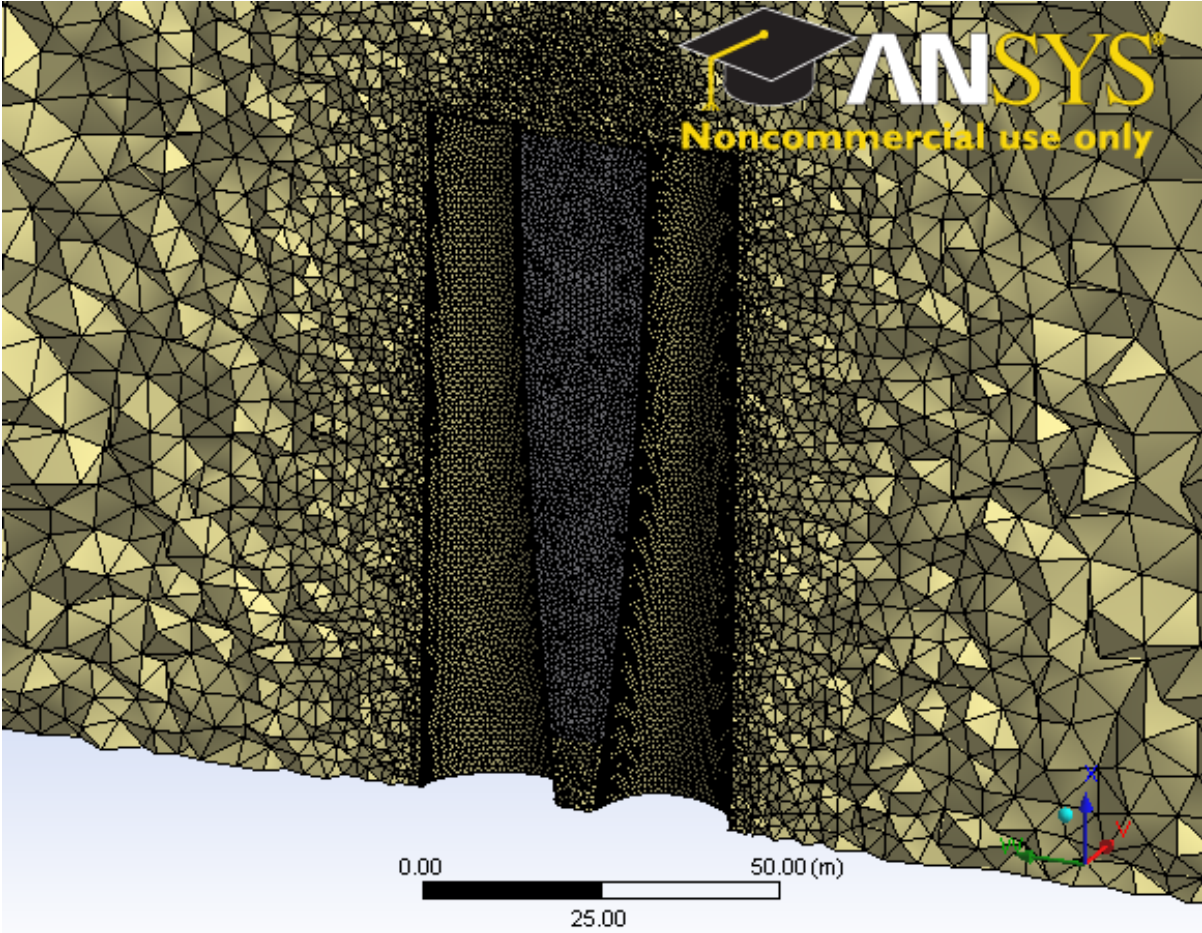


Figure 3.14: Mesh sliced lengthwise across *Turbine*

of the augmented power of the BAWT was reached. The resultant augmented powers plotted with respect to their mesh element densities. A Richardson extrapolation was performed using Matlab where the asymptote of the converging power solution is found. The extrapolated solution was then used as base point in determining the accuracy of the solution to the respective mesh sizings.

Figure 3.15 shows the comparative study of the four scaled meshes where the solutions appear to describe an asymptotic convergence of the augmented power to an extrapolated power of 346.9kW.

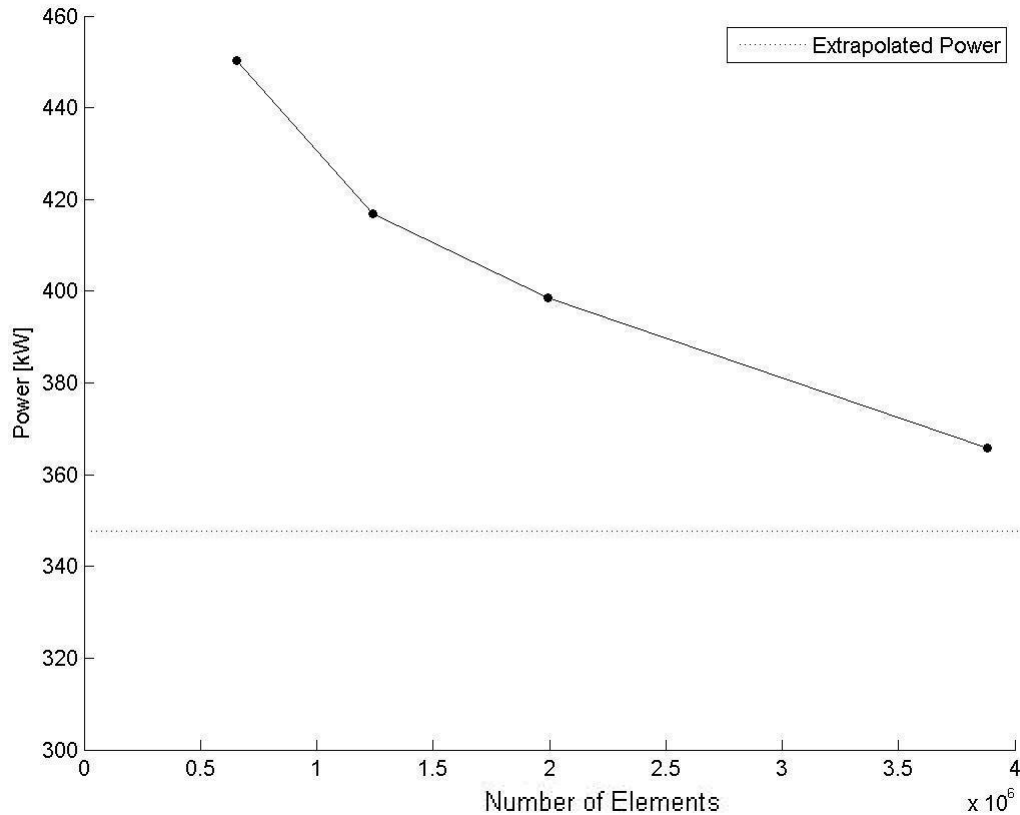


Figure 3.15: Steady state mesh convergence

Resultant deviations of the augmented power ratios compared to the extrapolated power ratio from the cases are shown in Table 3.3. Using a steady state solution it is shown the finest mesh has a deviation of 5.45% from the extrapolated power which is too high to conclude the solution of the discretized domain to be grid dependent. A solution is considered grid independent if there less than 1% deviation between the measured power and the extrapolated value.

The steady state augmented powers are noted to be high and unrealistic. This is due from the assumed steady state solution and the values were approximated with no transient fluctuations affecting turbulence in the flow resulting in the over evaluations of scalar variables. Thus a transient grid study

Mesh	Elements	Deviations from Extrapolated Result
1	656,637	29.8%
2	1,241,258	20.2%
3	1,994,056	14.9%
4	3,883,171	5.5%

Table 3.3: Steady state grid convergence and associated errors

was conducted to resolve this issue.

3.7 Time Step Study

Conversely, just like the grid convergence a study in time step size was done such that the transient turbulent behaviour and von Karman street is modeled and resulting turbine back pressure is simulated. A time-marching or dual-time scheme method used by ANSYS FLUENT which finds a converged steady state solution at the respective flow time and then advances the solution by the time step and converges another steady state solution for that time step, so on so forth.

Eddies are formed the flow through viscous shearing stemming from the flows surface friction from the ground and buildings. Eddies formed by the buildings separate from the surface, known as vortex shedding and migrate downstream with the flow. Length and time scales are needed to be resolved to obtain adequate turbulent characteristics within the flows discretized domain. Thus a time step study was performed using the previous resolved mesh number 4 of the grid study.

The effects of time step size where performed using three time step sizes of 0.1s, 1s and 10s. The convergence of power ratio was used to determine the appropriate time step. It should be noted the case of time step of 0.1s had not completed to a convergence value less than 0.5% of its mean extrapolated power ratio in over a hundred processing hours. Due to the vast amount of time needed to complete a full study using 0.1s time step, it was not considered. Conversely, solution convergence was not obtained using a 10s time step and fluctuations of the measured power ration varied 10%, thus is inappropriate for this study.

The case using 1s time step resolved to a converged value and the solution remained within a 0.5% deviation range for several hundred time step. Logically the 1s time step seemed most appropriate to begin with since the average element size to the discretized solution is of 1m and which are of similar size in scale. The processing time for solution convergence is shown in Table 3.4. Within the maximum allotted processing time Sharcnet provided was 100h. Using a time step of 0.1s and a grid size of $3.9 \cdot 10^6$ elements, the processing did not finish (DNF). For the larger time step of 10s, the solution did not converge (DNC).

The convergence time for the cases of one second time steps was around 24h of processing time with the use of 8 way parallel processing on Sharcnet's Guppy system. Guppy uses Inlet Xeon cores with 2.67 GHz and 24.0 GB RAM and cores are connected by a QDR InfiniBand. A sample read out from

Time Step Size [s]	Processing Time [h]	Power [kW]
0.1	> 100	DNF
1	< 20	106.2
10	< 4	DNC

Table 3.4: Convergence of power with respect to time step size

the generated output file FLUENT illustrates the processing time needed for one solution to complete.

```

CLU = gup
MY_QUEUE = mpi
HOST_NODEFILE = /var/spool/torque/aux//78529.gup-hn.guppy.sharcnet
NUMBER_PROCS = 8
NUMBER_NODES= 2
-----
Number cpus      = 8
Queue           = mpi
Jobid           = 78537.gup-hn.guppy.sharcnet
Version         = 3ddp
Journal file    = test.jou
Date job started = Thu Mar 31 21:22:46 EDT 2011
Date job finished = Fri Apr 1 19:11:57 EDT 2011
-----

```

3.8 Grid-Time Step Study

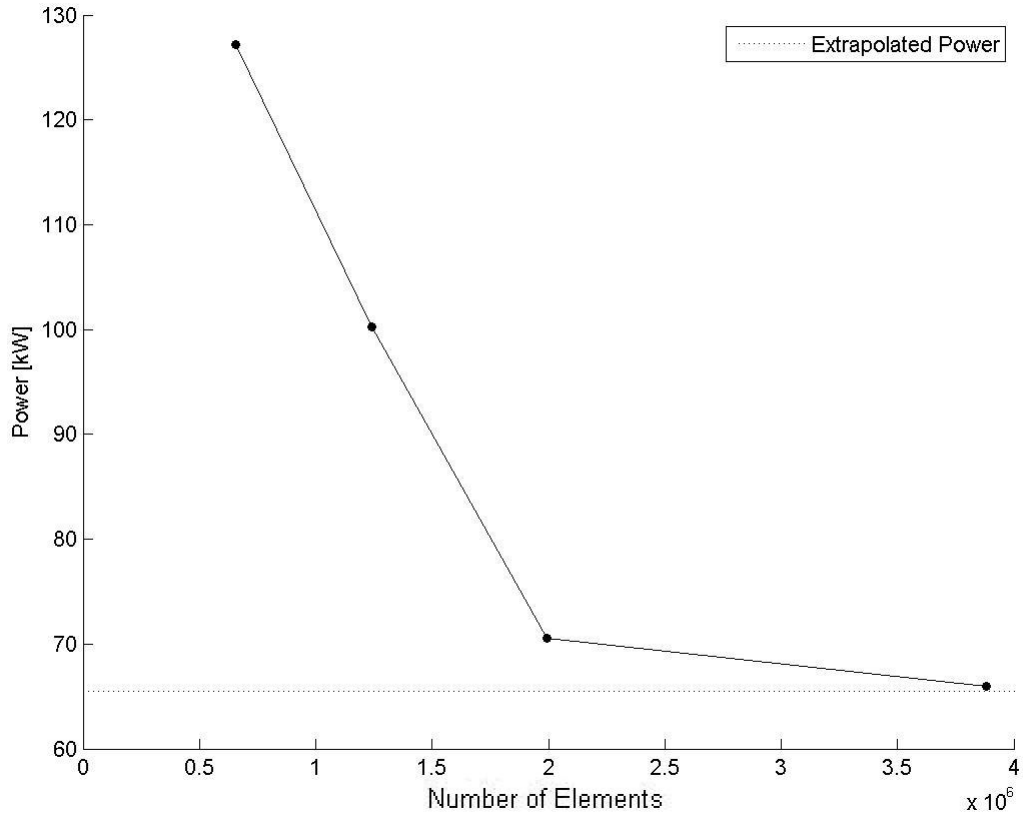
Simulations were tested for a length of time until results showed a steady mean of transient augmented power. The solution was considered converged when the change in power was less than 0.5% from the extrapolated mean over a few hundred time steps. Evaluating the mean power from $t = 0$ to time step $t = t_i$, defined in Equation 3.11 as

$$\bar{P}_i = \frac{\sum_{t=0}^{t=t_i} P_i}{N_i} \quad (3.11)$$

The assumed 1s time step from the previous time step study was used to conduct transient mesh independence study of the previous scaled meshes. Figure 3.16 shows convergence values of the mean augmented power ratio of the four meshes with respect to node density.

Deviations of the resultant grid-time convergence study are shown in Table 3.5. It can be seen that mesh 4 deviated from the extrapolated result by 0.66%.

For case tested for mesh and time convergence, no taper was applied to the BAWT but was analyzed with a wind incidence angle of 0° . It is assumed smaller vortex will be shed in tapered cases, thus the finer mesh should be used to capture the smaller vortex scales. Modeling the smaller turbulent scales more accurately will lead to better pressure fluctuation results aft of the turbine to better predict augmented power at the rotor. Therefore mesh 4 will be used for the purpose of this study.

Figure 3.16: Grid convergence at $t_i = 1s$

Mesh	Elements	Deviations from Extrapolated Result
1	656,637	94.0%
2	1,241,258	53.0%
3	1,994,056	7.7%
4	3,883,171	0.7%

Table 3.5: Steady state grid convergence

Chapter 4

Methodology

This section contains discussions of the approaches to the conditions for the solution boundaries, simulation parameters and the result criteria. Specified solution parameters for turbulent modeling were used to simulate the von Karman street. The analysis of power at the *Turbine* was used to determine solution convergence of the mean transient to a specified accuracy.

4.1 Boundary Conditions

Atmospheric boundary layer (ABL). ABL is the naturally occurring velocity profile developed when air passes over Earths terrain. Viscous forces become dominant near the terrain where shear forces resist fluid momentum until zero velocity is reached at the surface. Zero velocity at the surface is considered a no slip condition.

A commonly used model to define the velocity profile of ABL is the logarithmic law (Log-Law). A Log-Law defining the boundary layer over a flat plate was derived by Prandtl was also found to be valid to define the ABL near the Earths surface [15]. Velocity profile from a referenced height of 60m is used to calculate the velocity profile for any reference wind speed. ABL defined by Holmes [15] was simplified with defining a surface roughness, z_o of 0.03m and represented as Equation 4.1[19]

$$u_{(z)} = 1.31u_p \frac{\ln\left(\frac{z}{z_o}\right)}{\ln\left(\frac{60}{z_o}\right)} \quad (4.1)$$

where u_p is the potential wind speed 10m above ground and z is the elevation height.

The Log-Law profile was used with the velocity inlet condition to define the ABL normal to the *Inlet* boundary with a 10% turbulence intensity suggested by ANSYS when the inlet turbulent characteristics are unknown. Figure 4.1 shows the ABL velocity vectors and stream lines along a segment of the domain.

A gauge pressure of 0Pa far field was chosen for pressure at the *Outlet* condition.

Symmetry conditions were imposed on the *Sides* and *Top* boundaries of the domain to artificially

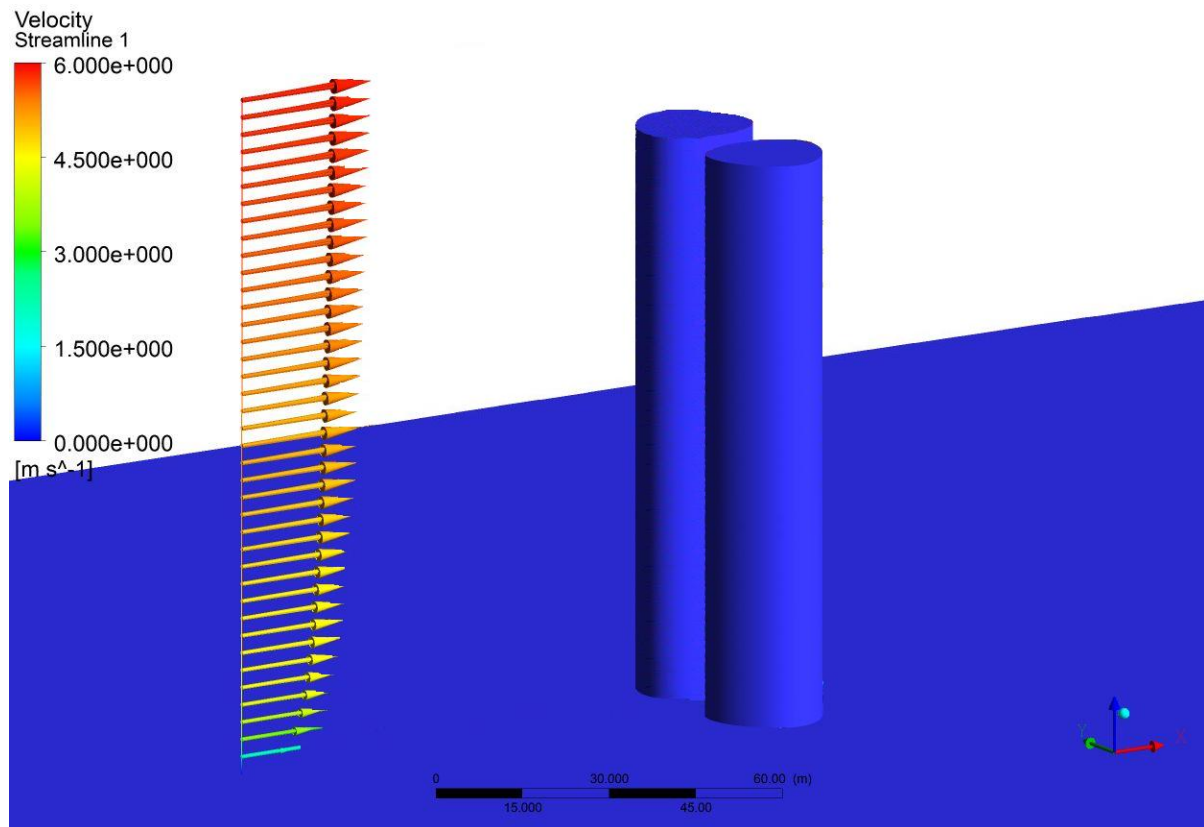


Figure 4.1: Log-Law velocity profile of ABL

simulate a greater domain space. Flow variables are allowed to develop along these symmetry boundaries where the normal gradients of the flow variables are equated to zero. Normal gradients however are not zero at the *Walls* and *Ground* boundaries. A no-slip condition is used for the two boundaries where the surface roughness z_o of 0.03m is defined for the *Ground* to simulate terrain. The *Walls* are assumed to be smooth [22] thus zero surface roughness was used.

The *Turbine* boundary was defined with a porous jump condition where a pressure drop was applied to simulate the presence of a turbine. A simplified Navier-Stokes equation for momentum derived in Appendix C was used to define the pressure drop across the *Turbine* in Equation C.2 as

$$\Delta P = -C_2 \frac{1}{2} \rho u^2 \Delta m \quad (4.2)$$

where ρ is the density of the fluid, C_2 is the momentum loss term corresponding to the pressure loss coefficient defined by Hans Hamm as 0.4 [14], u is the velocity magnitude normal to the cell face, and Δm is the thickness of the porous jump.

4.2 Solution Parameters

The solver used for this CFD analysis is FLUENT (ANSYS Inc.). This solver was chosen because of its reputation for solving both high and low Reynolds flows and around bluff bodies and the ability to obtain good boundary layer flow characteristics in all flow regimes. A density-based implicit solver was used where only Navier-Stokes equations are solved simultaneously using algebraic multi-grid (AMG) solver. A second-order upwind scheme recommended by ANSYS for accuracy in solving the discretized solution domain using the finite volume method was used.

The shear stress transport (SST) $k-\omega$ model was chosen over traditional $k-\epsilon$ model for its accuracy in solving adverse pressure gradients induced by wall bounded turbulent structures [2]. Mentor developed the SST which incorporates the qualities of models $k-\epsilon$ and $k-\omega$ by using a blend factor to activate the $k-\omega$ to calculate shear stress at low Reynolds number within the flow boundary layers and at far field where negligible shear stresses occur the $k-\epsilon$ model is activated.

4.3 Solution Criteria

The power of the wind at the *Turbine* boundary was used to measure mean transient conditions and is derived in Equation 4.3.

$$\overline{P}_i = \frac{\sum_{t=0}^{t=t_i} P_i}{N_i} \quad (4.3)$$

The solution is said to be completed when consistent mean transient conditions are obtained in the simulations. The solution was determined to be found if augmented power remains to within a 0.5%

deviation from the extrapolated mean of the augmented power for several hundred seconds.

The extrapolated mean augmented power was calculated using built in Richardson extrapolation function within Matlab to calculate the convergence value of mean augmented power. Plots of the solution convergence is shown in Figure 4.2 and Figure 4.3 is the associated error with respect to the converged value.

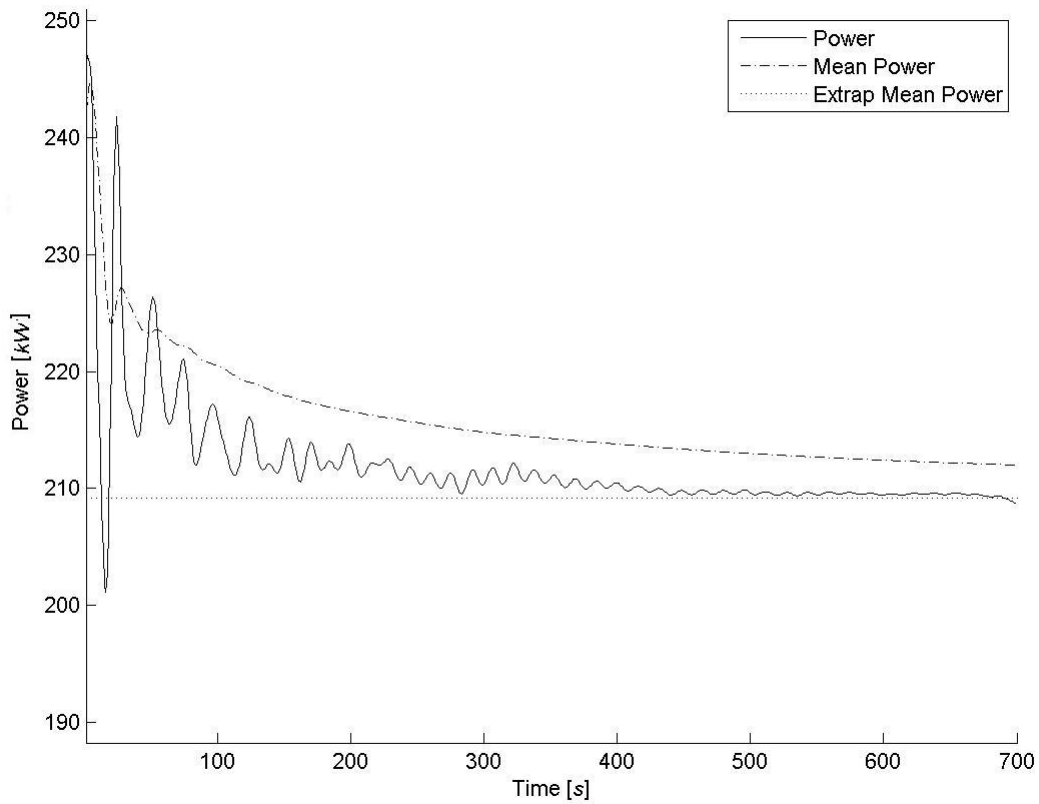


Figure 4.2: Mean time power convergence study ($R_t = 0.33$, $R_x = 0$, $R_y = 1$, $\alpha = 0^\circ$)

Various BAWT configurations produced oscillations of the augmented power at high incidence angles and wide spread. Pressure fluctuations formed from vortex shedding occurring at the *Turbine* boundary. An oscillating solution was considered converged when the augmented power oscillations maintain consistent amplitude for several hundred seconds as shown in Figure 4.4.

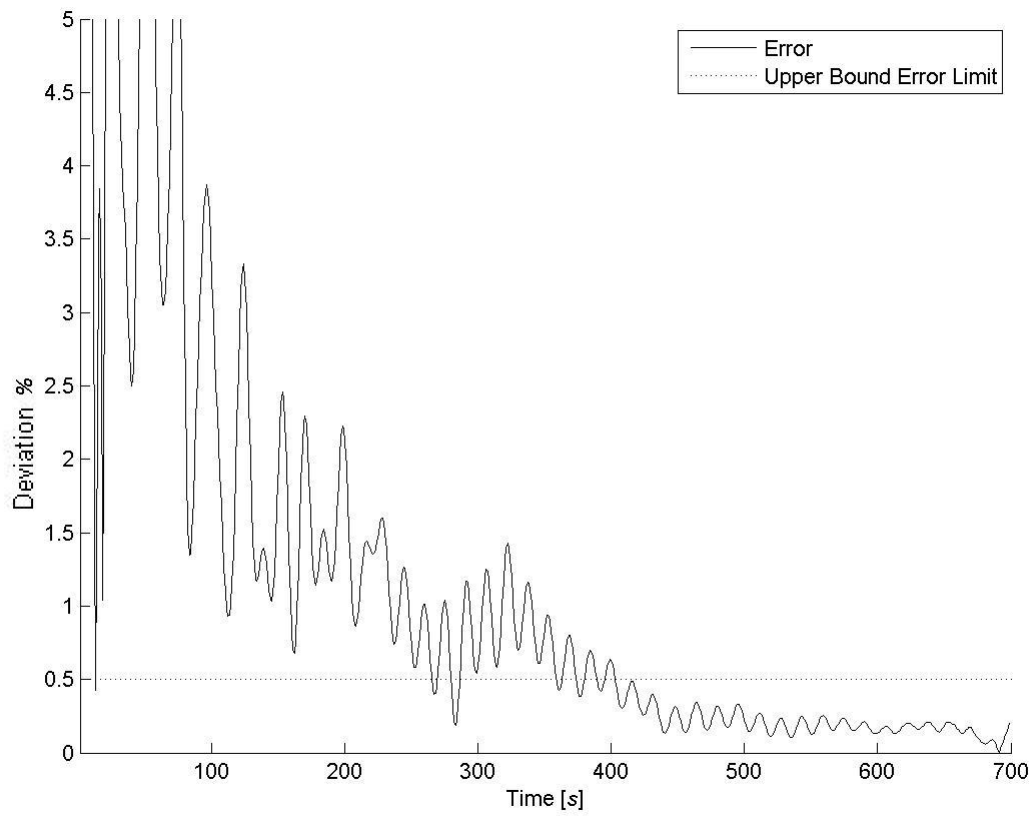


Figure 4.3: Error convergence study ($R_t = 0.33$, $R_x = 0$, $R_y = 1$, $\alpha = 0^\circ$)

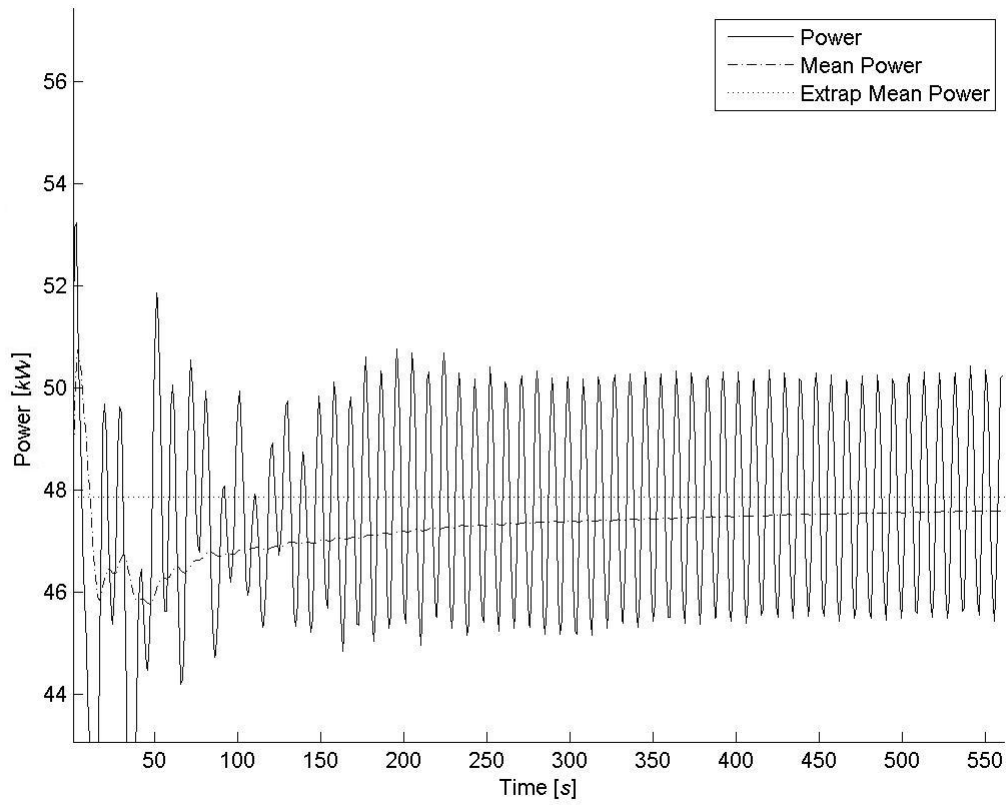


Figure 4.4: Mean time power coverage study ($R_t = 0.33$, $R_x = 0.5$, $R_y = 1$, $\alpha = 60^\circ$)

4.4 Augmented Power

Power is the rate of energy of a mass flow of air passing through a rotor swept area is defined as,

$$\frac{\delta E}{\delta t} = P = \int \int_A \epsilon \rho (V \cdot n) \delta A \quad (4.4)$$

Where n , is the normal vector of the sweeping area and ϵ is the energy per unit mass,

$$\epsilon = u + \frac{1}{2}V^2 + gz \quad (4.5)$$

Simplifications are made by neglecting internal energy and the hydrostatic terms. Due to the incompressibility of the fluid and lack of heat transfer the internal energy is constant, the fluid is gravitational the potential energy remains constant thus they can be negated reducing the equation to the kinetic energy of the fluid.

$$\epsilon = \frac{1}{2}V^2 \quad (4.6)$$

Substituting equation (4.6) into the rate of energy equation (4.4) to give energy flux as

$$P = \frac{1}{2}\rho \int \int_A V^2 (V \cdot n) \delta A \quad (4.7)$$

The density, ρ remains constant and can be taken outside of the integral and ∂A is the *Turbine* area. *Turbine* area is as function of building spread factor written as Equation 4.8

$$A = y(z)z \quad (4.8)$$

The change in area is then found as

$$\partial A = z\partial y + y(z)\partial z \quad (4.9)$$

The first term of the 4.9 is dropped because the *Turbine* only varies in the y -direction. Thus change in *Turbine* area becomes

$$\partial A = y(z)\partial z \quad (4.10)$$

Equation 4.10 can be substituted back into Equation 4.7 and simplifications are made

$$P = \frac{1}{2}\rho \int \int_A V^2 (V \cdot n) \delta A \quad (4.11)$$

$$P = \frac{1}{2}\rho \int_{10}^{100} V(z)^3 y(z) \partial z \quad (4.12)$$

The integration in Equation 4.12 is calculated from height of 10m to 100m where the *Turbine* boundary is situated.

Chapter 5

Results

An analysis of the data obtained from this study is synthesised and presented in various sections to illustrate the purpose of this study. ANSYS FLUENT software was used to perform transient simulations of 76 BAWT cases where their wind augmentation performance was measured with respect to four wind incidence angles. The BAWT performances were measured by various criteria of augmentation of both velocity and power, and the ratio of augmented power to unaugmented power. Also along with analysing their power ratings using three different wind regimes with equivalent frequencies, power rating was obtained from the sum of the product of the augmented power and the frequency of the wind incidence angle.

Figures 5.1 5.2 shows all data relevant to the results sections. Only BAWT configuration with R_x values at 0.5 are presented. This was done because change in results varied minutely with the change in R_x for all cases.

5.1 Velocity Augmentation

One of the purposes of this study was to determine the velocity augmentation factor the BAWT configurations have on the imposing wind. The augmented velocity is the average normal velocity at the *Turbine* boundary. The unaugmented wind speed was taken as the average normal velocity of the ABL through *Turbine* boundary. Augmentation factors were calculated by normalizing the augmented velocity with the unaugmented velocity. The BAWT velocity augmentation factors were obtained for each of the various wind incidence angles and are shown in Figure 5.3.

It can be seen from Figure 5.3 that augmentation factors for all BAWT configurations are at their highest at zero wind incidence angle and a gradual decrease occurs with increasing angles. Looking at the results for zero wind incidence angles, it is noted there the highest value of 1.3 is obtained for the case with no taper, R_t is 0. Velocity augmentation factors are shown to decrease by 1.5% and 4.6% with the increasing in taper from 0.33 and 0.66 respectively while and keeping an equivalent turbine capture area with a spread factor of 0.

Rt	Ry	Rx	WIA	Vabl [m/s]	V2 [m/s]	V2/Vabl	Palb [kW]	P [kW]	P/Pabl	Area [m ²]	Density [kW/m ²]
0	0	0	0	5.28	6.85	1.30	49.0	106.2	2.17	540	0.197
			20	5.28	6.81	1.29	49.0	103.1	2.11	540	0.191
			40	5.28	6.03	1.14	49.0	81.4	1.66	540	0.151
			60	5.28	5.59	1.06	49.0	57.5	1.17	540	0.106
0.33	0	0	0	5.28	6.56	1.24	49.0	95.4	1.95	540	0.177
			20	5.28	6.54	1.24	49.0	93.3	1.90	540	0.173
			40	5.28	6.00	1.14	49.0	73.1	1.49	540	0.135
			60	5.28	4.76	0.90	49.0	45.5	0.93	540	0.084
		0.5	0	5.28	6.77	1.28	49.0	100.3	2.05	540	0.186
			20	5.28	6.59	1.25	49.0	92.3	1.89	540	0.171
			40	5.28	5.94	1.13	49.0	71.5	1.46	540	0.132
			60	5.28	4.98	0.94	49.0	47.3	0.97	540	0.088
		1	0	5.28	6.68	1.27	49.0	98.3	2.01	540	0.182
			20	5.28	6.52	1.24	49.0	92.5	1.89	540	0.171
			40	5.28	6.00	1.14	49.0	70.8	1.45	540	0.131
			60	5.28	5.26	1.00	49.0	50.9	1.04	540	0.094
	0.5	0	0	5.34	5.94	1.11	92.3	159.0	1.72	986.8	0.161
			20	5.34	6.20	1.16	92.3	143.6	1.56	986.8	0.145
			40	5.34	5.59	1.05	92.3	106.9	1.16	986.8	0.108
			60	5.34	3.71	0.69	92.3	48.8	0.53	986.8	0.049
		0.5	0	5.34	6.41	1.20	92.2	158.9	1.72	986.8	0.161
			20	5.34	6.19	1.16	92.2	143.1	1.55	986.8	0.145
			40	5.34	5.32	1.00	92.2	99.6	1.08	986.8	0.101
			60	5.34	3.54	0.66	92.2	52.4	0.57	986.8	0.053
		1	0	5.34	6.38	1.19	92.3	157.3	1.70	986.8	0.159
			20	5.34	6.08	1.14	92.3	138.5	1.50	986.8	0.140
			40	5.34	5.40	1.01	92.3	107.8	1.17	986.8	0.109
			60	5.34	2.98	0.56	92.3	33.8	0.37	986.8	0.034
1	0	0	5.36	6.20	1.16	135.6	209.2	1.54	1433.5	0.146	
		20	5.36	5.89	1.10	135.6	179.5	1.32	1433.5	0.125	
		40	5.36	5.04	0.94	135.6	126.2	0.93	1433.5	0.088	
		60	5.36	3.10	0.58	135.6	47.5	0.35	1433.5	0.033	
	0.5	0	5.36	6.18	1.15	135.5	208.8	1.54	1433.5	0.146	
		20	5.36	5.92	1.10	135.5	184.1	1.36	1433.5	0.128	
		40	5.36	5.26	0.98	135.5	129.0	0.95	1433.5	0.090	
		60	5.36	3.32	0.62	135.5	47.9	0.35	1433.5	0.033	
	1	0	5.36	6.22	1.16	135.6	210.5	1.55	1433.5	0.147	
		20	5.36	5.97	1.11	135.6	186.3	1.37	1433.5	0.130	
		40	5.36	5.25	0.98	135.6	128.8	0.95	1433.5	0.090	
		60	5.36	3.19	0.59	135.6	44.7	0.33	1433.5	0.031	

Figure 5.1: Results

0.66	0	0	0	5.28	5.38	1.02	49.1	89.4	1.82	540	0.166
			20	5.28	6.26	1.19	49.1	77.2	1.57	540	0.143
			40	5.28	4.59	0.87	49.1	60.3	2.78	540	0.112
			60	5.28	2.90	0.55	49.1	30.3	0.62	540	0.056
		0.5	0	5.28	6.55	1.24	49.0	91.0	1.86	540	0.168
			20	5.28	6.26	1.19	49.0	81.2	1.66	540	0.150
			40	5.28	5.64	1.07	49.0	60.0	1.23	540	0.111
			60	5.28	4.22	0.80	49.0	32.2	0.66	540	0.060
		1	0	5.28	6.41	1.22	49.1	87.3	1.78	540	0.162
			20	5.28	6.22	1.18	49.1	79.4	1.62	540	0.147
			40	5.28	5.68	1.08	49.1	60.4	1.23	540	0.112
			60	5.28	3.72	0.71	49.1	28.2	0.58	540	0.052
	0.5	0	0	5.36	5.94	1.11	134.5	181.7	1.35	1420.4	0.128
			20	5.36	5.63	1.05	134.5	158.8	1.18	1420.4	0.112
			40	5.36	4.89	0.91	134.5	103.6	0.77	1420.4	0.073
			60	5.36	3.00	0.56	134.5	36.4	0.27	1420.4	0.026
		0.5	0	5.36	5.90	1.10	134.3	178.1	1.33	1420.4	0.125
			20	5.36	5.71	1.06	134.3	161.5	1.20	1420.4	0.114
			40	5.36	4.62	0.86	134.3	91.2	0.68	1420.4	0.064
			60	5.36	2.60	0.48	134.3	27.9	0.21	1420.4	0.020
		1	0	5.36	5.91	1.10	134.5	179.8	1.34	1420.4	0.127
			20	5.36	5.63	1.05	134.5	155.1	1.15	1420.4	0.109
			40	5.36	4.77	0.89	134.5	99.1	0.74	1420.4	0.070
			60	5.36	3.00	0.56	134.5	34.2	0.25	1420.4	0.024
1	0	0	5.38	5.68	1.06	219.9	256.9	1.17	2300.8	0.112	
		20	5.38	5.39	1.00	219.9	220.9	1.01	2300.8	0.096	
		40	5.38	4.54	0.84	219.9	135.3	0.62	2300.8	0.059	
		60	5.38	2.88	0.54	219.9	43.9	0.20	2300.8	0.019	
	0.5	0	5.38	5.66	1.05	219.5	255.7	1.17	2300.8	0.111	
		20	5.38	5.37	1.00	219.5	218.1	0.99	2300.8	0.095	
		40	5.38	4.35	0.81	219.5	122.0	0.56	2300.8	0.053	
		60	5.38	2.80	0.52	219.5	41.4	0.19	2300.8	0.018	
	1	0	5.38	5.68	1.06	219.5	258.9	1.18	2300.8	0.113	
		20	5.38	5.39	1.00	219.5	217.3	0.99	2300.8	0.094	
		40	5.38	4.54	0.84	219.5	127.0	0.58	2300.8	0.055	
		60	5.38	2.88	0.54	219.5	44.0	0.20	2300.8	0.019	

Figure 5.2: Results continued

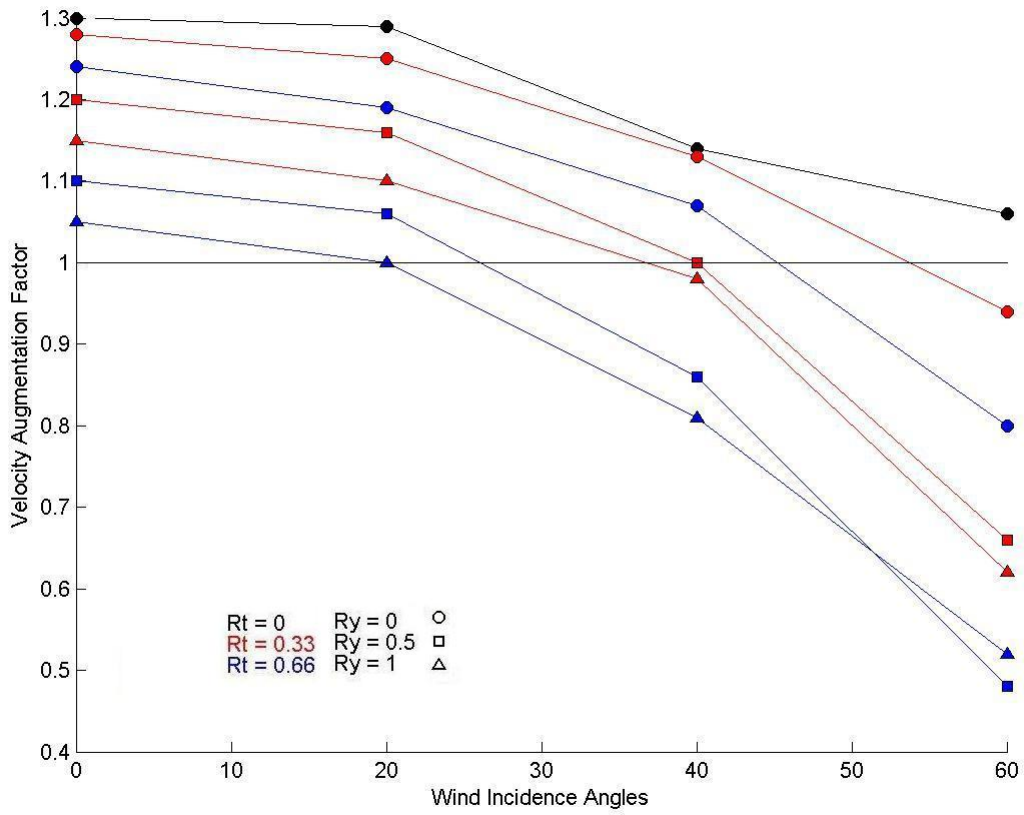


Figure 5.3: Velocity augmentation factors

The spread factor R_y is shown to have a negative effect on velocity augmentation factors for all cases. At zero incidence angle and using spread factor of 1 and 0.5 for cases of taper R_t 0.33 and 0.66 respectively, augmentation factors decreased from their 0 spread configuration by 10.2% and 11.3% and respectively. These results correlate to the law of continuity well, which states the incompressible flow must increase velocity through the BAWT gap region to maintain mass flow conservation. The velocity is also related to the pressure through the system where greater pressure differentials create higher velocities.

Figure 5.3 also illustrates the angles at which the BAWT configurations produce no velocity augmentation. Augmentation factors below 1 depict a decrease in performance values comparative to the free stream ABL. The BAWT configuration with taper 0.66 and spread of 1 is shown to prove no augmentation for incidence at 20° and poor augmentation for angles greater than 20° . Positive augmentation remains for at higher angles with decrease in spread factor, and the decrease in taper. The BAWT with 0 taper and 0 spread factors maintained to generate the highest augmentation factor for all incidence angles.

5.2 Augmented Power

This section analyses the augmented power delivered to the turbine capture area for all BAWT configurations with a comparison to the power in the ABL at the *Turbine* boundary.

5.2.1 Total Power

The total power within the flow at the *Turbine* boundary was obtained from the integral power developed normal to the *Turbine* boundary. Total power was obtained for each BAWT and was graphed in correlation to the four wind incidence angles shown in Figure 5.4.

Figure 5.4 shows there is a clear case when taper is 0.66 with spread factor of 1 generates the greatest energy of 255.7kW at the *Turbine* at 0° wind incidence. It is interesting to note from the previous section, this case provided the least velocity augmentation but outperforms in power generation. Moreover, the tapered cases with 0 spread factors which produce the highest wind augmentation factors result in generating the least power. This suggests the study of wind power generation is sensitive to changes in the capture area of turbines.

For the cases with spread factor of 0 with equivalent capture areas of 540m^2 , the total augmented power of the three cases for taper of 0, 0.33 and 0.66 are 106.2kW, 100.3kW, and 91kW respectively with a difference of 10.6%–11.7%. Changes in capture area produce wide degree of augmented power for the BAWT configurations. When spread factor was increased from 0 to 0.5, the *Turbine* boundary area increased 82.7% and 165.5% for tapers 0.33 and 0.66 respectively. This increased area augments the total power by 108.2% and 95.8% for the tapered cases of 0.33 and 0.66 respectively.

The configuration with the lowest power production at 0° wind incidence angle is taper ratio of 0.66 with spread factor of 0. This resulted from the lack of velocity augmentation through the BAWT where the flow does not accelerate comparably to the cases with increases in taper ratio and 0 spread factor.

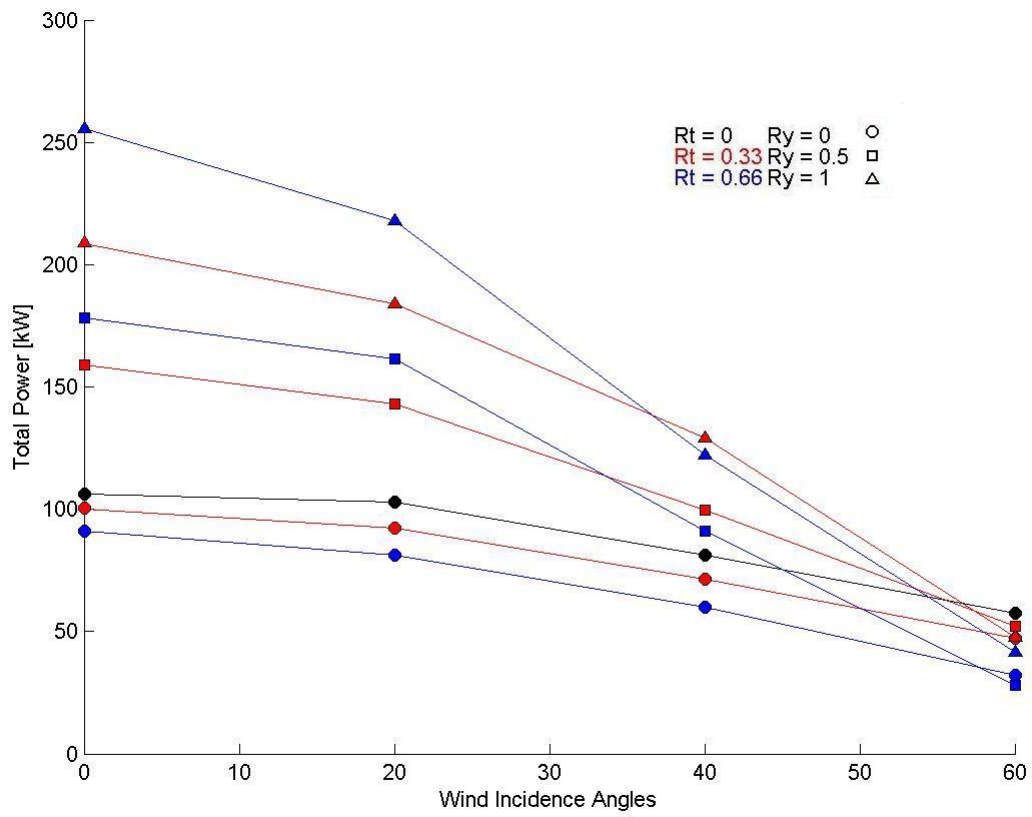


Figure 5.4: Total Power

Looking at Figure 5.4 from the best configuration to operate at 60° is the configuration with 0 taper. It outperforms configurations with taper at maximum spread factor of 1 by 20.1% and 38.8% for tapers of 0.33 and 0.66 respectively. Power values decrease with increasing wind incidence angle. This is an adequate result with correlations to the venturi effect with respect to incidence where venturi factor decreased as a result of the lack of low pressures aft of the BAWT system.

The case where taper is 0.33 at max spread factor of 1 surpasses the total power of cases with taper 0.66 and 0 is at a wind incidence angle of 30° – 40° . The difference in total power is 6.75kW, a difference of 5.6% and 15.6% at 40° and 60° wind incidence angles respectively. The two cases are surpassed by case of 0 taper between 50° – 60° . The measured powers at wind incidence angles of 60° are; 41.4kW, 47.9kW, and 57.5kW, with a difference of 38.8% and 20% with respect to the cases when taper of 0.33 and 0.66, both spread factors at 1 respectively. The critical factor controlling power production is the building spread which maximize turbine capture area, and higher wind augmentation factor plays a minimal role in the overall total power of a BAWT.

5.2.2 Power Augmentation Factor

Power augmentation factor determines how much power augmentation the specific BAWT configurations have in comparison to the ABL. The power augmentation factor is the ratio of the measured augmented total power to the total power from an unaugmented ABL. Power augmentation factors were measured for each BAWT configuration at each of the wind incidence angles and are plotted in Figure 5.5.

An average drop in power augmentation factor of 0.5 occurs when spread increases from 0 to 0.5 and an average drop of 0.2 occurs from 0.5 to 1. Power augmentation factor of 1 occurs just below 50° for spread factor of 0 and occurs at 30° and 20° with $Ry = 0.5$ and $Ry = 1$ respectively. A factor of 1 shows when a BAWT system produces no increase in total power compared to the power available in the ABL.

5.3 Power Rating

This study looked into defining the power rating of BAWT configurations varying wind regimes. Power rating is defined as the sum products of the augmented power and corresponding wind frequencies of the wind regime. Wind regimes are frequency of the measured wind directions based on the statistical averaged for a particular location.

Frequency of wind regimes are location dependent and any specified frequencies would be arbitrary. For this study three even frequency regime distributions are analysed where their frequencies of the wind incidence angles are equivalent and the regimes sum total of the frequencies equate 100%. Also a case study with a wind regime based on referenced statistical yearly averages at a referenced location is studied for a more realistic analysis of BAWT power rating.

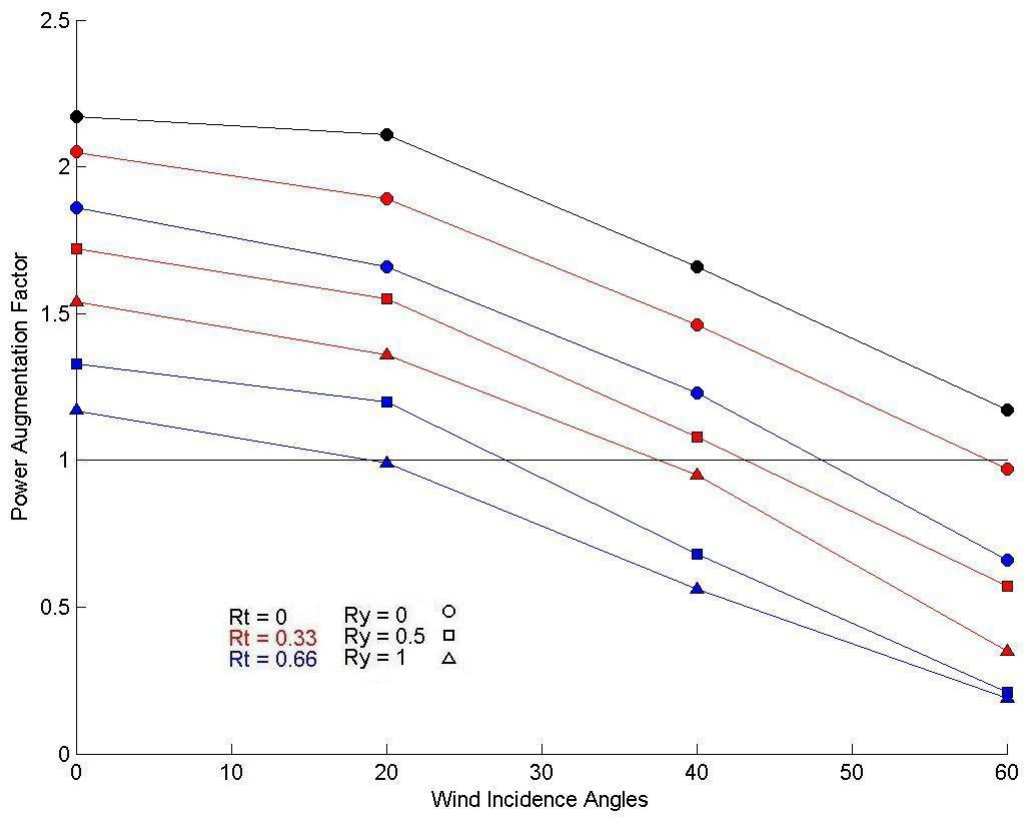


Figure 5.5: Power augmentation factors

Wind Regime	Frequencies						
High	14.3%	14.3%	14.3%	14.3%	14.3%	14.3%	14.3%
Medium	-	20%	20%	20%	20%	20%	-
Low	-	-	33.3%	33.3%	33.3%	-	-

Table 5.1: Incidence angles and relative frequencies of wind regimes

5.3.1 Even Frequency Regimes

This section is sub divided into three sub sections each pertaining to the analysis of each wind regime given in Table 5.1. The power ratings are plotted with respect to their turbine capture area.

High Regime

The high wind regime incorporates all wind incidence angles tested ranging from 0° – 60° . Since the study contained a symmetry plain through the BAWT at 0° , the negative reflective angles are taken into account creating a wind azimuth of $\pm 60^\circ$. The frequencies of the seven incidence angle are assumed to be equal value of 14.3% to sum 100%. The rated power for the BAWT system for a high wind regime is shown in Figure 5.6.

Figure 5.6 depicts the power ratings for each BAWT configuration in the high regime with respect to the turbine capture area. Figure 5.6 shows when spread factor is constant at 0, the power rating is highest for cases of 0 taper and produces a power rating of 84kW. The other ratings vary 12.9% and 38.2% for tapers of 0.33 and 0.66 respectively from the case of 0 taper.

It is interesting to note there are two cases of similar power ratings. The cases of tapered 0.33 and 0.5 spread factor is rated at 105.9kW and case of 0.66 taper and spread factor of 0.5 is rated at 108.5kW with a difference of 2.4%. The greater power rating developed by wind augmentation is counter balanced by a greater capture area.

For the case of 0.33 taper and spread factor of 1 the power rating is 22% higher than case of 0.66 taper at its maximum spread factor of 1 with equivalent *Turbine* areas. The velocity augmentation becomes the defining factor for energy capture rating.

Medium Regime

The medium wind regime incorporates the wind incidence angles ranging from 0° – 40° . Symmetry plane previously mentioned used at 0° bisecting the BAWT generating a wind azimuth of $\pm 40^\circ$. Equal frequencies for each wind incidence angle are 20% summing to 100%. Figure 5.7 depicts the power rating the BAWT configurations in the medium regime.

Equivalent trends to that of the high regime are produced for the medium regime were the results appear as scaled high regime results. For a constant spread factor of 0 of all tapered cases, the highest power rating of 95.1kW is from the case with no taper, with an 11.3% and 29.6% difference in power ratings from cases when taper is 0.33 and 0.66 respectively.

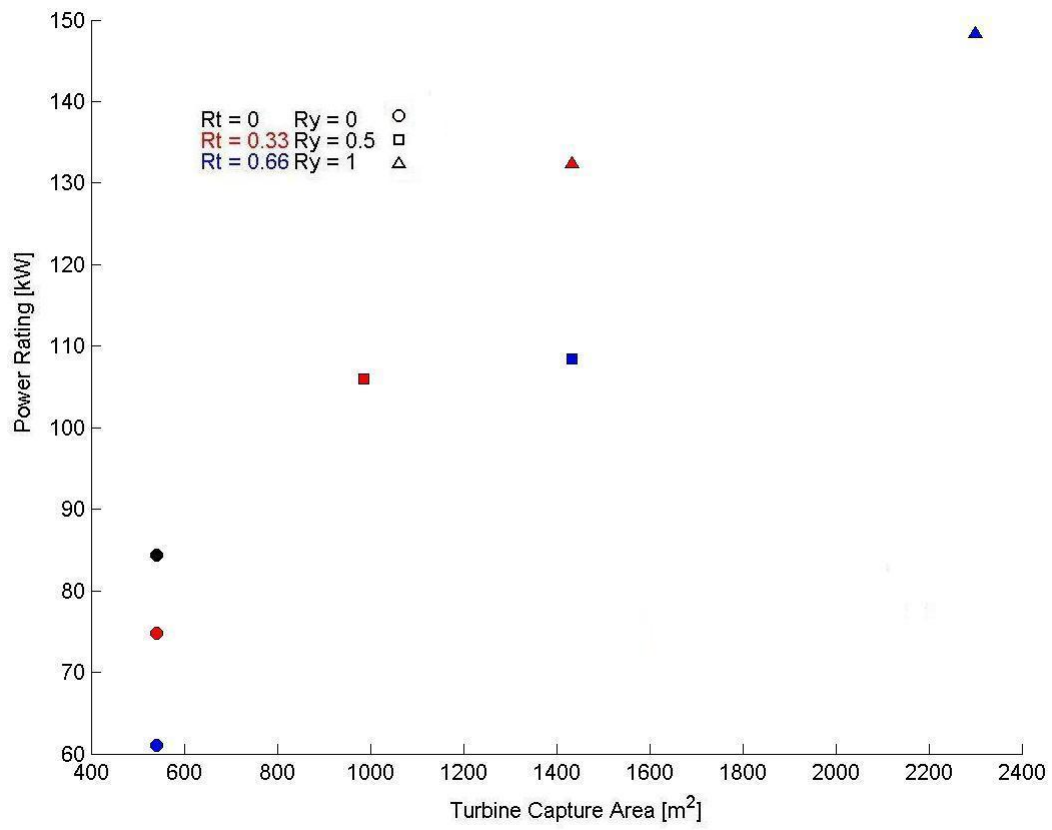


Figure 5.6: Power rating for high regime

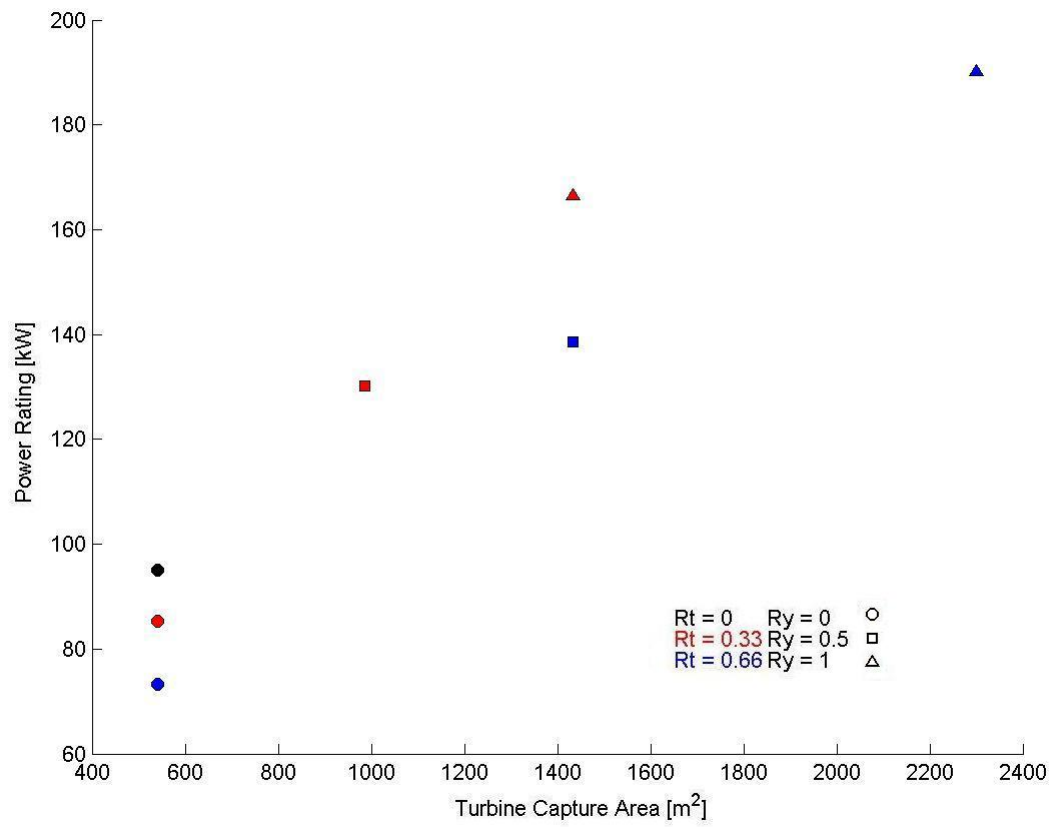


Figure 5.7: Power rating for medium regime

The two same cases are in close proximity also within the medium regime. Their values of 130.3kW and 138.8kW for the cases of taper at 0.33 with spread factor of 0.5 and case of taper 0.66% with spread factory of 0.5 respectively. The difference of these values is 6.4%. When the case of 0.33 taper has capture area equal to case with taper 0.66, a difference of 20% is shown.

The highest energy captures obtained from all tapers were generated at their max spread factors where turbine capture area is maximized. These values are given in Table 5.3 were the differences compared to the case of 0 taper are 75.1% and 100% from tapers of 0.33 and 0.66 respectively.

Low Regime

The low wind regime incorporates the wind incidence angles ranging from 0° – 20° with a symmetry plane at 0° generates a wind azimuth of $\pm 20^\circ$. Equal frequencies of each wind incidence angle are 33.3% summing to 100%. Figure 5.8 depicts the power rating of each BAWT configuration for a low regime.

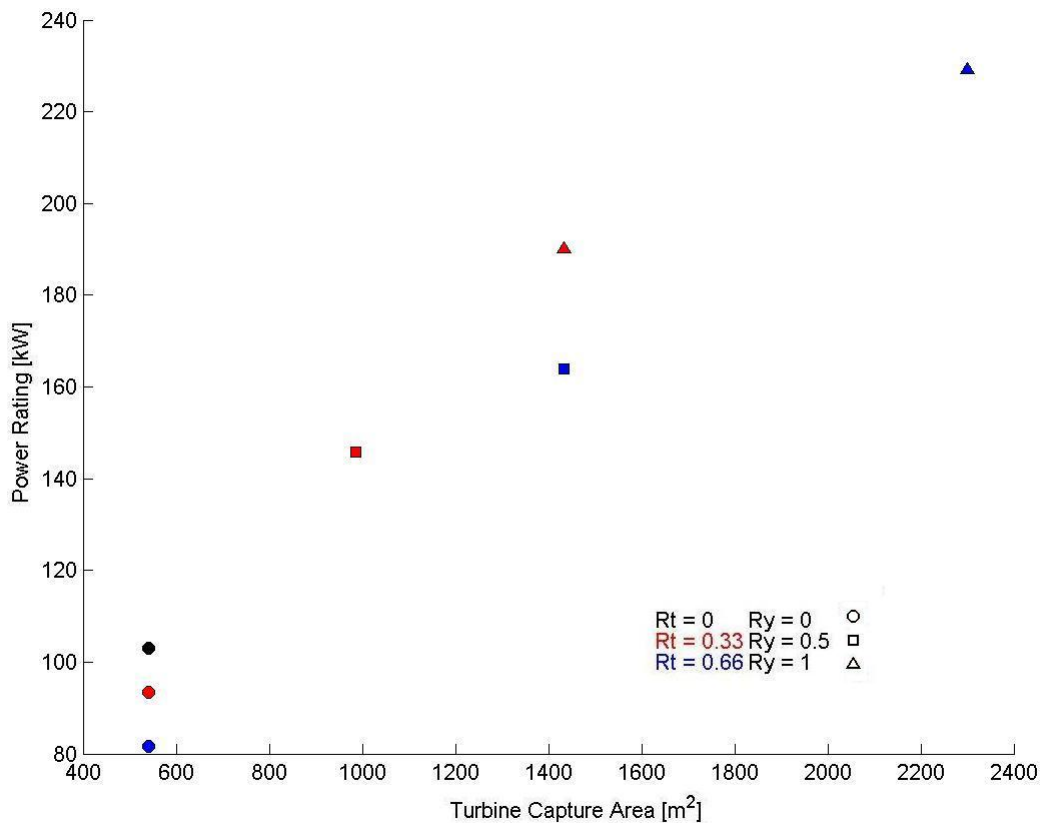


Figure 5.8: Power rating for low regime

Comparisons of the tapered cases with 0 spread factor generate differences of 10.2% and 22.8% for cases with taper 0.33 and 0.66 when compared to 0 taper of power rating of 103.1kW. There is a close

Incidence Angle	-60°	-40°	-20°	0°	20°	40°	60°
Toronto Island Regime	5.9%	6.5%	5.9%	6.5%	5.9%	5%	6.5%

Table 5.2: Wind regime of Toronto Island

grouping of configurations that is noted within Figure 5.8. The values for of these configurations are shown in Table 5.3.

The differences of cases of 0.33 taper with spread factor of 0.5 and 0.66 taper at spread factor 0.5 is 12.5%. When the 0.33 taper case increases to spread factor of 1, it then out performs the 0.66 taper with an equal turbine capture area by 20.5%. Power rating is maximized for each taper case when maximum spread factor and turbine capture area is reached. The power rating increases 84.5% and 122.4% from tapered cases 0.33 and 0.66 with respect to the case of 0 taper.

5.3.2 Wind Regime Case Study

The previous power ratings made use of an even frequency distribution across the evaluated wind regimes which generates an over evaluates the power rating. A more realistic approach is taking in the section where measured values of yearly averaged wind characteristics are referenced from the Toronto Island Airport, Toronto, Ontario. The wind regime's frequency was obtained by from a wind rose plot and used to calculate the power rating. Finally power ratings for all the BAWT configurations analysed are made and compared.

A wind rose plot is essential in determining the appropriate site for wind turbines and BAWT systems. It states three main characteristics of the wind engineers need to determine if a location is suitable in harvesting wind. The three characteristics are: speed, direction and frequency. A wind rose plot from the Toronto Island Airport was select for this study for its comparable ABL to the simulated ABL. Winds are coming off the water where the surface roughness is low and close to that of the simulated 0.03m surface roughness. Figure 5.9 is the wind rose plot of the Toronto Island Airport.

It can be seen from 5.10 the dominant wind direction is of West South West direction. Thus the BAWT system was oriented to face into that direction and have the BAWT's plane of symmetry directed West South West. Figure 5.10 illustrates the orientation of the BAWT system and it's encompassing wind azimuth of $\pm 60^\circ$.

The sectors for the wind rose plot are separated by 22.5° and it was assumed the sectors are close enough to the simulated wind sectors of 20° . The wind incidence angles and their frequencies are tabulated in Table 5.2.

Similarly to the previous section, power rating was defined as the sum products of the augmented power and corresponding wind frequencies of the wind regime. It is noted the sum of the frequency for the regime within the BAWT azimuth totals 42.2%, hence a lower power rating will incur. The power ratings for the BAWT configurations are presented in Figure 5.11.

Figure 5.11 depicts the power ratings for each BAWT configuration Toronto Island Airport wind regime with respect to the turbine capture area. Figure 5.11 shows when spread factor is constant at

Toronto Island (TORONTOI)

Statistics based on observations taken between 2/2007 - 3/2011 daily from 7 am to 7 pm local time.

Month of year	Jan	Feb	Mar	Apr	May	Jun	Jul	Aug	Sep	Oct	Nov	Dec	SUM
	01	02	03	04	05	06	07	08	09	10	11	12	1-12
Dominant <u>Wind dir.</u>	↗	↖	↖	↖	↖	↖	↖	↖	↖	↖	↖	↖	↖
Wind probability > = 4 Beaufort (%)	49	43	42	47	36	26	14	21	26	34	40	48	35
Average <u>Wind speed</u> (Knots)	12	11	11	11	10	8	7	8	8	9	10	12	9
Average air temp. (°C)	-2	-1	2	8	13	19	22	22	18	12	6	0	9
Select month (Help)	Jan	Feb	Mar	Apr	May	Jun	Jul	Aug	Sep	Oct	Nov	Dec	Year

Wind dir. distribution Toronto Island all year

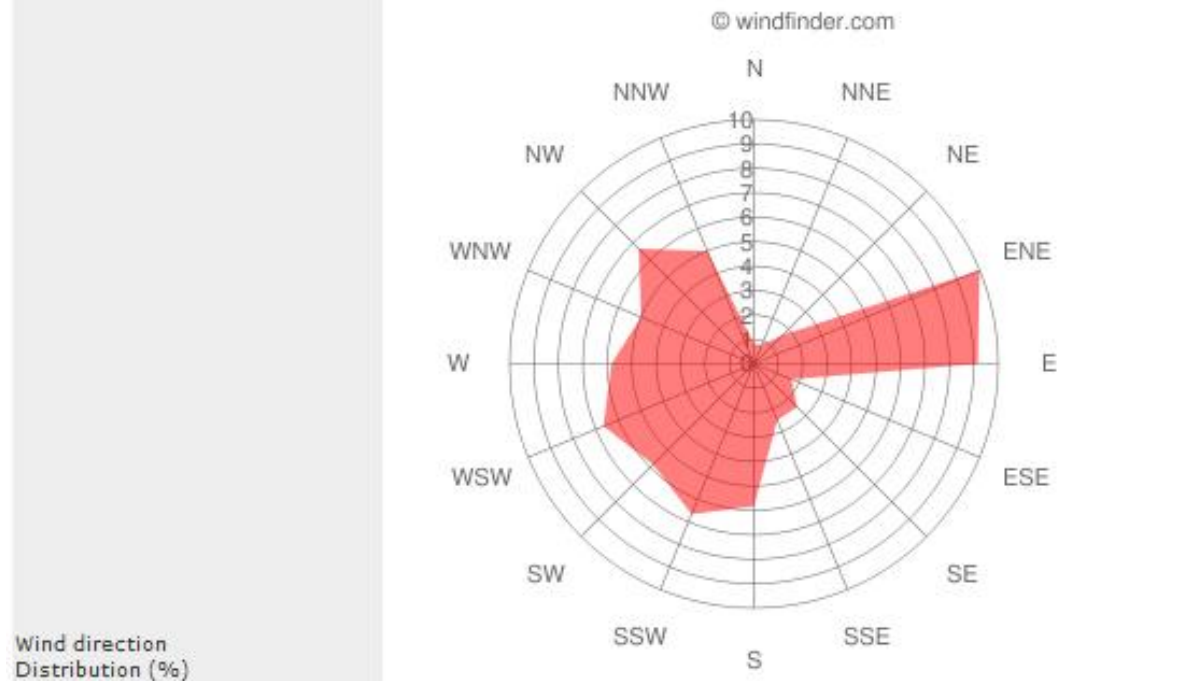


Figure 5.9: Toronto Island yearly average wind rose plot [4]

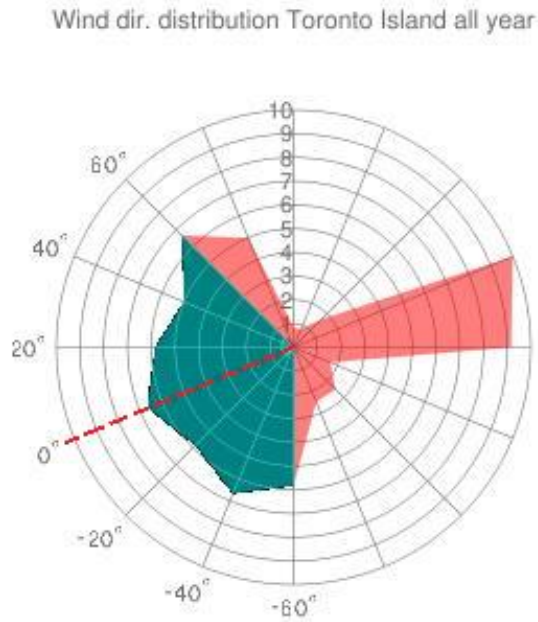


Figure 5.10: BAWT azimuth on wind rose plot
[4]

0, the power rating is highest for cases of 0 taper and produces a power rating of 35.6kW. The other ratings vary 13% and 34.8% for tapers of 0.33 and 0.66 respectively from the case of 0 taper.

The cases of tapered 0.33 and 0.5 spread factor is rated at 45.2kW and case of 0.66 taper and spread factor of 0.5 is rated at 44.6kW with a difference of 1.3%. The greater power rating developed by wind augmentation is counter balanced by a greater capture area.

For the case of 0.33 taper and spread factor of 1 the power rating is 25.8% higher than case of 0.66 taper at spread factor of 0.5 with equivalent *Turbine* areas. The velocity augmentation becomes the defining factor for energy capture rating. Comparing the rating for the tapered cases at their maximum spread factor and maximum turbine capture area, there is little increase in power rating. There is a 9.6% difference in power rating between the two configurations suggesting no real gains occur in power rating.

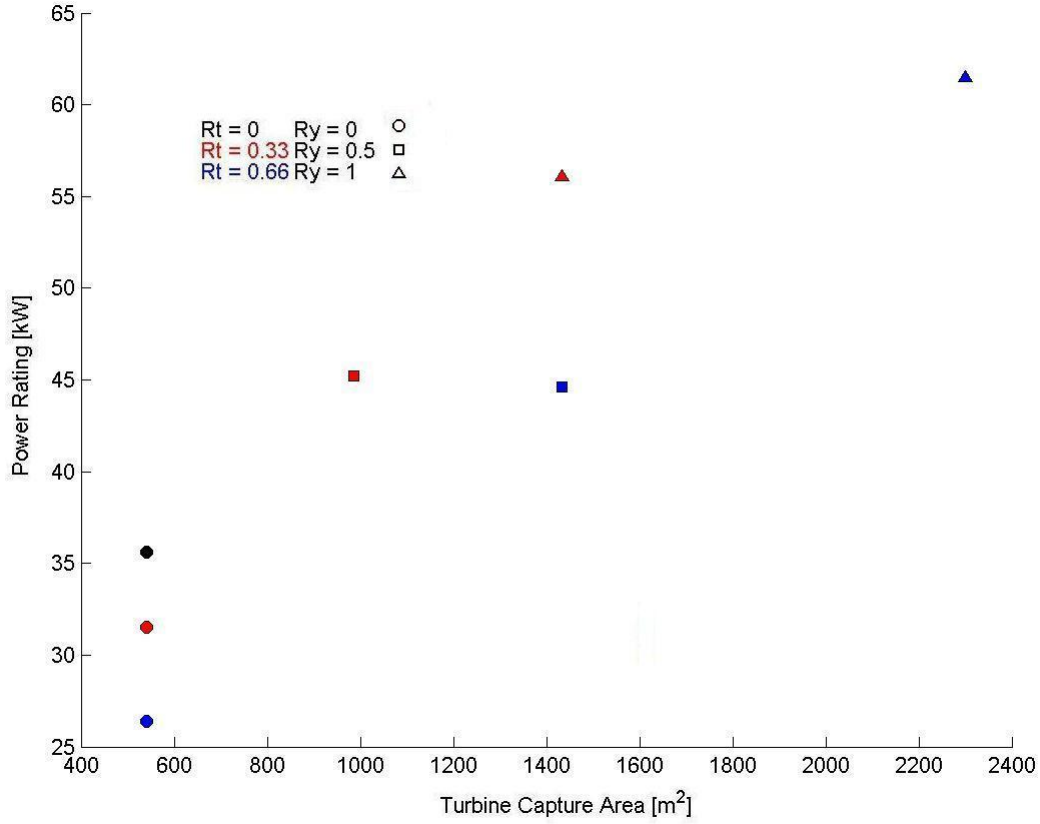


Figure 5.11: Power rating for Toronto Island case study

Taper	Turbine Area [m²]	Wind Regime Power Rating [kW]			
		High	Medium	Low	Toronto Island
0	540	84.4	95.1	103.1	35.6
0.33	540	74.7	85.4	93.5	31.5
0.33	986.7	105.9	130.3	145.7	45.2
0.33	1433.5	132.3	166.5	190.2	56.1
0.66	540	61.1	73.3	81.7	26.4
0.66	1433.5	108.5	138.6	164.0	44.6
0.66	2300.8	148.3	190.2	229.2	61.5

Table 5.3: Power rating for the wind regimes

Chapter 6

Conclusion

It should be noted the simulated turbines was simplified using a porous jump boundary condition with a one-dimensional pressure drop approximation. Turbine turbulent factors such as rotational effects and tip losses were not taken into account within the simplified porous jump boundary.

The key aim of this study was to find a BAWT geometry which provides greatest velocity augmentation, total augmented power and overall power rating with respect to different wind regimes. This thesis utilized an optimized two dimensional BAWT footprint for low wind incidence angles derived from the work of Hans Hamm [14] where parabolic parameter definitions were imposed on the three dimensional extruding of the BAWT configuration.

Also important in this investigation was the modeling of ABL to obtain realistic flow characteristics. Proper modeling of the von Karman street developed the pressure cascade to influence the pressure upstream and ultimately the BAWT augmented power at the turbine.

In summary:

1. Augmentation factor correlates with continuity law and venturi effect
2. The BAWT configuration with no taper produced highest augmentation
3. The BAWT with greatest spread factor and taper produced lowest augmentation
4. Turbine capture area is the primary factor in generating best captured power
5. Velocity augmentation is a secondary factor in producing best capture power
6. Best configuration may lay between a taper ratio of 0.33 and 0.66 at max spread of 1

6.1 Future Work

Future analysis would be to model BAWT systems and include other building obstructions for the wind. Perhaps obstructions can act as a diverter or channel to provide consistent and high wind regime

frequencies to BAWT. A realistic urban ABL maybe modeled for the study which may generate different BAWT profiles for greatest power augmentation.

Furthe study can also be made in varying the original gap size for greater range of turbine capture area. A trade of study of the gap area between the buildings and the turbine sweeping area and the number of turbines used can be done. Direct modelling of rotating turbines can generate the rotational effects and tip losses which occur in real flows across turbines.

The cross-section of the BAWT system can also be varied with height. The variation of the 2D parameters set by Hamm can be varied as a function of height and potentially a new parameter of twist may be incorporated. The design may also incorporate a bi-directional flow where the turbines can counter rotate and receive wind from the other end and generate power.

Lastly an optimization routine can be utilized in directing the researcher in the direction of the optimal BAWT configurations according to the imposed various constraints.

Appendix A

Parabolic BAWT Profile Formulation

It was mentioned in the Methodology section the BAWT profile follows a parabolic profile for each of the three parameters. This section derives the the parabolic profile as a function of the buildings height. The base parabolic equation is defined as

$$P(z) = az^2 + bz + c \quad (\text{A.1})$$

where a , b and c are constants to the parabolic equation. It was assumed there to be no change in the profile at the building roof 100m high, thus differentiating Equation A.1 and substituting the defined variables we get

$$\partial P(z) = 2az + b$$

$$\partial P(z) = 0 \quad @ \quad z = 100$$

$$\partial 0 = 2a(100) + b$$

$$b = -200a$$

$$P(z) = az^2 - 200bz + c \quad (\text{A.2})$$

Also, the parabolic profile is 0 at the ground when $z = 0\text{m}$. Substituting the known variables into Equation A.2

$$\begin{aligned} P(z) &= 0 \quad @ \quad z = 0 \\ c &= 0 \end{aligned}$$

$$P(z) = az^2 - 200bz \tag{A.3}$$

Also known is the roof top offset parameter $\chi\varnothing_o$ which from the referenced base diameter $\varnothing_o = 20\text{m}$ is substituted into Equation A.3

$$\begin{aligned} P(z) &= 20\chi \quad @ \quad z = 100 \\ 20\chi &= a(100)^2 - 200(100)a \\ \chi &= -500a \\ a &= -\frac{\chi}{500} \end{aligned}$$

Substituting a back into Equation A.3

$$\begin{aligned} P(z) &= -\left(\frac{\chi}{500}\right)z^2 + 200\left(\frac{\chi}{500}\right)z \\ &= \frac{z(200-z)}{500}\chi \\ P(z) &= \frac{z(200-z)}{500}\chi \end{aligned} \tag{A.4}$$

Equation A.4 is the derived parabolic profile defining the BAWT taper and forward lean parameters. Spread factor has an added constant at the end of A.4 which defines the initial gap of 3m set by the referenced model of Hans Hamm. Thus the parabolic function for spread factor is given as

$$P(z) = \frac{z(200-z)}{500}\chi + 3 \tag{A.5}$$

Appendix B

Bodies of Influence

Bodies of influence are used to control element sizing at specified locations within the control volume without modeling an internal body. Two bodies of influence were used to define the vortex street with varying element sizes of influence. The sizes were varied from finest located up the center of the of BAWT system with a gradual coarsening in the bodies of influent as they move further downstream in the domain.

A body of influence of 120m diameter encapsulated the BAWT system and was extended downstream to the outlet area to capture the von Karman street. Figure B.1 shows the bodies of influence encapsulating the BAWT system as domed structures which are stretched downstream in the von Karman street.

The length of the medium body of influence was defined by the assumption vortex would dissipate enough kinetic energy and extend turbulent length scale to be captured in the coarser body of influence after three shedding periods. The frequency of shedding was determined from the Strouhal numbers defined by Zdrakovich for flows over cylinders at flow Reynolds nuber $1 \cdot 10^6$ defined in Table B.1.

The distance a vortex propagates from a body after three periods is found by multiplying the inverse of frequency and the potential wind speed define in Equation B.1.

$$l_{vp} = f_r^{-1} u_p \tag{B.1}$$

Table B.1 shows the resultant vortex propagation distances from a cylinder using flow Strouhal num-

Strouhal Numbers	Frequency [Hz]	Periods [s]	Propagation Distance [m]
0.18	0.0374	26.7	334
0.50	0.1040	9.6	120

Table B.1: Vortex propagation distances after three periods with respect to Strouhal numbers

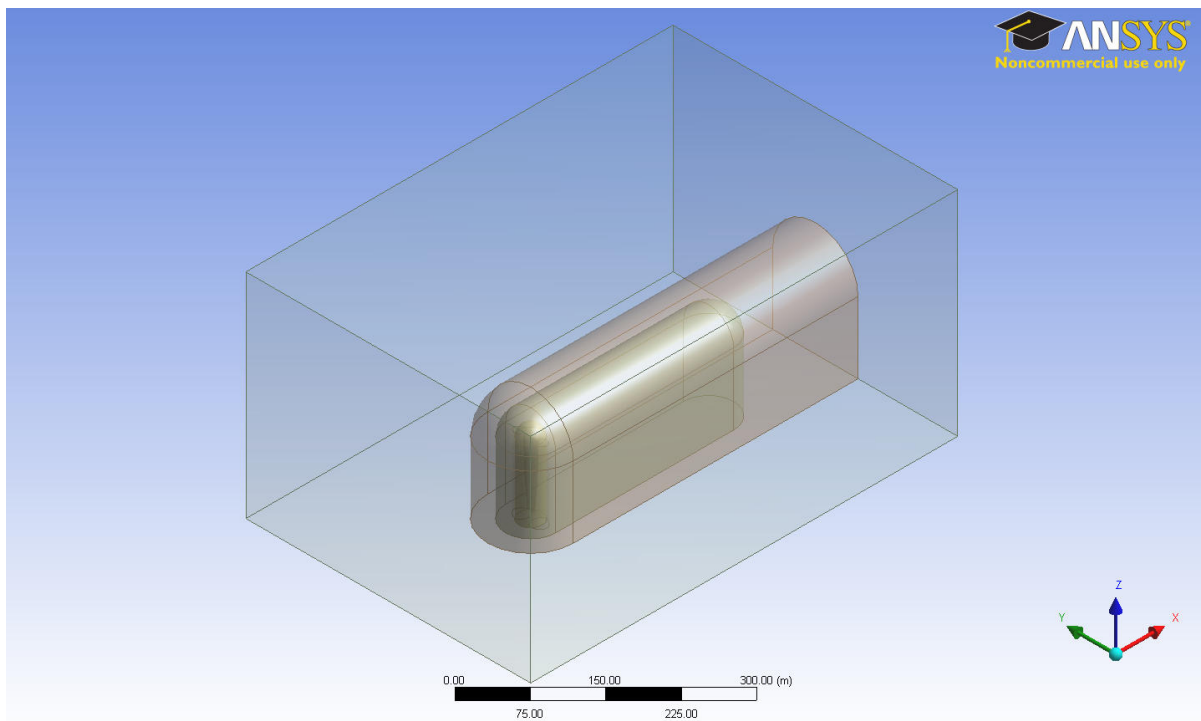


Figure B.1: Body of influence

bers. Zdravkovich defines Strouhal numbers to fall within the range from 0.18–0.50 which is dependent on the turbulence model chosen for analysis.

Since there is a range of Strouhal numbers it was assumed any number may appear within this study. Therefore the largest propagation distance was used which corresponds to the lowest shedding frequency from a Strouhal number of 0.18.

Figures B.2 and B.3 show the turbulent von Karman street formed behind the BAWT systems. They depict vortex bubbles to remain within the defined bodies of influence for the modelling of the upstream pressure cascade.

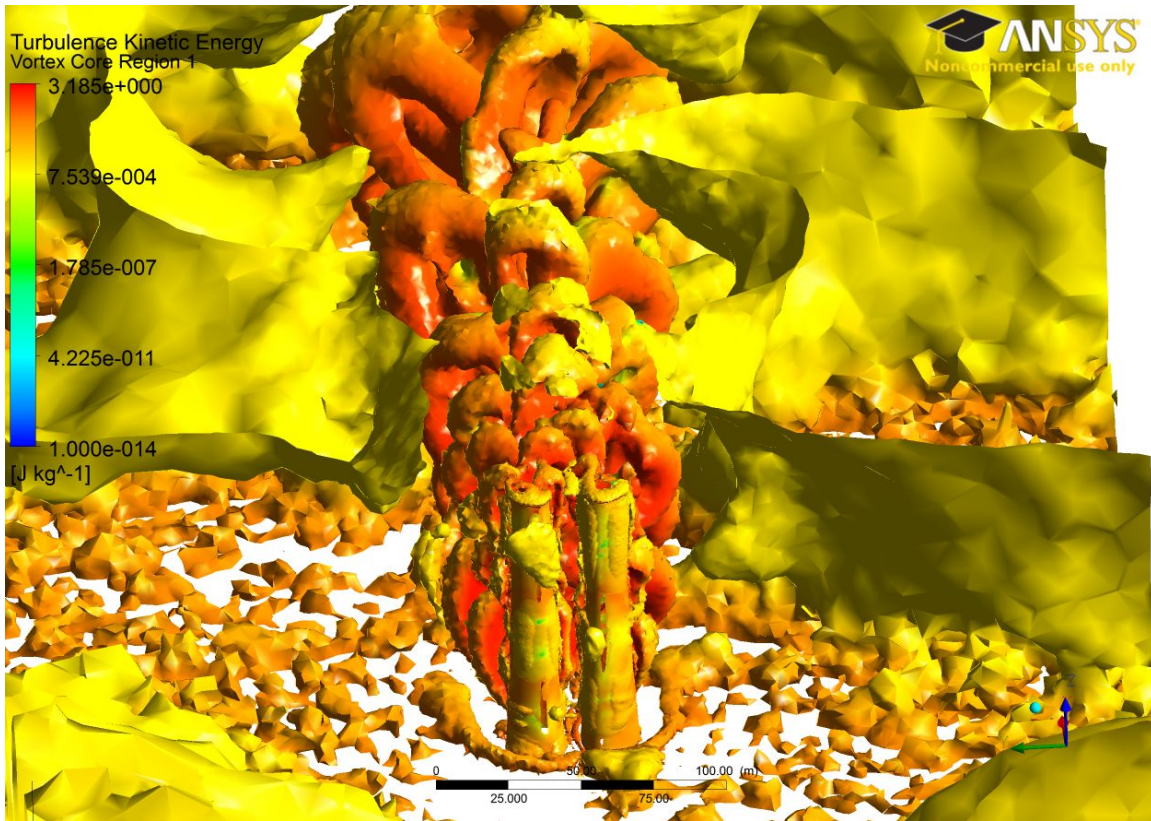


Figure B.2: Q-Criterion Iso Surface with Turbulent kinetic energy variations ($R_t = 0.33$, $R_x = 0.5$, $R_y = 0.5$ and $\alpha = 0^\circ$)

Also in the two Figures B.2 and B.3, three separation bubbles are visibly defined within the 330m length of the *Fine Body of Influence*. Thus it can be said the $k-\omega$ (SST) model, near-wall modeling and vortex shedding produces a pressure cascade well enough for the purpose of this study.

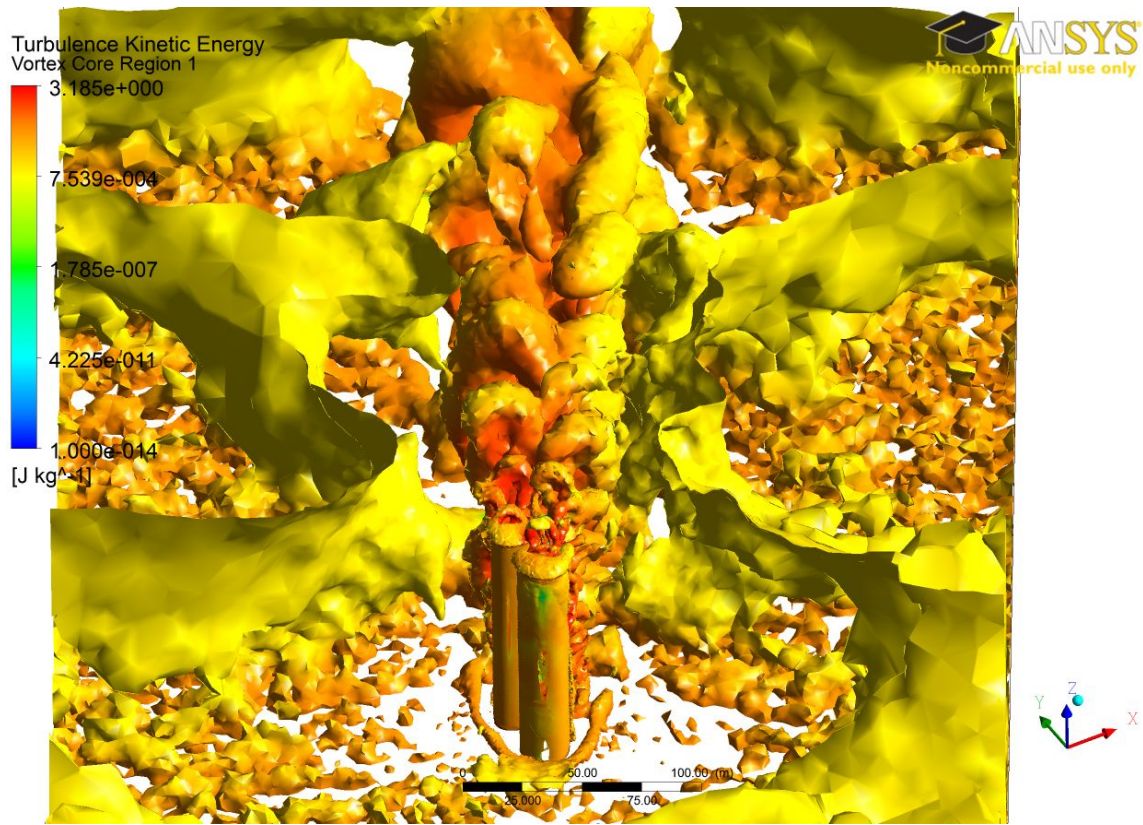


Figure B.3: Q-Criterion Iso Surface with Turbulent kinetic energy variations ($R_t = 0$ and $\alpha = 60^\circ$)

Appendix C

Porous Jump

Turbines were modeled using the porous jump boundary condition at the *Turbine* boundary. The Navier-Stokes equations with the addition of momentum source terms were used to model the porous media. The Navier-Stokes equations with momentum source terms are given below in Cartesian coordinates in Equation C.1

$$\Delta P = - \left(\frac{\mu}{\alpha} \nu + C_2 \frac{1}{2} \rho u^2 \right) \Delta m \quad (\text{C.1})$$

μ is the fluid viscosity, ν is the dynamic viscosity, α is the permeability of the porous media. Two source terms account for the viscous losses and inertial loss when the fluid passes through the porous jump *Turbine* boundary condition. The first term is called the Darcy term which is the instantaneous discharge rate of a fluid through a porous medium.

The simplification does not incorporate the effects and flow characteristics of the vortex shedding created by the rotating blades, thus omitting three dimensional wake and tip effects. The simplified modeled turbine consists of no porous media therefore no viscous losses incur thus the Darcy term is dropped and porous jump is defined by Equation C.2.

$$\Delta P = -C_2 \frac{1}{2} \rho u^2 \Delta m \quad (\text{C.2})$$

To maintain consistency with the work from Hans Hamm [14] his arbitrary pressure coefficient $C_2 = 0.4$ was used for the pressure loss coefficient of the porous jump with a unit length of $\Delta m = 1$.

Figure C.1 illustrates the pressure drop through the mid section of the BAWT along the x -axis at a height of 60m. The pressure drop across the turbine was measured from the difference of the measured pressures at the *Turbine* capture area and 1m downstream. The pressure difference of the cell values are calculated to be $\Delta P = -11.49\text{Pa}$.

Verification of the pressure drop found at the porous section is based on the fluid velocity entering the porous jump boundary and was measured to be 6.71m/s. Using equation C.2 the pressure drop

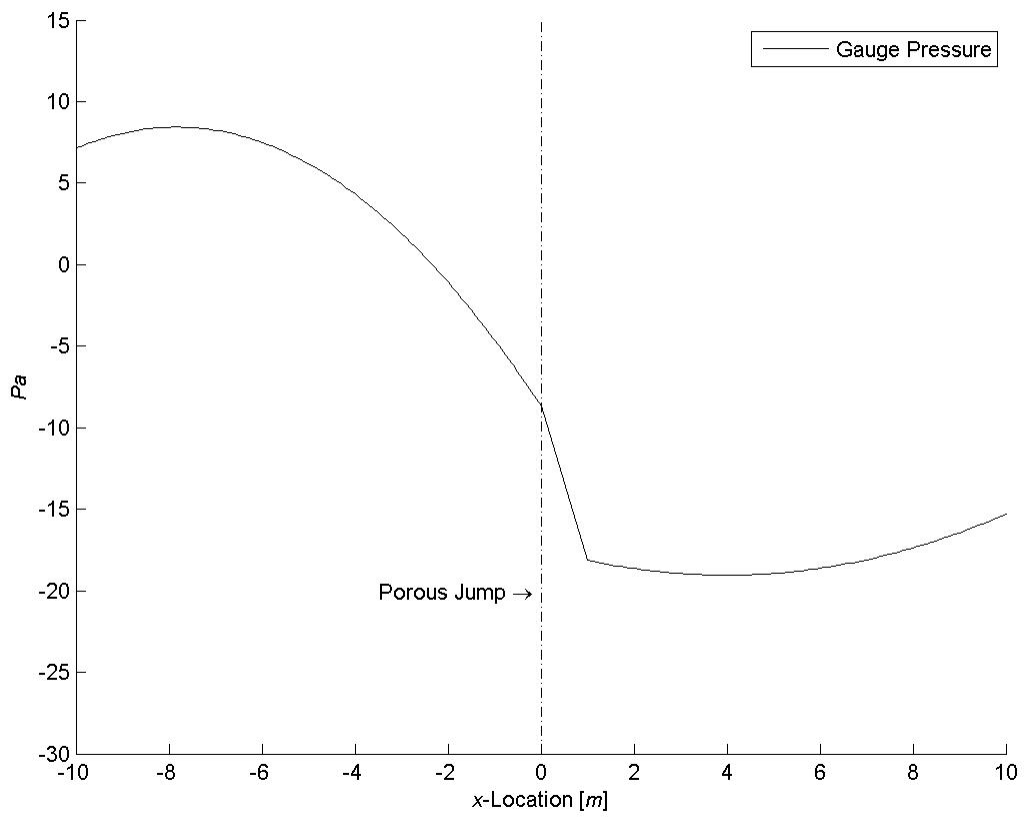


Figure C.1: Pressure reading through BAWT a model

across the porous media was found to be -11.04Pa with a difference of 4.1% from the measured value.

$$\begin{aligned}\Delta P &= -\left(0.4\frac{1}{2}(1.225)(6.713)^2\right) (1) \\ &= -11.04Pa\end{aligned}$$

Appendix D

Figures

This section shows the pressure contours on the BAWT *Walls*, *Ground* and a pressure contour of the center plane through the BAWT projected on the fall boundary *Side* boundary. Also stream lines depict the turbulence aft of the BAWT.

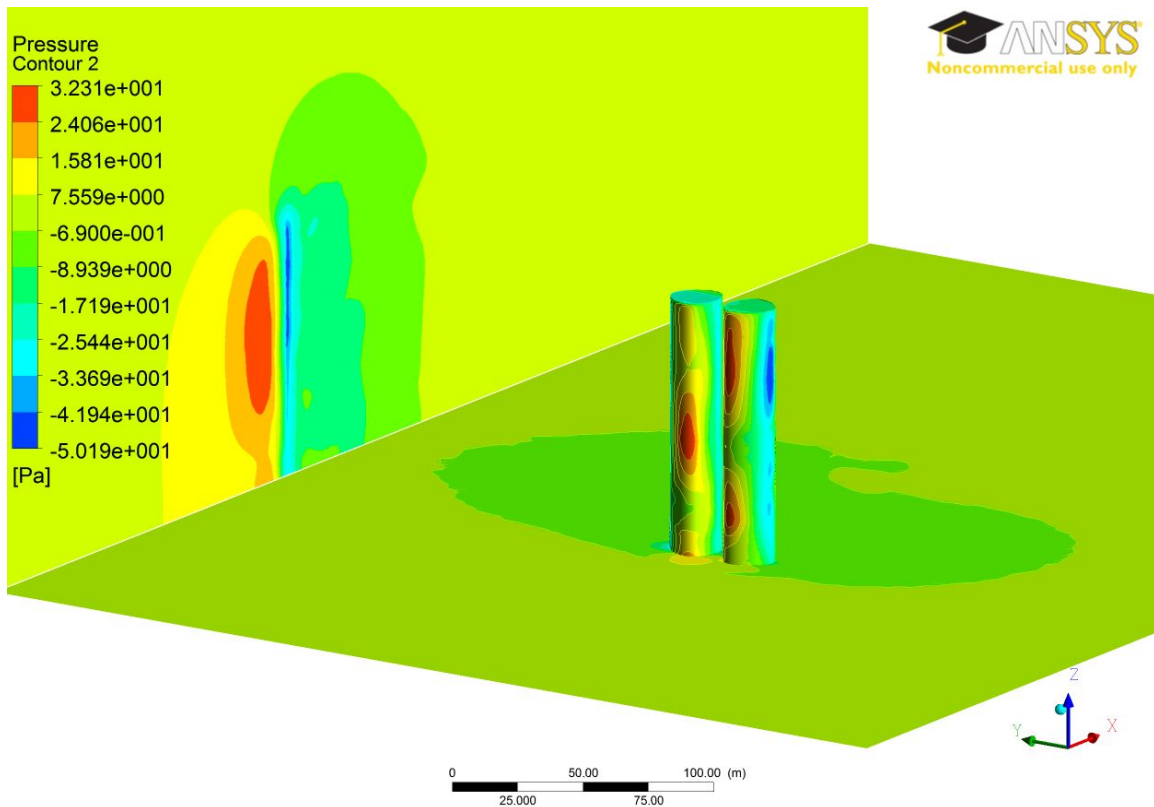


Figure D.1: Contour of pressure on BAWT walls the pressure contour through the mid-plane projected on the domain side wall

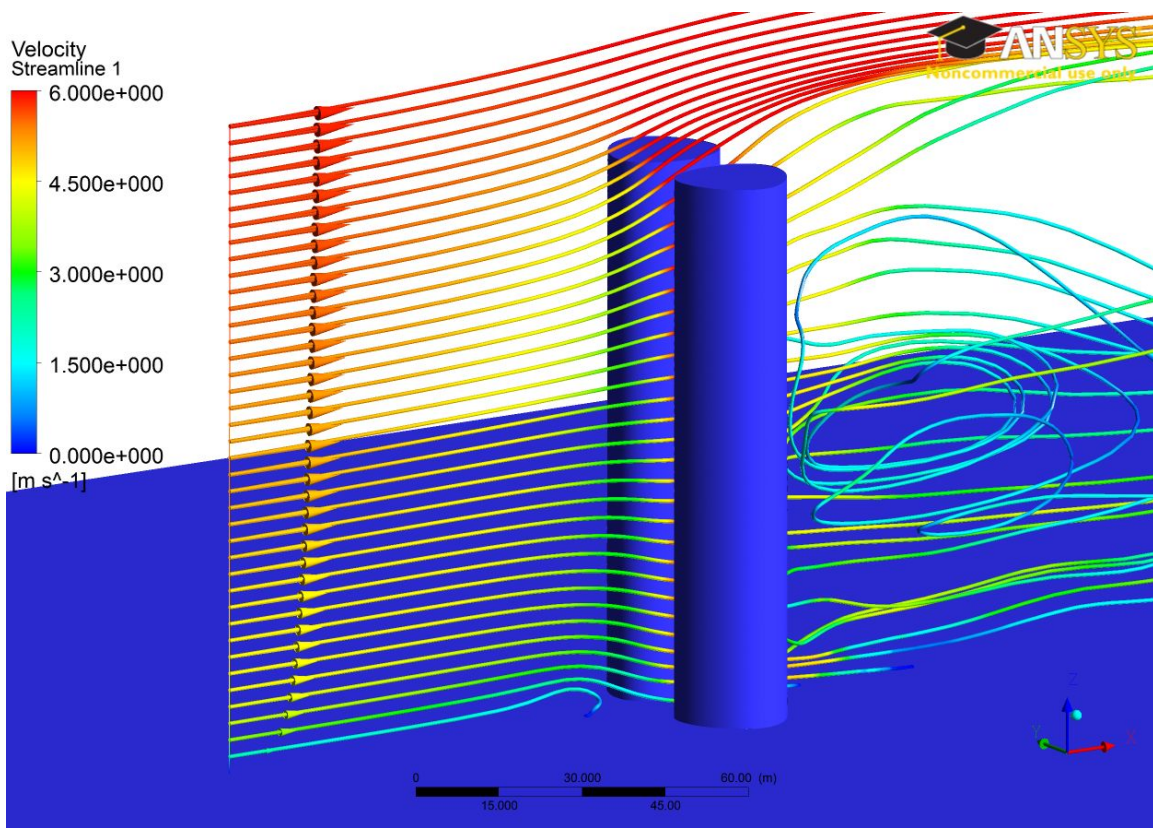


Figure D.2: Flow stream lines ($R_t = 0$, $R_x = 0$, $R_y = 0$ and $\alpha = 0$)

Appendix E

Velocity Inlet ABL UDF

This section shows the user defined function (UDF) for FLUENT created to define the ABL for the velocity inlet condition at the *Inlet* boundary.

```
/******  
abl_udf.c  
UDF for specifying steady-state velocity profile boundary condition  
*****/  
#include "udf.h"  
  
DEFINE_PROFILE(inlet_u_velocity, thread, position)  
{  
    real x[ND_ND];  
    face_t f;  
    real z,zo,zref,ln,lnref,vel;  
  
    vel = 4.16;  
    zo = 0.03;  
    zref = 60;  
    lnref = log10(zref/zo);  
  
    begin_f_loop(f,thread)  
    {  
        F_CENTROID(x,f,thread);  
  
        z=x[2];  
  
        ln = log10(z/zo);  
  
        F_PROFILE(f,thread,position)= (1.31*vel*ln)/lnref;  
    }  
    end_f_loop(f, thread)  
}
```


Appendix F

FLUENT Journal Scripting

The journal scrip was create to submit bash jobs to FLUENT for processing. The journal script defined the BAWT configurations used and the model set up and solution configurations.

```
/file/set-batch-options no yes no
/file/read-case SGE_0_WORKDIR/MeshFiles/Rt_RT/Rx_RX_Ry_RY/FFF.Rt_RT_Rx_RX_Ry_RY_AOA_ANGLE.msh
/define/user-defined/compiled-functions compile SGE_0_WORKDIR/SUBDIR/libudf yes SGE_0_WORKDIR/SUBDIR/
    libudf/abl_udf.c "" SGE_0_WORKDIR/SUBDIR/libudf/abl_udf.c ""
/define/user-defined/compiled-functions load SGE_0_WORKDIR/SUBDIR/libudf
/define/custom-field-functions/define "abl" VIN*1.31*log10((z_coordinate)/0.03)/log10(60/0.03)
/define/custom-field-functions/define "power_aug" 1/2*density*(x_velocity)^3
/define/custom-field-functions/define "power_abl" 1/2*density*(abl)^3
/define/custom-field-functions/define "initial_u_velocity" abl*cos(ANGLE*PI/180)
/define/custom-field-functions/define "initial_v_velocity" abl*sin(ANGLE*PI/180)
/define/models/solver/density-based-implicit yes
/define/models/energy yes
/define/models/viscous kw-sst yes
/define/boundary-conditions/velocity-inlet inlet no no yes yes yes yes "udf" "inlet_u_velocity::libudf" no
    300 no yes 10 1 no 0
/define/boundary-conditions/pressure-outlet outlet no 0 no 300 no no yes yes no 0.7 no 1 no no
/define/boundary-conditions/wall ground 0 no 0 no no no 0 no no no 0.03 no 0.5
/define/boundary-conditions/wall leftbuilding 0 no 0 no no no 0 no no no 0 no 0.5
/define/boundary-conditions/copy-bc leftbuilding rightbuilding leftbuildingtop rightbuildingtop ()
/solve/set/discretization-scheme/amg-c 1
/solve/set/discretization-scheme/k 1
/solve/set/discretization-scheme/omega 1
/solve/set/under-relaxation/k 0.8
/solve/set/under-relaxation/omega 0.8
/solve/set/under-relaxation/turb-viscosity 1
/solve/monitors/residual/criterion-type 1
/solve/monitors/residual/monitor yes yes yes yes yes yes yes
/solve/set/flow-warnings no
/solve/initialize/set-defaults k 0.7
/solve/initialize/set-defaults omega 1
/solve/initialize/set-defaults temperature 300
/solve/initialize/initialize-flow
/solve/patch Model-fluid () x-velocity no yes initial_u_velocity
/solve/patch Model-fluid () y-velocity no yes initial_v_velocity
/solve/initialize/set-fmg-initialization 5 0.001 10 0.001 50 0.001 500 0.001 500 0.001 100 0.75 yes
/solve/initialize/fmg-initialization yes
/solve/iterate 50
/define/boundary-conditions/modify-zones zone-type turbine porous-jump
```

```
/define/boundary-conditions/porous-jump turbine 1e+10 1 0.4
/solve/iterate 100
/define/models/unsteady-2nd-order yes
/solve/monitors/surface/set-monitor x-velocity-turbineinlet "Area-Weighted Average" x-velocity turbine ()
    no no yes "ave_x_velocity_turbineinlet_area_weighted" 1 yes flow
/solve/monitors/surface/set-monitor abl-velocity-turbineinlet "Area-Weighted Average" abl turbine () no no
    yes "ave_abl_velocity_turbineinlet_area_weighted" 1 yes flow
/solve/monitors/surface/set-monitor mass-flow-rate-turbineinlet "Mass Flow Rate" turbine () no no yes
    "mass_flow_rate_turbineinlet" 1 yes flow
/solve/monitors/surface/set-monitor augmented-power "Integral" power_aug turbine () no no yes "power_aug" 1
    yes flow
/solve/monitors/surface/set-monitor non-augmented-power "Integral" power_abl turbine () no no yes
    "power_abl" 1 yes flow
/file/auto-save data-frequency 200
/solve/set time-step TIME_STEP
/solve/dual-time-iterate N_TIME_STEPS N_ITERATIONS
/file/write-case Rt_RT_Rx_RX_Ry_RY_AOA_ANGLE.cas.gz
/file/write-data Rt_RT_Rx_RX_Ry_RY_AOA_ANGLE.dat.gz
/report/summary yes "report.sum"
/exit
```

Appendix G

Shell Bash Script

Shell scripts were created to automate the journal scrip variations defining the solution criteria for FLUENT and aswell the submission of bash cases.

```
#!/bin/sh

vin_array="4.16";
taper_ratio="0 0.33 0.66";
x_position="0 0.5 1";
y_position="0 0.5 1";
angle_of_incidence="0 20 40 60";

n_iterations="20";
time_step="1";
run_time="700";
n_time_steps="700";

for RT in $taper_ratio; do
  for RX in $x_position; do
    for RY in $y_position; do
      for AOA in $angle_of_incidence; do
        for VIN in $vin_array; do
          subdir='Rt_'$RT'_Rx_'$RX'_Ry_'$RY'_AOA_'$AOA;
          mkdir -p $subdir;
          mkdir -p $subdir/libudf;
          mkdir -p $subdir/udf;
          mkdir -p $subdir/udf/libudf;
          cp -r libudf/* $subdir/libudf/
          sed -e 's#SGE_O_WORKDIR#`pwd`#g' -e 's/VIN/'$VIN'/g' udf/abl_udf.c > $subdir/libudf/abl_udf.c
          sed -e 's#SGE_O_WORKDIR#`pwd`#g' -e 's/RX/'$RX'/g'
          -e 's/RX/'$RX'/g'
          -e 's/RY/'$RY'/g'
          -e 's/RT/'$RT'/g'
          -e 's/N_ITERATIONS/'$n_iterations'/g'
          -e 's/N_TIME_STEPS/'$n_time_steps'/g'
          -e 's/TIME_STEP/'$time_step'/g'
          -e 's/VIN/'$VIN'/g'
          -e 's/ANGLE/'$AOA'/g'
          -e 's/SUBDIR/'$subdir'/g' test.jou > $subdir/test.jou

          cd $subdir;
          sqsub -r 100h --nompirun -q mpi -n 8 -o ofile%J fluent 3ddp test2.jou
          cd ..
        done
      done
    done
  done
done
```

```
done
done
done
done
```

Appendix H

FLUENT CFD Code Settings

A sample results file produced by FLUENT describing the CFD code settings.

```
FLUENT
Version: 3d, dp, dbns imp, sstk,
        transient (3d, double precision, density-based implicit,
                  SST k-omega, transient)
```

```
Release: 12.1.2
```

```
Title:
```

```
Models
```

```
-----
```

Model	Settings
Space	3D
Time	Unsteady, 2nd-Order Implicit
Viscous	k-omega turbulence model
Heat Transfer	Enabled
Solidification and Melting	Disabled
Radiation	None
Species Transport	Disabled
Coupled Dispersed Phase	Disabled
Pollutants	Disabled
Pollutants	Disabled
Soot	Disabled

```
Material Properties
```

```
-----
```

```
Material: air (fluid)
```

Property	Units	Method	Value(s)
Density	kg/m3	constant	1.225
Cp (Specific Heat)	j/kg-k	constant	1006.43
Thermal Conductivity	w/m-k	constant	0.0242
Viscosity	kg/m-s	constant	1.7894e-05
Molecular Weight	kg/kgmol	constant	28.966
Thermal Expansion Coefficient	1/k	constant	0
Speed of Sound	m/s	none	#f

APPENDIX H. FLUENT CFD CODE SETTINGS

Material: aluminum (solid)

Property	Units	Method	Value(s)
Density	kg/m3	constant	2719
Cp (Specific Heat)	j/kg-k	constant	871
Thermal Conductivity	w/m-k	constant	202.4

Cell Zone Conditions

Zones

name	id	type
model-fluid	4	fluid

Setup Conditions

model-fluid

Condition	Value
Material Name	air
Specify source terms?	no
Source Terms	()
Specify fixed values?	no
Local Coordinate System for Fixed Velocities	no
Fixed Values	()
Motion Type	0
X-Velocity Of Zone (m/s)	0
Y-Velocity Of Zone (m/s)	0
Z-Velocity Of Zone (m/s)	0
Rotation speed (rad/s)	0
X-Origin of Rotation-Axis (m)	0
Y-Origin of Rotation-Axis (m)	0
Z-Origin of Rotation-Axis (m)	0
X-Component of Rotation-Axis	0
Y-Component of Rotation-Axis	0
Z-Component of Rotation-Axis	1
Deactivated Thread	no
Laminar zone?	no
Set Turbulent Viscosity to zero within laminar zone?	yes
Porous zone?	no
Conical porous zone?	no
X-Component of Direction-1 Vector	1
Y-Component of Direction-1 Vector	0
Z-Component of Direction-1 Vector	0
X-Component of Direction-2 Vector	0
Y-Component of Direction-2 Vector	1
Z-Component of Direction-2 Vector	0
X-Component of Cone Axis Vector	1
Y-Component of Cone Axis Vector	0
Z-Component of Cone Axis Vector	0
X-Coordinate of Point on Cone Axis (m)	1
Y-Coordinate of Point on Cone Axis (m)	0
Z-Coordinate of Point on Cone Axis (m)	0
Half Angle of Cone Relative to its Axis (deg)	0
Direction-1 Viscous Resistance (1/m2)	0
Direction-2 Viscous Resistance (1/m2)	0
Direction-3 Viscous Resistance (1/m2)	0
Direction-1 Inertial Resistance (1/m)	0

APPENDIX H. FLUENT CFD CODE SETTINGS

```

Direction-2 Inertial Resistance (1/m)      0
Direction-3 Inertial Resistance (1/m)      0
C0 Coefficient for Power-Law              0
C1 Coefficient for Power-Law              0
Porosity                                  1
Solid Material Name                       aluminum
    
```

Boundary Conditions

Zones

```

name          id  type
-----
turbine       3   porous-jump
ground        7   wall
inlet         8   velocity-inlet
leftbuilding  9   wall
leftbuildingtop 10  wall
outlet        11  pressure-outlet
rightbuilding 12  wall
rightbuildingtop 13  wall
symmetry      14  symmetry
    
```

Setup Conditions

turbine

```

Condition                                     Value
-----
Face Permeability (m2)                       1e+10
Porous Medium Thickness (m)                   1
Pressure-Jump Coefficient (C2) (1/m)         0.4
    
```

ground

```

Condition                                     Value
-----
Wall Thickness (m)                            0
Heat Generation Rate (w/m3)                   0
Material Name                                 aluminum
Thermal BC Type                               1
Temperature (k)                               300
Heat Flux (w/m2)                              0
Convective Heat Transfer Coefficient (w/m2-k) 0
Free Stream Temperature (k)                   300
Wall Motion                                   0
Shear Boundary Condition                      0
Define wall motion relative to adjacent cell zone? yes
Apply a rotational velocity to this wall?     no
Velocity Magnitude (m/s)                      0
X-Component of Wall Translation                1
Y-Component of Wall Translation                0
Z-Component of Wall Translation                0
Define wall velocity components?              no
X-Component of Wall Translation (m/s)         0
Y-Component of Wall Translation (m/s)         0
Z-Component of Wall Translation (m/s)         0
External Emissivity                           1
External Radiation Temperature (k)            300
Wall Roughness Height (m)                     0.03
Wall Roughness Constant                       0.5
    
```

APPENDIX H. FLUENT CFD CODE SETTINGS

```

Rotation Speed (rad/s) 0
X-Position of Rotation-Axis Origin (m) 0
Y-Position of Rotation-Axis Origin (m) 0
Z-Position of Rotation-Axis Origin (m) 0
X-Component of Rotation-Axis Direction 0
Y-Component of Rotation-Axis Direction 0
Z-Component of Rotation-Axis Direction 1
X-component of shear stress (pascal) 0
Y-component of shear stress (pascal) 0
Z-component of shear stress (pascal) 0
Surface tension gradient (n/m-k) 0
Specularity Coefficient 0

```

inlet

Condition	Value
Velocity Specification Method	2
Reference Frame	0
Velocity Magnitude	(profile udf inlet_u_velocity::libudf)
Coordinate System	0
X-Velocity (m/s)	0
Y-Velocity (m/s)	0
Z-Velocity (m/s)	0
X-Component of Flow Direction	1
Y-Component of Flow Direction	0
Z-Component of Flow Direction	0
X-Component of Axis Direction	1
Y-Component of Axis Direction	0
Z-Component of Axis Direction	0
X-Coordinate of Axis Origin (m)	0
Y-Coordinate of Axis Origin (m)	0
Z-Coordinate of Axis Origin (m)	0
Angular velocity (rad/s)	0
Temperature (k)	300
Turbulent Specification Method	1
Turbulent Kinetic Energy (m2/s2)	1
Specific Dissipation Rate (1/s)	1
Turbulent Intensity (%)	10
Turbulent Length Scale (m)	1
Hydraulic Diameter (m)	1
Turbulent Viscosity Ratio	1
Outflow Gauge Pressure (pascal)	0
is zone used in mixing-plane model?	no

leftbuilding

Condition	Value
Wall Thickness (m)	0
Heat Generation Rate (w/m3)	0
Material Name	aluminum
Thermal BC Type	1
Temperature (k)	300
Heat Flux (w/m2)	0
Convective Heat Transfer Coefficient (w/m2-k)	0
Free Stream Temperature (k)	300
Wall Motion	0
Shear Boundary Condition	0
Define wall motion relative to adjacent cell zone?	yes
Apply a rotational velocity to this wall?	no
Velocity Magnitude (m/s)	0

APPENDIX H. FLUENT CFD CODE SETTINGS

```

X-Component of Wall Translation      1
Y-Component of Wall Translation      0
Z-Component of Wall Translation      0
Define wall velocity components?     no
X-Component of Wall Translation (m/s) 0
Y-Component of Wall Translation (m/s) 0
Z-Component of Wall Translation (m/s) 0
External Emissivity                  1
External Radiation Temperature (k)   300
Wall Roughness Height (m)           0
Wall Roughness Constant              0.5
Rotation Speed (rad/s)              0
X-Position of Rotation-Axis Origin (m) 0
Y-Position of Rotation-Axis Origin (m) 0
Z-Position of Rotation-Axis Origin (m) 0
X-Component of Rotation-Axis Direction 0
Y-Component of Rotation-Axis Direction 0
Z-Component of Rotation-Axis Direction 1
X-component of shear stress (pascal)  0
Y-component of shear stress (pascal)  0
Z-component of shear stress (pascal)  0
Surface tension gradient (n/m-k)     0
Specularity Coefficient              0

```

leftbuildingtop

Condition	Value
Wall Thickness (m)	0
Heat Generation Rate (w/m3)	0
Material Name	aluminum
Thermal BC Type	1
Temperature (k)	300
Heat Flux (w/m2)	0
Convective Heat Transfer Coefficient (w/m2-k)	0
Free Stream Temperature (k)	300
Wall Motion	0
Shear Boundary Condition	0
Define wall motion relative to adjacent cell zone?	yes
Apply a rotational velocity to this wall?	no
Velocity Magnitude (m/s)	0
X-Component of Wall Translation	1
Y-Component of Wall Translation	0
Z-Component of Wall Translation	0
Define wall velocity components?	no
X-Component of Wall Translation (m/s)	0
Y-Component of Wall Translation (m/s)	0
Z-Component of Wall Translation (m/s)	0
External Emissivity	1
External Radiation Temperature (k)	300
Wall Roughness Height (m)	0
Wall Roughness Constant	0.5
Rotation Speed (rad/s)	0
X-Position of Rotation-Axis Origin (m)	0
Y-Position of Rotation-Axis Origin (m)	0
Z-Position of Rotation-Axis Origin (m)	0
X-Component of Rotation-Axis Direction	0
Y-Component of Rotation-Axis Direction	0
Z-Component of Rotation-Axis Direction	1
X-component of shear stress (pascal)	0
Y-component of shear stress (pascal)	0
Z-component of shear stress (pascal)	0

APPENDIX H. FLUENT CFD CODE SETTINGS

Surface tension gradient (n/m-k) 0
 Specularity Coefficient 0

outlet

Condition	Value
Gauge Pressure (pascal)	0
Backflow Total Temperature (k)	300
Backflow Direction Specification Method	2
Coordinate System	0
X-Component of Flow Direction	1
Y-Component of Flow Direction	0
Z-Component of Flow Direction	0
X-Component of Axis Direction	1
Y-Component of Axis Direction	0
Z-Component of Axis Direction	0
X-Coordinate of Axis Origin (m)	0
Y-Coordinate of Axis Origin (m)	0
Z-Coordinate of Axis Origin (m)	0
Turbulent Specification Method	0
Backflow Turbulent Kinetic Energy (m2/s2)	0.7
Backflow Specific Dissipation Rate (1/s)	1
Backflow Turbulent Intensity (%)	10
Backflow Turbulent Length Scale (m)	1
Backflow Hydraulic Diameter (m)	1
Backflow Turbulent Viscosity Ratio	10
is zone used in mixing-plane model?	no
Radial Equilibrium Pressure Distribution	no
Specify targeted mass flow rate	no
Targeted mass flow (kg/s)	1
Upper Limit of Absolute Pressure Value (pascal)	5000000
Lower Limit of Absolute Pressure Value (pascal)	1

rightbuilding

Condition	Value
Wall Thickness (m)	0
Heat Generation Rate (w/m3)	0
Material Name	aluminum
Thermal BC Type	1
Temperature (k)	300
Heat Flux (w/m2)	0
Convective Heat Transfer Coefficient (w/m2-k)	0
Free Stream Temperature (k)	300
Wall Motion	0
Shear Boundary Condition	0
Define wall motion relative to adjacent cell zone?	yes
Apply a rotational velocity to this wall?	no
Velocity Magnitude (m/s)	0
X-Component of Wall Translation	1
Y-Component of Wall Translation	0
Z-Component of Wall Translation	0
Define wall velocity components?	no
X-Component of Wall Translation (m/s)	0
Y-Component of Wall Translation (m/s)	0
Z-Component of Wall Translation (m/s)	0
External Emissivity	1
External Radiation Temperature (k)	300
Wall Roughness Height (m)	0
Wall Roughness Constant	0.5

APPENDIX H. FLUENT CFD CODE SETTINGS

```

Rotation Speed (rad/s)                0
X-Position of Rotation-Axis Origin (m) 0
Y-Position of Rotation-Axis Origin (m) 0
Z-Position of Rotation-Axis Origin (m) 0
X-Component of Rotation-Axis Direction 0
Y-Component of Rotation-Axis Direction 0
Z-Component of Rotation-Axis Direction 1
X-component of shear stress (pascal)    0
Y-component of shear stress (pascal)    0
Z-component of shear stress (pascal)    0
Surface tension gradient (n/m-k)        0
Specularity Coefficient                 0

```

rightbuildingtop

Condition	Value
Wall Thickness (m)	0
Heat Generation Rate (w/m3)	0
Material Name	aluminum
Thermal BC Type	1
Temperature (k)	300
Heat Flux (w/m2)	0
Convective Heat Transfer Coefficient (w/m2-k)	0
Free Stream Temperature (k)	300
Wall Motion	0
Shear Boundary Condition	0
Define wall motion relative to adjacent cell zone?	yes
Apply a rotational velocity to this wall?	no
Velocity Magnitude (m/s)	0
X-Component of Wall Translation	1
Y-Component of Wall Translation	0
Z-Component of Wall Translation	0
Define wall velocity components?	no
X-Component of Wall Translation (m/s)	0
Y-Component of Wall Translation (m/s)	0
Z-Component of Wall Translation (m/s)	0
External Emissivity	1
External Radiation Temperature (k)	300
Wall Roughness Height (m)	0
Wall Roughness Constant	0.5
Rotation Speed (rad/s)	0
X-Position of Rotation-Axis Origin (m)	0
Y-Position of Rotation-Axis Origin (m)	0
Z-Position of Rotation-Axis Origin (m)	0
X-Component of Rotation-Axis Direction	0
Y-Component of Rotation-Axis Direction	0
Z-Component of Rotation-Axis Direction	1
X-component of shear stress (pascal)	0
Y-component of shear stress (pascal)	0
Z-component of shear stress (pascal)	0
Surface tension gradient (n/m-k)	0
Specularity Coefficient	0

symmetry

Condition	Value

Solver Settings

Equations

Equation	Solved
Flow	yes
Turbulence	yes

Numerics

Numeric	Enabled
Absolute Velocity Formulation	yes

Unsteady Calculation Parameters

Time Step (s)	1
Max. Iterations Per Time Step	20

Relaxation

Variable	Relaxation Factor
Turbulent Kinetic Energy	0.8
Specific Dissipation Rate	0.8
Turbulent Viscosity	1
Solid	1

Linear Solver

Variable	Solver Type	Termination Criterion	Residual Reduction Tolerance
Flow	F-Cycle	0.1	
Turbulent Kinetic Energy	Flexible	0.1	0.7
Specific Dissipation Rate	Flexible	0.1	0.7

Discretization Scheme

Variable	Scheme
Flow	Second Order Upwind
Turbulent Kinetic Energy	Second Order Upwind
Specific Dissipation Rate	Second Order Upwind

Time Marching

Parameter	Value
Solver	Implicit
Physical Time Step	1
Courant Number	5

Solution Limits

Quantity	Limit
Minimum Absolute Pressure	1
Maximum Absolute Pressure	5e+10
Minimum Temperature	1
Maximum Temperature	5000

APPENDIX H. FLUENT CFD CODE SETTINGS

Minimum Turb. Kinetic Energy	1e-14
Minimum Spec. Dissipation Rate	1e-20
Maximum Turb. Viscosity Ratio	100000

Appendix I

Sample Output File

A sample output file of FLUENT's processing for a case along with calculations of the iterations for the first and last time steps.

Cluster: Gup

Welcome to ANSYS FLUENT 12.1.4

Copyright 2009 ANSYS Inc.

All Rights Reserved. Unauthorized use, distribution or duplication is prohibited. ANSYS and FLUENT are trademarks or registered trademarks of ANSYS, Inc. or its subsidiaries in the United States or other countries.

Loading "/opt/sharcnet/ansys/12.1.1/v121/fluent/fluent12.1.4/lib/flprim.dmp.1119-64"
Done.

```
-----  
This is a version of FLUENT intended for use by students,  
academic staff, and faculty. Usage of studentFLUENT is  
limited to the terms and conditions specified in the  
Clickwrap Software License Agreement for studentFLUENT.  
-----
```

Host spawning Node 0 on machine "gup7" (unix).

```
/opt/sharcnet/ansys/12.1.1/v121/fluent/fluent12.1.4/bin/fluent -r12.1.4 3ddp -node -alnamd64 -t8  
-pinfiniband -mpi=openmpi -cnf=/var/spool/torque/aux//78547.gup-hn.guppy.sharcnet -ssh -mport  
10.36.14.7:10.36.14.7:52642:0
```

```
Starting fixfiledes /opt/sharcnet/ansys/12.1.1/v121/fluent/fluent12.1.4/multiport/mpi/lnamd64/openmpi/bin/  
mpirun --app /tmp/fluent-appfile.5984
```

```
-----  
ID      Comm.  Hostname  O.S.      PID      Mach ID HW ID  Name  
-----  
n7      openmpi gup6      Linux-64  2111     1       7      Fluent Node  
n6      openmpi gup6      Linux-64  2110     1       6      Fluent Node  
n5      openmpi gup6      Linux-64  2109     1       5      Fluent Node  
n4      openmpi gup6      Linux-64  2108     1       4      Fluent Node  
host    net     gup7      Linux-64  5851     0       19     Fluent Host  
n3      openmpi gup7      Linux-64  6188     0       3      Fluent Node  
n2      openmpi gup7      Linux-64  6187     0       2      Fluent Node  
n1      openmpi gup7      Linux-64  6186     0       1      Fluent Node  
n0*     openmpi gup7      Linux-64  6185     0       0      Fluent Node  
-----
```

```

Selected system interconnect: InfiniBand
-----

> /file/set-batch-options no yes no

> /file/read-case /scratch/amacquar/guppy/MeshFiles/FFF.Rt_1_Rx_0_Ry_0_AOA_0.msh

Multicore processors detected. Processor affinity set!

Reading "/scratch/amacquar/guppy/MeshFiles/FFF.Rt_1_Rx_0_Ry_0_AOA_0.msh"...
.....

419064 nodes, binary.
27651 nodes, binary.
3540180 mixed interior faces, zone 1, binary.
  323 mixed interior faces, zone 2, binary.
  387 mixed interior faces, zone 3, binary.
13358 mixed wall faces, zone 7, binary.
 1766 triangular velocity-inlet faces, zone 8, binary.
11721 triangular wall faces, zone 9, binary.
 1064 triangular wall faces, zone 10, binary.
 2324 triangular pressure-outlet faces, zone 11, binary.
11709 triangular wall faces, zone 12, binary.
 1022 triangular wall faces, zone 13, binary.
  9218 mixed symmetry faces, zone 14, binary.
1667771 mixed cells, zone 4, binary.

Building...
  mesh
    auto partitioning mesh by Metis (fast),
    distributing mesh
      parts.....,
      faces.....,
      nodes.....,
      cells.....,
  materials,
Loading material properties database...
  interface,
  domains,
  zones,
    symmetry
    rightbuildingtop
    rightbuilding
    outlet
    leftbuildingtop
    leftbuilding
    inlet
    ground
    model-fluid
    turbineout
    turbine
    interior-model-fluid
  parallel,
Done.

> /define/user-defined/compiled-functions compile
/scratch/amacquar/guppy/Rt_1_Rx_0_Ry_0_AOA_0/libudf yes
Give C-Source file names:
/scratch/amacquar/guppy/Rt_1_Rx_0_Ry_0_AOA_0/libudf/abl_udf.c ""
Give header file names:
/scratch/amacquar/guppy/Rt_1_Rx_0_Ry_0_AOA_0/libudf/abl_udf.c ""

```

APPENDIX I. SAMPLE OUTPUT FILE

Done.

```
> /define/user-defined/compiled-functions load /scratch/amacquar/guppy/Rt_3_Rx_0_Ry_0_AOA_0/libudf
```

```
Opening library "/scratch/amacquar/guppy/Rt_1_Rx_0_Ry_0_AOA_0/libudf"...
Library "/scratch/amacquar/guppy/Rt_1_Rx_0_Ry_0_AOA_0/libudf/lnamd64/3ddp_host/libudf.so" opened
inlet_u_velocity
```

Done.

```
Opening library "/scratch/amacquar/guppy/Rt_1_Rx_0_Ry_0_AOA_0/libudf"...
Library "/scratch/amacquar/guppy/Rt_1_Rx_0_Ry_0_AOA_0/libudf/lnamd64/3ddp_node/libudf.so" opened
```

```
> /define/custom-field-functions/define "abl"Enter Custom Field Function:
4.16*1.31*log10((z_coordinate+0.03)/0.03)/log10(60/0.03)
```

```
> /define/custom-field-functions/define "power_aug"Enter Custom Field Function: 1/2*density*(x_velocity)^3
```

```
> /define/custom-field-functions/define "power_abl"Enter Custom Field Function: 1/2*density*(abl)^3
```

```
> /define/custom-field-functions/define "initial_u_velocity"Enter Custom Field Function: abl*cos(0*PI/180)
```

```
> /define/custom-field-functions/define "initial_v_velocity"Enter Custom Field Function: abl*sin(0*PI/180)
```

```
> /define/models/solver/density-based-implicit yes
```

```
> /define/models/energy yes
```

```
> /define/models/viscous kw-sst yes
```

```
> /define/boundary-conditions/velocity-inlet (inlet)
inlet no no yes yes yes yes profile names list: ("udf")
"udf" data names list: ("inlet_u_velocity::libudf")
"inlet_u_velocity::libudf" no 300 no yes 10 1 no 0
```

```
> /define/boundary-conditions/pressure-outlet (outlet)
outlet no 0 no 300 no no yes yes no 0.7 no 1 no no
```

```
> /define/boundary-conditions/wall (ground leftbuilding leftbuildingtop rightbuilding rightbuildingtop)
ground 0 no 0 no no no 0 no no no 0.03 no 0.5
```

```
> /define/boundary-conditions/wall (ground leftbuilding leftbuildingtop rightbuilding rightbuildingtop)
leftbuilding 0 no 0 no no no 0 no no no 0 no 0.5
```

```
> /define/boundary-conditions/copy-bc leftbuilding rightbuilding leftbuildingtop rightbuildingtop ()Copy
leftbuilding boundary conditions to rightbuildingtop
Copy leftbuilding boundary conditions to leftbuildingtop
Copy leftbuilding boundary conditions to rightbuilding
```

```
> /solve/set/discretization-scheme/amg-c 1
> /solve/set/discretization-scheme/k 1
> /solve/set/discretization-scheme/omega 1
> /solve/set/under-relaxation/k 0.8
> /solve/set/under-relaxation/omega 0.8
> /solve/set/under-relaxation/turb-viscosity 1
> /solve/monitors/residual/criterion-type 1
The requested convergence criterion type is not available
> /solve/monitors/residual monitor yes yes yes yes yes yes yes
> /solve/set/flow-warnings no
> /solve/initialize/set-defaults k 0.7
> /solve/initialize/set-defaults omega 1
> /solve/initialize/set-defaults temperature 300
> /solve/initialize/initialize-flow
> /solve/patch Model-fluid () x-velocity no yes initial_u_velocity
> /solve/patch Model-fluid () y-velocity no yes initial_v_velocity
> /solve/initialize/set-fmg-initialization

Customize your FMG initialization:
5
  set FMG parameters on levels ..

  residual reduction on level 10.001    number of cycles on level 110
  residual reduction on level 20.001    number of cycles on level 250
  residual reduction on level 30.001    number of cycles on level 3500
  residual reduction on level 40.001    number of cycles on level 4500
  residual reduction on level 5 [coarsest grid]0.001    number of cycles on level 5100

Number of FMG (and FAS geometric multigrid) levels: 5
* FMG customization summary:
* residual reduction on level 0 [finest grid] is: 0.001
* number of cycles on level 0 is: 1
* residual reduction on level 1 is: 0.001
* number of cycles on level 1 is: 10
* residual reduction on level 2 is: 0.001
* number of cycles on level 2 is: 50
* residual reduction on level 3 is: 0.001
* number of cycles on level 3 is: 500
* residual reduction on level 4 is: 0.001
* number of cycles on level 4 is: 500
* residual reduction on level 5 [coarsest grid] is: 0.001
* number of cycles on level 5 is: 100
* FMG customization complete
0.75 yes

> /solve/initialize/fmg-initialization yes
```

APPENDIX I. SAMPLE OUTPUT FILE

>> Reordering domain using Reverse Cuthill-McKee method:

zones, cells, faces, done.

Bandwidth reduction = 212011/3632 = 58.37

Done.

Creating multigrid levels...

```
Grid Level 0: 1667771 cells, 3593072 faces,      0 nodes;   8 clusters
Grid Level 1: 68420 cells, 1208751 faces, 446715 nodes;   8 clusters
Grid Level 1: 68420 cells, 394031 faces, 446715 nodes
Grid Level 2: 13343 cells, 843777 faces, 446715 nodes;   8 clusters
Grid Level 2: 13343 cells, 94638 faces, 446715 nodes
Grid Level 3: 3222 cells, 642109 faces, 446715 nodes;   8 clusters
Grid Level 3: 3222 cells, 25488 faces, 446711 nodes
Grid Level 4: 843 cells, 496894 faces, 446715 nodes;   8 clusters
Grid Level 4: 843 cells, 7123 faces, 446707 nodes
Grid Level 5: 225 cells, 380680 faces, 446715 nodes;   8 clusters
Grid Level 5: 225 cells, 1950 faces, 446664 nodes
```

Done.

FMG: Converge FAS on level 5 [eps = 0.001000, max-iter=100]

```
..... -> Normalized residual = 0.0855078
..... -> Normalized residual = 0.0246967
..... -> Normalized residual = 0.00570638
..... -> Normalized residual = 0.00443262
..... -> Normalized residual = 0.00648771
..... -> Normalized residual = 0.00698003
..... -> Normalized residual = 0.00627502
..... -> Normalized residual = 0.00488412
..... -> Normalized residual = 0.00328286
..... -> Normalized residual = 0.00183126
```

FMG: FAS reached maximum iterations.

Normalized residual = 0.00183126

FMG: Finished work on level = 5

FMG: Interpolate solution on next level . . . end

FMG: Converge FAS on level 4 [eps = 0.001000, max-iter=500]

```
..... -> Normalized residual = 0.031736
..... -> Normalized residual = 0.00571157
..... -> Normalized residual = 0.00403975
..... -> Normalized residual = 0.00188588
.....
```

FMG: FAS converged.

FMG: Finished work on level = 4

FMG: Interpolate solution on next level . . . end

FMG: Converge FAS on level 3 [eps = 0.001000, max-iter=500]

```
..... -> Normalized residual = 0.054006
..... -> Normalized residual = 0.0101748
..... -> Normalized residual = 0.00622941
..... -> Normalized residual = 0.00342219
..... -> Normalized residual = 0.0020179
..... -> Normalized residual = 0.00138015
....
```

FMG: FAS converged.

FMG: Finished work on level = 3

FMG: Interpolate solution on next level . . . end

FMG: Converge FAS on level 2 [eps = 0.001000, max-iter=50]

..... -> Normalized residual = 0.115932
 -> Normalized residual = 0.024402
 -> Normalized residual = 0.0138924
 -> Normalized residual = 0.0149562
 -> Normalized residual = 0.00540462

FMG: FAS reached maximum iterations.
 Normalized residual = 0.00540462

FMG: Finished work on level = 2

FMG: Interpolate solution on next level . . . end

FMG: Converge FAS on level 1 [eps = 0.001000, max-iter=10]

..... -> Normalized residual = 1.31067

FMG: FAS reached maximum iterations.
 Normalized residual = 1.31067

FMG: Finished work on level = 1

FMG: Interpolate solution on next level . . . end

0.->1.->2.->3.->4.->5.<<<<<

> /solve/iterate 50

iter	continuity	x-velocity	y-velocity	z-velocity	energy	k	omega	time/iter
1	1.0000e+00	1.0000e+00	1.0000e+00	1.0000e+00	1.0000e+00	3.0235e-03	6.8717e-02	0:02:47 49
2	6.7912e-01	4.2026e-01	4.1741e-01	1.0000e+00	7.3245e-01	3.0472e-03	5.5440e-02	0:02:41 48
3	2.9705e-01	2.8333e-01	2.8343e-01	1.0000e+00	3.0660e-01	3.0738e-03	4.9367e-02	0:02:36 47
4	1.3025e-01	2.0877e-01	2.0897e-01	1.0000e+00	1.3797e-01	3.0826e-03	4.4259e-02	0:02:31 46
5	1.1859e-01	1.1128e-01	1.1178e-01	7.3986e-01	1.2322e-01	3.0834e-03	3.9836e-02	0:02:27 45
6	1.1182e-01	4.4597e-02	4.3268e-02	4.2092e-01	1.2563e-01	3.0805e-03	3.6217e-02	0:02:23 44
7	9.9991e-02	1.9496e-02	1.4249e-02	2.8511e-01	1.1058e-01	3.0783e-03	3.3571e-02	0:02:19 43
8	8.5705e-02	1.5012e-02	9.4597e-03	2.4849e-01	9.4347e-02	3.0778e-03	3.1693e-02	0:02:15 42
9	7.3269e-02	1.3348e-02	8.8468e-03	2.4551e-01	7.9407e-02	3.0791e-03	2.9607e-02	0:02:11 41
10	6.4289e-02	1.0405e-02	6.6346e-03	2.3049e-01	6.8137e-02	3.0810e-03	2.7960e-02	0:02:08 40
11	5.2366e-02	7.9446e-03	5.1138e-03	1.8296e-01	5.4377e-02	3.0823e-03	2.7064e-02	0:02:04 39
12	4.3439e-02	6.7013e-03	3.9818e-03	1.5310e-01	4.4493e-02	3.0831e-03	2.6562e-02	0:02:01 38
13	3.6549e-02	6.1999e-03	3.2576e-03	1.4222e-01	3.6894e-02	3.0833e-03	2.5153e-02	0:01:57 37
14	3.0111e-02	5.8833e-03	2.8713e-03	1.3508e-01	2.9578e-02	3.0833e-03	2.3627e-02	0:01:54 36
15	2.3907e-02	5.4675e-03	2.6960e-03	1.2443e-01	2.2164e-02	3.0831e-03	2.2235e-02	0:01:51 35
16	1.8975e-02	4.9116e-03	2.5796e-03	1.0935e-01	1.6022e-02	3.0844e-03	2.1515e-02	0:01:48 34
17	1.7249e-02	4.2337e-03	2.4264e-03	9.2835e-02	1.4402e-02	3.0881e-03	2.0987e-02	0:01:44 33
18	1.8976e-02	3.5788e-03	2.1787e-03	7.8994e-02	1.7637e-02	3.0938e-03	2.0475e-02	0:01:41 32
19	2.1914e-02	3.0765e-03	1.8024e-03	7.0451e-02	2.1797e-02	3.1027e-03	1.9977e-02	0:01:38 31
20	2.4315e-02	2.7396e-03	1.4048e-03	6.5945e-02	2.4632e-02	3.1158e-03	1.9386e-02	0:01:35 30
21	2.5889e-02	2.5306e-03	1.1076e-03	6.2770e-02	2.5899e-02	3.1348e-03	1.8571e-02	0:01:32 29
22	2.7448e-02	2.2556e-03	9.2190e-04	5.8480e-02	2.6575e-02	3.1617e-03	1.7784e-02	0:01:28 28
23	2.8287e-02	1.8348e-03	8.0674e-04	5.1310e-02	2.6128e-02	3.1915e-03	1.7175e-02	0:01:25 27
24	2.6370e-02	1.4351e-03	5.7988e-04	4.1284e-02	2.3435e-02	3.2276e-03	1.6525e-02	0:01:22 26
25	2.2826e-02	1.0334e-03	3.2453e-04	2.8205e-02	1.9707e-02	3.2643e-03	1.6024e-02	0:01:19 25
26	1.9555e-02	8.1748e-04	2.9358e-04	1.7540e-02	1.6557e-02	3.3006e-03	1.5625e-02	0:01:16 24

APPENDIX I. SAMPLE OUTPUT FILE

```

27 1.7178e-02 7.8342e-04 3.6729e-04 1.4107e-02 1.4356e-02 3.3283e-03 1.5215e-02 0:01:13 23
28 1.5753e-02 7.5118e-04 3.8920e-04 1.4843e-02 1.3059e-02 3.3384e-03 1.4839e-02 0:01:09 22
29 1.5072e-02 6.7562e-04 3.6519e-04 1.5238e-02 1.2454e-02 3.3460e-03 1.4516e-02 0:01:06 21
30 1.4902e-02 5.7821e-04 3.1427e-04 1.5030e-02 1.2320e-02 3.3482e-03 1.4210e-02 0:01:03 20
31 1.5012e-02 5.0188e-04 2.6311e-04 1.4250e-02 1.2440e-02 3.3373e-03 1.3949e-02 0:01:00 19
32 1.5238e-02 4.6158e-04 2.2707e-04 1.3269e-02 1.2664e-02 3.3258e-03 1.3749e-02 0:00:57 18
33 1.5362e-02 4.4433e-04 1.9920e-04 1.2389e-02 1.2808e-02 3.3106e-03 1.3621e-02 0:00:54 17
iter continuity x-velocity y-velocity z-velocity energy k omega time/iter
34 1.5431e-02 4.4539e-04 1.7822e-04 1.1756e-02 1.2905e-02 3.2879e-03 1.3522e-02 0:00:50 16
35 1.5488e-02 4.4915e-04 1.6048e-04 1.1359e-02 1.2987e-02 3.2706e-03 1.3382e-02 0:00:47 15
36 1.5542e-02 4.5035e-04 1.4599e-04 1.1055e-02 1.3059e-02 3.2440e-03 1.3215e-02 0:00:44 14
37 1.5506e-02 4.3891e-04 1.3626e-04 1.0633e-02 1.3045e-02 3.2227e-03 1.3019e-02 0:00:41 13
38 1.5388e-02 4.1922e-04 1.2910e-04 9.9980e-03 1.2952e-02 3.1977e-03 1.2814e-02 0:00:38 12
39 1.5200e-02 3.9423e-04 1.2336e-04 9.2670e-03 1.2792e-02 3.1775e-03 1.2575e-02 0:00:35 11
40 1.4967e-02 3.6702e-04 1.1871e-04 8.5283e-03 1.2593e-02 3.1588e-03 1.2330e-02 0:00:31 10
41 1.4703e-02 3.4151e-04 1.1446e-04 7.9066e-03 1.2370e-02 3.1375e-03 1.2074e-02 0:00:28 9
42 1.4439e-02 3.2263e-04 1.1050e-04 7.4215e-03 1.2149e-02 3.1180e-03 1.1818e-02 0:00:25 8
43 1.4107e-02 3.0833e-04 1.0713e-04 7.0246e-03 1.1868e-02 3.0967e-03 1.1575e-02 0:00:22 7
44 1.3705e-02 2.9682e-04 1.0447e-04 6.6753e-03 1.1518e-02 3.0780e-03 1.1357e-02 0:00:19 6
iter continuity x-velocity y-velocity z-velocity energy k omega time/iter
45 1.3225e-02 2.8510e-04 1.0226e-04 6.3112e-03 1.1084e-02 3.0603e-03 1.1160e-02 0:00:16 5
46 1.2672e-02 2.7126e-04 1.0017e-04 5.9207e-03 1.0564e-02 3.0447e-03 1.0978e-02 0:00:13 4
47 1.2105e-02 2.5521e-04 9.7985e-05 5.4943e-03 1.0023e-02 3.0292e-03 1.0805e-02 0:00:09 3
48 1.1590e-02 2.3748e-04 9.5424e-05 5.0659e-03 9.5343e-03 3.0158e-03 1.0634e-02 0:00:06 2
49 1.1181e-02 2.2073e-04 9.2462e-05 4.6594e-03 9.1585e-03 3.0039e-03 1.0461e-02 0:00:03 1
50 1.0903e-02 2.0646e-04 8.9502e-05 4.3164e-03 8.9199e-03 2.9926e-03 1.0288e-02 0:00:00 0

> /define/boundary-conditions/modify-zones zone-type turbine porous-jump

> /define/boundary-conditions/porous-jump (turbine)
turbine 1e+10 0.075 0.4

> /solve/iterate 100
iter continuity x-velocity y-velocity z-velocity energy k omega time/iter
50 1.0903e-02 2.0646e-04 8.9502e-05 4.3164e-03 8.9199e-03 2.9926e-03 1.0288e-02 0:05:15 100
51 1.0738e-02 1.9542e-04 8.6704e-05 4.0412e-03 8.7955e-03 2.9818e-03 1.0111e-02 0:05:17 99
52 1.0656e-02 1.8713e-04 8.4109e-05 3.8172e-03 8.7451e-03 2.9721e-03 9.9349e-03 0:05:12 98
53 1.0640e-02 1.8063e-04 8.1919e-05 3.6313e-03 8.7449e-03 2.9630e-03 9.7594e-03 0:05:08 97
54 1.0666e-02 1.7521e-04 8.0030e-05 3.4730e-03 8.7700e-03 2.9548e-03 9.5960e-03 0:05:05 96
55 1.0717e-02 1.7014e-04 7.8341e-05 3.3275e-03 8.8087e-03 2.9476e-03 9.4481e-03 0:05:01 95
56 1.0764e-02 1.6527e-04 7.6763e-05 3.1884e-03 8.8388e-03 2.9407e-03 9.3103e-03 0:04:57 94
57 1.0764e-02 1.6025e-04 7.5114e-05 3.0602e-03 8.8281e-03 2.9347e-03 9.1810e-03 0:04:54 93
58 1.0735e-02 1.5518e-04 7.3667e-05 2.9467e-03 8.7964e-03 2.9294e-03 9.0559e-03 0:04:51 92
59 1.0688e-02 1.5051e-04 7.2405e-05 2.8490e-03 8.7518e-03 2.9241e-03 8.9356e-03 0:04:47 91
60 1.0618e-02 1.4613e-04 7.1307e-05 2.7713e-03 8.6899e-03 2.9189e-03 8.8206e-03 0:04:44 90
iter continuity x-velocity y-velocity z-velocity energy k omega time/iter
61 1.0530e-02 1.4242e-04 7.0266e-05 2.7129e-03 8.6157e-03 2.9140e-03 8.7085e-03 0:04:41 89
62 1.0421e-02 1.3932e-04 6.9128e-05 2.6680e-03 8.5239e-03 2.9091e-03 8.6002e-03 0:04:37 88
63 1.0306e-02 1.3675e-04 6.7901e-05 2.6346e-03 8.4293e-03 2.9044e-03 8.4961e-03 0:04:34 87
64 1.0195e-02 1.3483e-04 6.6541e-05 2.6114e-03 8.3375e-03 2.9000e-03 8.3949e-03 0:04:31 86
65 1.0104e-02 1.3338e-04 6.5063e-05 2.5927e-03 8.2632e-03 2.8960e-03 8.2999e-03 0:04:28 85
66 1.0035e-02 1.3234e-04 6.3518e-05 2.5756e-03 8.2070e-03 2.8923e-03 8.2087e-03 0:04:25 84
67 9.9826e-03 1.3150e-04 6.1927e-05 2.5572e-03 8.1641e-03 2.8890e-03 8.1197e-03 0:04:22 83
68 9.9417e-03 1.3070e-04 6.0305e-05 2.5328e-03 8.1308e-03 2.8861e-03 8.0307e-03 0:04:18 82
69 9.9115e-03 1.2988e-04 5.8727e-05 2.5000e-03 8.1062e-03 2.8836e-03 7.9414e-03 0:04:15 81
70 9.8880e-03 1.2893e-04 5.7246e-05 2.4581e-03 8.0869e-03 2.8814e-03 7.8521e-03 0:04:12 80
71 9.8653e-03 1.2786e-04 5.5924e-05 2.4058e-03 8.0683e-03 2.8794e-03 7.7619e-03 0:04:09 79
iter continuity x-velocity y-velocity z-velocity energy k omega time/iter
72 9.8396e-03 1.2679e-04 5.4753e-05 2.3451e-03 8.0473e-03 2.8776e-03 7.6701e-03 0:04:06 78
73 9.8085e-03 1.2562e-04 5.3713e-05 2.2770e-03 8.0219e-03 2.8761e-03 7.5769e-03 0:04:03 77
74 9.7737e-03 1.2439e-04 5.2846e-05 2.2056e-03 7.9936e-03 2.8749e-03 7.4827e-03 0:03:59 76
75 9.7373e-03 1.2322e-04 5.2138e-05 2.1326e-03 7.9639e-03 2.8739e-03 7.3875e-03 0:03:56 75

```

APPENDIX I. SAMPLE OUTPUT FILE

76	9.7013e-03	1.2214e-04	5.1560e-05	2.0588e-03	7.9346e-03	2.8731e-03	7.2904e-03	0:03:53	74
77	9.6615e-03	1.2117e-04	5.1076e-05	1.9869e-03	7.9023e-03	2.8726e-03	7.1909e-03	0:03:50	73
78	9.6225e-03	1.2036e-04	5.0672e-05	1.9183e-03	7.8705e-03	2.8724e-03	7.0912e-03	0:03:47	72
79	9.5838e-03	1.1970e-04	5.0270e-05	1.8538e-03	7.8390e-03	2.8724e-03	6.9914e-03	0:03:44	71
80	9.5488e-03	1.1920e-04	4.9894e-05	1.7957e-03	7.8105e-03	2.8727e-03	6.8917e-03	0:03:40	70
81	9.5197e-03	1.1891e-04	4.9508e-05	1.7445e-03	7.7868e-03	2.8733e-03	6.7919e-03	0:03:37	69
82	9.4989e-03	1.1881e-04	4.9114e-05	1.7005e-03	7.7699e-03	2.8740e-03	6.6914e-03	0:03:34	68
iter	continuity	x-velocity	y-velocity	z-velocity	energy	k	omega	time/iter	
83	9.4877e-03	1.1886e-04	4.8712e-05	1.6635e-03	7.7609e-03	2.8749e-03	6.5915e-03	0:03:31	67
84	9.4818e-03	1.1905e-04	4.8284e-05	1.6319e-03	7.7562e-03	2.8759e-03	6.4921e-03	0:03:28	66
85	9.4799e-03	1.1934e-04	4.7836e-05	1.6054e-03	7.7547e-03	2.8771e-03	6.3929e-03	0:03:25	65
86	9.4790e-03	1.1967e-04	4.7357e-05	1.5840e-03	7.7540e-03	2.8784e-03	6.2939e-03	0:03:22	64
87	9.4798e-03	1.1999e-04	4.6837e-05	1.5671e-03	7.7548e-03	2.8798e-03	6.1968e-03	0:03:18	63
88	9.4803e-03	1.2020e-04	4.6295e-05	1.5527e-03	7.7552e-03	2.8813e-03	6.1009e-03	0:03:15	62
89	9.4840e-03	1.2031e-04	4.5722e-05	1.5399e-03	7.7584e-03	2.8828e-03	6.0078e-03	0:03:12	61
90	9.4889e-03	1.2019e-04	4.5148e-05	1.5263e-03	7.7624e-03	2.8844e-03	5.9182e-03	0:03:09	60
91	9.4923e-03	1.1983e-04	4.4564e-05	1.5118e-03	7.7652e-03	2.8861e-03	5.8313e-03	0:03:06	59
92	9.4927e-03	1.1928e-04	4.3955e-05	1.4976e-03	7.7654e-03	2.8879e-03	5.7479e-03	0:03:03	58
93	9.4869e-03	1.1849e-04	4.3362e-05	1.4828e-03	7.7607e-03	2.8896e-03	5.6684e-03	0:03:00	57
iter	continuity	x-velocity	y-velocity	z-velocity	energy	k	omega	time/iter	
94	9.4751e-03	1.1749e-04	4.2789e-05	1.4683e-03	7.7510e-03	2.8915e-03	5.5910e-03	0:02:57	56
95	9.4521e-03	1.1630e-04	4.2240e-05	1.4547e-03	7.7322e-03	2.8934e-03	5.5164e-03	0:02:53	55
96	9.4159e-03	1.1494e-04	4.1696e-05	1.4370e-03	7.7025e-03	2.8953e-03	5.4443e-03	0:02:50	54
97	9.3638e-03	1.1342e-04	4.1149e-05	1.4179e-03	7.6598e-03	2.8973e-03	5.3744e-03	0:02:47	53
98	9.2983e-03	1.1189e-04	4.0597e-05	1.4014e-03	7.6062e-03	2.8993e-03	5.3076e-03	0:02:44	52
99	9.2191e-03	1.1037e-04	4.0030e-05	1.3866e-03	7.5415e-03	2.9013e-03	5.2436e-03	0:02:41	51
100	9.1281e-03	1.0886e-04	3.9478e-05	1.3724e-03	7.4670e-03	2.9034e-03	5.1829e-03	0:02:38	50
101	9.0275e-03	1.0744e-04	3.8928e-05	1.3586e-03	7.3845e-03	2.9056e-03	5.1269e-03	0:02:35	49
102	8.9189e-03	1.0616e-04	3.8350e-05	1.3453e-03	7.2956e-03	2.9078e-03	5.0753e-03	0:02:31	48
103	8.8086e-03	1.0507e-04	3.7757e-05	1.3318e-03	7.2052e-03	2.9101e-03	5.0287e-03	0:02:28	47
104	8.7023e-03	1.0414e-04	3.7158e-05	1.3186e-03	7.1180e-03	2.9125e-03	4.9874e-03	0:02:25	46
iter	continuity	x-velocity	y-velocity	z-velocity	energy	k	omega	time/iter	
105	8.6054e-03	1.0342e-04	3.6553e-05	1.3051e-03	7.0385e-03	2.9150e-03	4.9514e-03	0:02:22	45
106	8.5193e-03	1.0286e-04	3.5939e-05	1.2913e-03	6.9679e-03	2.9175e-03	4.9199e-03	0:02:19	44
107	8.4480e-03	1.0248e-04	3.5325e-05	1.2776e-03	6.9094e-03	2.9201e-03	4.8928e-03	0:02:16	43
108	8.3920e-03	1.0222e-04	3.4731e-05	1.2636e-03	6.8635e-03	2.9227e-03	4.8694e-03	0:02:13	42
109	8.3547e-03	1.0203e-04	3.4155e-05	1.2497e-03	6.8328e-03	2.9254e-03	4.8504e-03	0:02:09	41
110	8.3367e-03	1.0190e-04	3.3603e-05	1.2363e-03	6.8179e-03	2.9281e-03	4.8345e-03	0:02:06	40
111	8.3380e-03	1.0182e-04	3.3078e-05	1.2227e-03	6.8188e-03	2.9309e-03	4.8211e-03	0:02:03	39
112	8.3529e-03	1.0169e-04	3.2600e-05	1.2088e-03	6.8309e-03	2.9336e-03	4.8094e-03	0:02:00	38
113	8.3802e-03	1.0154e-04	3.2170e-05	1.1952e-03	6.8531e-03	2.9364e-03	4.7981e-03	0:01:57	37
114	8.4160e-03	1.0138e-04	3.1769e-05	1.1813e-03	6.8822e-03	2.9392e-03	4.7865e-03	0:01:54	36
115	8.4542e-03	1.0117e-04	3.1384e-05	1.1675e-03	6.9134e-03	2.9420e-03	4.7736e-03	0:01:51	35
iter	continuity	x-velocity	y-velocity	z-velocity	energy	k	omega	time/iter	
116	8.4924e-03	1.0093e-04	3.1031e-05	1.1536e-03	6.9446e-03	2.9447e-03	4.7587e-03	0:01:48	34
117	8.5239e-03	1.0057e-04	3.0713e-05	1.1397e-03	6.9703e-03	2.9473e-03	4.7417e-03	0:01:44	33
118	8.5470e-03	1.0016e-04	3.0407e-05	1.1261e-03	6.9892e-03	2.9498e-03	4.7231e-03	0:01:41	32
119	8.5619e-03	9.9675e-05	3.0104e-05	1.1125e-03	7.0014e-03	2.9521e-03	4.7025e-03	0:01:38	31
120	8.5658e-03	9.9119e-05	2.9812e-05	1.0987e-03	7.0046e-03	2.9543e-03	4.6801e-03	0:01:35	30
121	8.5576e-03	9.8505e-05	2.9520e-05	1.0846e-03	6.9979e-03	2.9563e-03	4.6576e-03	0:01:32	29
122	8.5380e-03	9.7863e-05	2.9214e-05	1.0706e-03	6.9818e-03	2.9581e-03	4.6355e-03	0:01:28	28
123	8.5104e-03	9.7181e-05	2.8900e-05	1.0569e-03	6.9593e-03	2.9596e-03	4.6137e-03	0:01:25	27
124	8.4708e-03	9.6438e-05	2.8573e-05	1.0436e-03	6.9268e-03	2.9609e-03	4.5925e-03	0:01:22	26
125	8.4232e-03	9.5672e-05	2.8231e-05	1.0308e-03	6.8879e-03	2.9618e-03	4.5722e-03	0:01:19	25
126	8.3707e-03	9.4889e-05	2.7877e-05	1.0182e-03	6.8451e-03	2.9623e-03	4.5535e-03	0:01:16	24
iter	continuity	x-velocity	y-velocity	z-velocity	energy	k	omega	time/iter	
127	8.3151e-03	9.4100e-05	2.7510e-05	1.0064e-03	6.7996e-03	2.9625e-03	4.5371e-03	0:01:13	23
128	8.2584e-03	9.3282e-05	2.7142e-05	9.9512e-04	6.7532e-03	2.9622e-03	4.5228e-03	0:01:09	22
129	8.2028e-03	9.2457e-05	2.6770e-05	9.8465e-04	6.7078e-03	2.9614e-03	4.5108e-03	0:01:06	21
130	8.1486e-03	9.1621e-05	2.6402e-05	9.7487e-04	6.6634e-03	2.9601e-03	4.5006e-03	0:01:03	20
131	8.0941e-03	9.0793e-05	2.6029e-05	9.6588e-04	6.6188e-03	2.9583e-03	4.4917e-03	0:01:00	19
132	8.0406e-03	8.9971e-05	2.5670e-05	9.5761e-04	6.5751e-03	2.9558e-03	4.4838e-03	0:00:57	18

APPENDIX I. SAMPLE OUTPUT FILE

```

133 7.9872e-03 8.9162e-05 2.5319e-05 9.4972e-04 6.5315e-03 2.9527e-03 4.4767e-03 0:00:54 17
134 7.9342e-03 8.8383e-05 2.4981e-05 9.4219e-04 6.4881e-03 2.9490e-03 4.4696e-03 0:00:51 16
135 7.8796e-03 8.7624e-05 2.4645e-05 9.3491e-04 6.4435e-03 2.9447e-03 4.4619e-03 0:00:47 15
136 7.8231e-03 8.6926e-05 2.4317e-05 9.2756e-04 6.3972e-03 2.9397e-03 4.4534e-03 0:00:44 14
137 7.7635e-03 8.6289e-05 2.3987e-05 9.2001e-04 6.3485e-03 2.9339e-03 4.4441e-03 0:00:41 13
iter continuity x-velocity y-velocity z-velocity energy k omega time/iter
138 7.7025e-03 8.5714e-05 2.3665e-05 9.1241e-04 6.2986e-03 2.9275e-03 4.4339e-03 0:00:38 12
139 7.6410e-03 8.5193e-05 2.3350e-05 9.0457e-04 6.2483e-03 2.9204e-03 4.4227e-03 0:00:35 11
140 7.5782e-03 8.4752e-05 2.3039e-05 8.9659e-04 6.1970e-03 2.9127e-03 4.4114e-03 0:00:32 10
141 7.5143e-03 8.4359e-05 2.2739e-05 8.8852e-04 6.1448e-03 2.9042e-03 4.4001e-03 0:00:28 9
142 7.4512e-03 8.4048e-05 2.2436e-05 8.8034e-04 6.0931e-03 2.8952e-03 4.3887e-03 0:00:25 8
143 7.3896e-03 8.3788e-05 2.2143e-05 8.7206e-04 6.0428e-03 2.8856e-03 4.3769e-03 0:00:22 7
144 7.3298e-03 8.3558e-05 2.1847e-05 8.6362e-04 5.9939e-03 2.8754e-03 4.3647e-03 0:00:19 6
145 7.2726e-03 8.3374e-05 2.1568e-05 8.5509e-04 5.9472e-03 2.8648e-03 4.3523e-03 0:00:16 5
146 7.2200e-03 8.3279e-05 2.1290e-05 8.4656e-04 5.9042e-03 2.8538e-03 4.3402e-03 0:00:13 4
147 7.1724e-03 8.3227e-05 2.1019e-05 8.3802e-04 5.8653e-03 2.8424e-03 4.3281e-03 0:00:09 3
148 7.1307e-03 8.3209e-05 2.0759e-05 8.2950e-04 5.8312e-03 2.8307e-03 4.3159e-03 0:00:06 2
iter continuity x-velocity y-velocity z-velocity energy k omega time/iter
149 7.0975e-03 8.3242e-05 2.0507e-05 8.2107e-04 5.8041e-03 2.8187e-03 4.3042e-03 0:00:03 1
150 7.0739e-03 8.3330e-05 2.0260e-05 8.1260e-04 5.7849e-03 2.8066e-03 4.2937e-03 0:00:00 0

> /define/models/unsteady-2nd-order yes

> /solve/monitors/surface/set-monitor x-velocity-turbineinlet "Area-Weighted Average" x-velocity turbine
  () no no yes "ave_x_velocity_turbineinlet_area_weighted" 1 yes flow

> /solve/monitors/surface/set-monitor abl-velocity-turbineinlet "Area-Weighted Average" abl turbine () no
  no yes "ave_abl_velocity_turbineinlet_area_weighted" 1 yes flow

> /solve/monitors/surface/set-monitor mass-flow-rate-turbineinlet "Mass Flow Rate" turbine () no no yes
"mass_flow_rate_turbineinlet" 1 yes flow

> /solve/monitors/surface/set-monitor augmented-power "Integral" power_aug turbine () no no yes "power_aug"
  1 yes flow

> /solve/monitors/surface/set-monitor non-augmented-power "Integral" power_abl turbine () no no yes
  "power_abl" 1 yes flow

> /file/auto-save data-frequency 200

> /solve/set time-step 1

> /solve/dual-time-iterate 700 20

Updating solution at time levels N and N-1.
done.
iter continuity x-velocity y-velocity z-velocity energy k omega time/iter
150 7.0739e-03 8.3330e-05 2.0260e-05 8.1260e-04 5.7849e-03 2.8066e-03 4.2937e-03 0:01:03 20
151 7.0568e-03 8.3438e-05 2.0026e-05 8.0396e-04 5.7709e-03 2.7695e-03 4.2933e-03 0:01:01 19
152 7.0542e-03 8.3533e-05 1.9747e-05 7.9212e-04 5.7688e-03 2.6403e-03 4.2828e-03 0:00:58 18
153 7.0672e-03 8.3705e-05 1.9488e-05 7.8073e-04 5.7795e-03 2.5187e-03 4.2668e-03 0:00:55 17
154 7.0953e-03 8.3841e-05 1.9212e-05 7.6918e-04 5.8025e-03 2.4043e-03 4.2472e-03 0:00:51 16
155 7.1350e-03 8.4130e-05 1.8980e-05 7.5750e-04 5.8350e-03 2.2966e-03 4.2253e-03 0:00:48 15
156 7.1824e-03 8.4258e-05 1.8782e-05 7.4588e-04 5.8737e-03 2.1955e-03 4.2014e-03 0:00:45 14
157 7.2340e-03 8.4269e-05 1.8581e-05 7.3362e-04 5.9159e-03 2.1004e-03 4.1752e-03 0:00:42 13
158 7.2874e-03 8.4255e-05 1.8411e-05 7.2231e-04 5.9595e-03 2.0111e-03 4.1480e-03 0:00:38 12
159 7.3403e-03 8.4283e-05 1.8257e-05 7.1084e-04 6.0028e-03 1.9272e-03 4.1192e-03 0:00:35 11
160 7.3897e-03 8.4314e-05 1.8142e-05 7.0042e-04 6.0431e-03 1.8484e-03 4.0889e-03 0:00:32 10
iter continuity x-velocity y-velocity z-velocity energy k omega time/iter
161 7.4349e-03 8.4226e-05 1.8016e-05 6.9048e-04 6.0801e-03 1.7744e-03 4.0576e-03 0:00:29 9
162 7.4731e-03 8.3890e-05 1.7917e-05 6.7957e-04 6.1113e-03 1.7049e-03 4.0252e-03 0:00:26 8
163 7.5050e-03 8.3535e-05 1.7823e-05 6.6997e-04 6.1373e-03 1.6396e-03 3.9929e-03 0:00:22 7

```

APPENDIX I. SAMPLE OUTPUT FILE

```

164 7.5332e-03 8.3193e-05 1.7710e-05 6.6144e-04 6.1603e-03 1.5782e-03 3.9614e-03 0:00:19 6
165 7.5546e-03 8.2816e-05 1.7611e-05 6.5253e-04 6.1778e-03 1.5205e-03 3.9304e-03 0:00:16 5
166 7.5693e-03 8.2507e-05 1.7486e-05 6.4471e-04 6.1898e-03 1.4662e-03 3.8990e-03 0:00:13 4
167 7.5804e-03 8.1951e-05 1.7344e-05 6.3682e-04 6.1988e-03 1.4150e-03 3.8676e-03 0:00:10 3
168 7.5880e-03 8.1359e-05 1.7202e-05 6.2941e-04 6.2050e-03 1.3668e-03 3.8362e-03 0:00:06 2
169 7.5949e-03 8.0747e-05 1.7049e-05 6.2325e-04 6.2107e-03 1.3213e-03 3.8031e-03 0:00:03 1
170 7.6023e-03 8.0073e-05 1.6868e-05 6.1726e-04 6.2167e-03 1.2785e-03 3.7684e-03 0:00:00 0
Flow time = 1s, time step = 1
699 more time steps

```

```

*****
.....

```

```

*****

```

```

Updating solution at time levels N and N-1.
done.
  iter continuity x-velocity y-velocity z-velocity      energy          k      omega      time/iter
! 2985 solution is converged
  2985 7.7169e-04 5.5841e-06 6.4118e-07 1.3866e-04 6.3103e-04 7.5365e-04 5.5183e-04 0:01:14 20
! 2986 solution is converged
  2986 7.7994e-04 5.8968e-06 6.5650e-07 1.3966e-04 6.3777e-04 7.5339e-04 5.5250e-04 0:01:10 19
Flow time = 699s, time step = 699
1 more time step

```

```

Updating solution at time levels N and N-1.
done.
  iter continuity x-velocity y-velocity z-velocity      energy          k      omega      time/iter
! 2986 solution is converged
  2986 7.7994e-04 5.8968e-06 6.5650e-07 1.3966e-04 6.3777e-04 7.5339e-04 5.5250e-04 0:01:14 20
! 2987 solution is converged
  2987 7.9066e-04 6.0848e-06 6.5593e-07 1.4012e-04 6.4654e-04 7.5317e-04 5.5275e-04 0:01:10 19
Flow time = 700s, time step = 700

```

```

> /file/write-case Rt_1_Rx_0_Ry_0_AOA_0.cas.gz
/file/write-data Rt_1_Rx_0_Ry_0_AOA_0.dat.gz
/report/summary yes "report.sum"
/exit
*****

```

```

-----
Number cpus      = 8
Queue           = mpi
Jobid           = 78537.gup-hn.guppy.sharcnet
Version         = 3ddp
Journal file    = test.jou
Date job started = Thu Mar 31 21:22:46 EDT 2011
Date job finished = Fri Apr 1 19:11:57 EDT 2011
-----

```

Bibliography

- [1] *Bruce Wind Turbine*. Ontario Power Generation Inc., 2001.
- [2] *ANSYS FLUENT-Solver Theory*. ANSYS Inc., 2009.
- [3] *GISS Surface, Temperature Analysis*, volume 2. Goddard Institute for Space Studies, National Aeronautics and Space Administration, 2011.
- [4] *Wind and weater statistic Toronto Island*. Windfinder.com, 2011.
- [5] M. J. Blanch A. G. Duuton, J. A. Halliday. *The Feasibility of Building-Mounted/Integrated Wind Turbines (BUWTs): Achieving their potential for carbon emission reductions*. Energy Research Unit, CCLRC, 2005.
- [6] L. Bryans N. Jenkins D. Milborrow M. O'Malley R. Watson B. Fox, D. Flynn and O. Anaya-Lara. *Wind Power Integration: Connection and system operational aspects*. The Institute of Engineering and Technology, 2007.
- [7] P.W. Bearman and A.J. Wadcock. *The interaction between a pair of circular cylinders normal to a stream*. Fluid Mechanics, 61, 499., 1973.
- [8] L. Chen and J. Tu. *A Large-Eddy Simulation of Two Side-by-Side Circular Cylinders in Cross Flow*. Maritime Platforms Devision, DSTO Melbourne and School of Mechanical and Manufacturing Engineering, RMIT University, Australia.
- [9] Robert K. W. Dannecker and Andrew D. Grant. *Integrated Ducted Wind Turbine Module*. University of Strathclyde, Glasgow, UK, 2002.
- [10] L.G. Margolin F.F. Grinstein and W.J. Rider. *Implicit Large Eddy Simulation*. 2007.
- [11] M. Gaster. *Vortex shedding from slender cones at low Reynolds number*. Journal of Fluid Mechanics, 38, 565–576, 1969.
- [12] M. Gaster. *Vortex shedding from circular cylinders at low Reynolds number*. Journal of Fluid Mechanics, 46, 746–756, 1971.

-
- [13] Gorlov Alexander M. Silantyy Valentin M. Gorban, Alexander N. *Limits of the Turbine Efficiency for Free Fluid Flow*. Journal of Energy Resource Technology, ASME, Vol. 123, pg311-317 December, 2001.
- [14] H. Hamm. *Optimization of Wind Augmenters for Urban Power Generation*. Ryerson University, 2006.
- [15] J. D. Holmes. *Wind Loading of Structures*. Spoon Press, New York, NY, 2001.
- [16] X. Jiang and C.H. Lai. *Numerical Techniques for Direct and Large Eddy Simulation*. 2009.
- [17] H.J. Kim and P.A. Durbin. *Investigation of the flow between a pair of circular cylinders in the floppy regime*. Lewis Research Center, Cleveland, OHm USA, 1988.
- [18] C. W. Rowley M. A. Green and G. Haller. *Detection of Lagrangian coherent structures in three-dimensional turbulence*. Cambridge University Press, 2007.
- [19] S. Mertens. *Wind Energy in the Built Environment*. Multi-Science, United Kingdom, 2006.
- [20] United Nations. *Kyoto Protocol to the United Nations Framework Convention on Climate Change*. 1998.
- [21] P. Piccirillo and C.W. Van Atta. *An experimental study of vortex shedding behind linearly tapered cylinders at low Reynolds number*. Journal of Fluid Mechanics, 246, 163–195, 1993.
- [22] A. Harries S. Stankovic, N. Campbell. *Urban Wind Energy*. Sterling, VA: Earthscan, 2009.
- [23] Ian J. Sobey. *Oscillatory Flows at Intermediate Strouhal Number in Asymmetry Channels*. Journal of Fluid Mechanics, 125, pg359-373, 1982.
- [24] M. M. Zdravkovich. *Flow around Circular Cylinders; Volume 1. Fundamentals*. Oxford Science Publications, 1997.

